

Electronic Thesis and Dissertation Repository

August 2015

Morphology and Morphometry of Double Layered Ejecta Craters on Mars

Ryan Schwegman
The University of Western Ontario

Supervisor
Dr. Gordon Osinski
The University of Western Ontario Joint Supervisor
Dr. Livio Tornabene
The University of Western Ontario

Graduate Program in Geology
A thesis submitted in partial fulfillment of the requirements for the degree in Master of Science
© Ryan Schwegman 2015

Follow this and additional works at: <https://ir.lib.uwo.ca/etd>



Part of the [Geology Commons](#)

Recommended Citation

Schwegman, Ryan, "Morphology and Morphometry of Double Layered Ejecta Craters on Mars" (2015).
Electronic Thesis and Dissertation Repository. 3074.
<https://ir.lib.uwo.ca/etd/3074>

This Dissertation/Thesis is brought to you for free and open access by Scholarship@Western. It has been accepted for inclusion in Electronic Thesis and Dissertation Repository by an authorized administrator of Scholarship@Western. For more information, please contact wlsadmin@uwo.ca.

MORPHOLOGY AND MORPHOMETRY OF DOUBLE LAYERED EJECTA
CRATERS ON MARS

(Thesis format: Integrated Article)

by

Ryan Schwegman

Graduate Program in Geology: Planetary Science

A thesis submitted in partial fulfillment
of the requirements for the degree of
Master of Science

The School of Graduate and Postdoctoral Studies
The University of Western Ontario
London, Ontario, Canada

© Ryan Schwegman 2015

Abstract

Double layered ejecta (DLE) craters display two distinct layers of ejecta that appear to have been emplaced as a mobile, ground-hugging flow. While volatile content within the target, atmosphere, or some combination of the two is generally considered a major variable enhancing the mobility of ejecta, the presence of unconsolidated surface materials may also have some effect. This statement is studied further here, aiming to determine whether bulk target lithology and/or attributes of the surface have any effect on morphometric properties between DLEs situated on sedimentary targets to those on volcanic ones. Results suggest that ejecta mobility (the distance ejecta travels from the crater rim) generally increases with increasing latitude and may reflect volatile concentrations on Mars, while lobateness (sinuosity of the perimeter of ejecta) generally decreases with increasing latitude. Furthermore, DLEs on sedimentary targets appear to have a higher EM, on average, than those on volcanic targets.

Keywords

Mars; impact processes; cratering; layered ejecta; Mars, surface processes

Co-Authorship Statement

Chapter 2 is an article currently in review for publication titled “A comparative morphologic and morphometric study of double layered ejecta craters in volcanic terrains on Mars”. Co-authors are Dr. G. R. Osinski, Dr. L. L. Tornabene, Dr. E. Jones, and T. N. Harrison (Western University, London, ON). All data was collected by R. Schwegman. Dr. G. R. Osinski and Dr. L. L. Tornabene contributed to interpretations and structure of the overall article, as well as editorial suggestions.

Acknowledgments

I cannot thank anyone else before I thank Oz and Livio who have both been incredibly helpful and supportive throughout this whole process and I could not have asked for better supervisors. Also to Eriita who introduced me to Martian layered ejecta and helped me get started on this project.

Thank you to Bianca and Patrick for all their help with ArcGIS, my fellow American Zach, my office buddies Kathy, Becca, Roshni, Laura, Alex, and (British) Jon, and to (Canadian) Ryan. You all have been really awesome friends and I couldn't imagine what these past two years would have been like without you. Thanks also to Eric, Hun, Kayle, Tanya, Mary, and the rest of the former and current Ozlings who have helped me along the way.

I would also like to thank Mary Bourke as if it weren't for her introducing me to Oz, I would have never gotten this incredible opportunity to study in Canada. Thank you also to Jeffrey Byrnes and all the other undergraduate instructors at Oklahoma State University that provided me an education in geological sciences. I would most definitely not be where I am without their expertise.

I cannot forget my family for their unending support; Mom, Dad, Melissa, Debbie, Nick, and Bob, none of this would have been possible without you.

Thank you to my examiners Catherine Neish, Richard Grieve, and Ken McIsaac for their helpful and constructive comments.

And lastly, thank you Canada for letting me study in your great country.

Table of Contents

Abstract	ii
Co-Authorship Statement.....	iii
Acknowledgments.....	iv
Table of Contents	v
List of Tables	viii
List of Figures	ix
List of Appendices	xvii
Chapter 1	1
1 Introduction	1
1.1 Mars	2
1.2 Global Structure	4
1.3 Geologic History.....	6
1.3.1 Noachian Period.....	7
1.3.2 Hesperian Period.....	8
1.3.3 Amazonian Period.....	8
1.4 Cratering Rates and the Cratering Record on Mars	9
1.5 The Impact Cratering Process	10
1.5.1 Contact and Compression	11
1.5.2 Excavation.....	12
1.5.3 Modification.....	13
1.6 Ejecta Morphologies on Mars	15
1.6.1 Radial Ejecta	15
1.6.2 Layered Ejecta Morphologies	17
1.7 Double Layered Ejecta Emplacement Models.....	23

1.7.1	Schultz and Gault (1979) and Schultz (1992) Atmospheric Model.....	23
1.7.2	Mouginis-Mark (1981) and Boyce and Mouginis-Mark (2006) Model ...	24
1.7.3	Komatsu et al. (2007) Model	26
1.7.4	Osinski et al. (2011) Model	28
1.7.5	Weiss and Head (2013) Glacial Substrate Model	30
1.7.6	Wulf and Kenkmann (2015) Model.....	31
1.8	References.....	32
Chapter 2.....		43
2	A Comparative Morphologic and Morphometric Study of Double Layered Ejecta Craters in Volcanic Terrains on Mars	43
2.1	Introduction.....	43
2.2	Methodology	46
2.2.1	Study Areas	48
2.3	Results.....	52
2.3.1	Ejecta Mobility (EM).....	52
2.3.2	Lobateness (Γ)	57
2.3.3	Other Morphologic and Morphometric Attributes.....	61
2.4	Discussion.....	69
2.4.1	Effect of the Target Properties on Ejecta Mobility.....	69
2.4.2	Effect of the Target Properties on Lobateness.....	72
2.4.3	Radial Grooves.....	74
2.4.4	Hesperia Planum – An Outlier?	78
2.5	Concluding Remarks.....	78
2.6	References.....	80
Chapter 3.....		93
3	A Morphometric Comparison of Martian Double Layered Ejecta Craters and Implications for the Effect of Target Lithology.....	93

3.1 Introduction.....	93
3.2 Methodology.....	95
3.3 Results.....	99
3.3.1 Ejecta Mobility (EM).....	99
3.3.2 Lobateness (Γ).....	104
3.3.3 Morphology.....	107
3.4 Discussion.....	110
3.4.1 Effect of Target/Surface Properties on Ejecta Mobility and Lobateness	110
3.4.2 Ejecta Emplacement Chronology	116
3.5 Summary.....	117
3.6 References.....	118
Chapter 4.....	129
4 Conclusions.....	129
4.1 Future Work	131
4.2 References.....	133
Appendices.....	134
Curriculum Vitae	141

List of Tables

Table 1.1: Fact sheet of Earth and Mars.	4
Table 2.1: Study regions showing the number of DLEs corresponding to each geologic unit (See Scott and Tanaka, 1986 and Greeley and Guest, 1987 for full unit descriptions). The first letter of each unit represents each geologic period: A = Amazonian; H = Hesperian; N = Noachian.	51
Table 2.2: Average ejecta mobility (EM) and lobateness (Γ) for outer and inner layers of DLEs.	57
Table 2.3: Dust cover index (DCI) for each region.	75
Table 2.4: Average DCI for DLEs with grooves and without.	75
Table 3.1: Number of volcanic and non-volcanic DLEs within each region.....	96
Table 3.2: Study regions showing the number of DLEs corresponding to each geologic with regional interpretation (see Scott and Tanaka, 1986 and Greeley and Guest, 1987 for full unit descriptions).....	97
Table 3.3: Number of DLEs within each latitude bin.....	100
Table 3.4: Number of DLEs within each crater diameter bin.....	100
Table 3.5: Number of DLEs with or without radial grooves.	107
Table A.0.1 - Volcanic DLEs	134
Table A.0.2 - Non-volcanic DLEs	138

List of Figures

- Figure 1.1: A comparison of Earth and Mars. Image of Earth (Jan. 4, 2012) and Mars (April 1999) taken from the VIIRS instrument onboard Suomi NPP (*NASA/NOAA/GSFC/Suomi NPP/VIIRS/Norman Kuring*) and Mars Orbiter Camera (MOC) onboard Mars Global Surveyor (MGS) (*NASA/JPL/MSSS*) respectively. Size to scale. 3
- Figure 1.2: The 2001 global dust storm as seen from the Mars Orbiter Camera (MOC). Images centered on the Tharsis volcanic region. These images capture the 2001 global dust storm as southern winter transitions to spring (*NASA/JPL/MSSS*). 4
- Figure 1.3: The topography of Mars by the Mars Orbiter Laser Altimeter (MOLA). This map shows the general topography of Mars where blues and purples are lowest in elevation (Hellas Basin ~-7 km) and browns and whites are highest (Olympus Mons ~25 km). The global dichotomy is also apparent (mostly greens) and marks the boundary from the northern lowlands (blues) to the southern highlands (yellows and oranges). Image credit: *NASA/MOLA Science Team*. 6
- Figure 1.4: Geologic timescale of Mars compared to Earth. 7
- Figure 1.5: The impact cratering process as illustrated by Osinski, 2004. 11
- Figure 1.6: Examples of the three crater morphology types: (a) 4 km diameter simple crater located 316.10° E, 38.69° N (HiRISE image ID: ESP_020245_2190_RED); (b) 24 km diameter complex crater located 122.97° E, 4.06° N (CTX mosaic: P17_007752_1832_XN_03N237W; B19_016903_1828_XN_02N237W; P21_009189_1827_XN_02N236W); (c) 7.6 km diameter transitional crater located 277.77° E, 23.81° S (CTX image ID: G12_022818_1564_XN_23S082W). 15
- Figure 1.7: Winslow crater (1.1 km diameter) on Mars (59.16° E, 3.74° S) displaying a radial ejecta morphology (CTX image ID: P08_004313_1780_XI_02S301W). 16
- Figure 1.8: Ballistic sedimentation model (after Oberbeck, 1975). Material ejected out of the transient cavity follow ballistic trajectories where the innermost ejecta is ejected first (at the

steepest angles and highest velocities) and material closest to the rim is ejected later (at lower angles and velocities). The largest particles fall closer to the rim while smaller particles travel further. Airborne (primary) ejecta re-impacts the target and incorporates local material (secondary ejecta) into the developing ejecta blanket which then moves as a ground-hugging flow behind the primary ejecta curtain. The interaction of airborne (primary) ejecta (black circles) with the surface (dashed lines) are depicted in the three lower boxes. 17

Figure 1.9: The 3 common types of layered ejecta morphologies: (a) 12 km diameter single layered ejecta (SLE) crater located 80.47° E, 36.02° N (CTX mosaic: B05_011564_2163_XN_36N279W; P18_008083_2177_XN_37N280W); (b) Steinheim Crater, an 11 km diameter double layered ejecta (DLE) crater located 190.65° E, 54.57° N (CTX mosaic: G21_026302_2344_XN_54N169W; G02_018944_2348_XI_54N168W; P15_006945_2349_XN_54N169W; P17_007736_2349_XI_54N169W); (c) Tooting Crater, a 28 km diameter multiple layered ejecta (MLE) crater located 207.76° E, 23.21° N (THEMIS day IR 100m global mosaic)..... 21

Figure 1.10: Example of a LARLE (a) and pedestal (b) crater on Mars. (a) 5 km diameter crater located 266.37° E, 68.29° N (THEMIS day IR 100m global mosaic); (b) 3 km diameter crater located 91.78° E, 55.28° N (CTX mosaic: G23_027110_2354_XN_55N268W; G21_026477_2355_XN_55N267W)..... 22

Figure 1.11: Schematic diagram of the atmospheric model. Ejecta is emplaced ballistically in which finer particles are winnowed out of the advancing curtain from atmospheric drag. A vortex ring is produced by atmospheric turbulence which can then remobilize emplaced ejecta and deposit smaller material over initial ejecta. 24

Figure 1.12: Schematic diagram showing the inner layer being emplaced before the outer layer. Outer layer is emplaced as a base surge-like process, flowing over and beyond the inner layer and etching grooves into the inner layer..... 26

Figure 1.13: Schematic diagram showing the interaction of near-surface and atmospheric volatiles to produce a layered ejecta morphology..... 27

Figure 1.14: Schematic diagram showing emplacement of the outer layer first via ballistic sedimentation and radial flow. The inner layer is emplaced after as melt-rich material (within

transient cavity) that flows out and over crater rim via uplift during the crater modification stage. 30

Figure 1.15: Schematic diagram of the glacial substrate model. The outer layer is emplaced ballistically while the inner layer is emplaced via landslide mode off of the uplifted crater rim. Impact into a glacial substrate provides ample volatile concentrations to initiate slide mechanism of the inner layer. 31

Figure 1.16: Schematic diagram showing the outer layer being emplaced first as a debris flow mode and the inner layer being emplaced as a translational slide model. 32

Figure 2.1: Example of a double layered ejecta crater in the Syrtis Major region (75.46° E, 9.61° N). HRSC (IDs: H0230_0000_ND4 and H3025_0000_ND4) and THEMIS Day IR 100m mosaic. Scale bar 10 km. North is up. 45

Figure 2.2: Geologic map of Mars highlighting volcanic geologic units (shades of red) (modified after Skinner et al., 2006). DLEs are plotted in yellow. 49

Figure 2.3: Representative DLEs from each study region. Scale bars 10 km. North is up in all images. (a) N Tharsis (276.54° E, 39.73°), THEMIS Day IR 100m global mosaic. (b) Elysium (145.63° E, 9.63°), HRSC image ID: H2973_0000_ND4. (c) S Tharsis (301.04° E, -10.21°), CTX image ID: G22_026773_1700_XN_10S059W. (d) Hesperia Planum (119.51° E, -23.24°), CTX mosaic: B20_017312_1564_XN_23S240W, B18_016745_1551_XN_24S240W, B09_013066_1565_XN_23S240W. 50

Figure 2.4: Distribution of binned EM data on MOLA shaded relief map of Mars. Data is binned by 0.1 increments. (a) Outer layer EM. (b) Inner layer EM. 54

Figure 2.5: Ejecta mobility (EM) of outer layers. (a) Normalized frequency of EM values across latitude. EM values in legend are grouped in 0.5 intervals. Number of craters within a specific series is labeled within each respective bar while total number of craters in each latitude bin are labeled in white boxes. (b) Box plot showing the distribution of EM values within each region. Whiskers represent minimum and maximum values. Average (positive) latitudes are listed with each respective region. 55

Figure 2.6: Ejecta mobility (EM) of inner layers. (a) Normalized frequency of EM values across latitude. EM values in legend are grouped in 0.5 intervals. Number of craters in a specific series is labeled within each respective bar while total number of craters in each latitude bin are labeled in white boxes. (b) Box plot showing the distribution of EM values within each region. Whiskers represent minimum and maximum values. Average (positive) latitudes are listed with each respective region..... 56

Figure 2.7: Distribution of binned lobateness data on MOLA shaded relief map of Mars. Data is binned by 0.1 increments. (a) Outer layer EM. (b) Inner layer EM..... 58

Figure 2.8: Lobateness of outer layers. (a) Normalized frequency of lobateness values across latitude. Lobateness values in legend are grouped in 0.5 intervals. Number of craters in a specific series is labeled within each respective bar while total number of craters in each latitude bin are labeled in white boxes. (b) Box plot showing the distribution of lobateness values within each region. Whiskers represent minimum and maximum values. Average (positive) latitudes are listed with each respective region. 59

Figure 2.9: Lobateness of inner layers. (a) Normalized frequency of lobateness values across latitude. Lobateness values in legend are grouped in 0.5 intervals. Number of craters in a specific series is labeled within each respective bar while total number of craters in each latitude bin are labeled in white boxes. (b) Box plot showing the distribution of lobateness values within each region. Whiskers represent minimum and maximum values. Average (positive) latitudes are listed with each respective region. 60

Figure 2.10: DLEs located in Tharsis with grooves (a, b, c) and without grooves (d, e, f). All scale bars 10 km except b (5 km). North is up in all images. (a) N Tharsis (276.54° E, 39.73°), CTX mosaic: P12_005663_2185_XI_38N083W, B19_016884_2181_XI_38N083W; (b) N Tharsis (266.85° E, 31.69°), CTX image ID: P13_006204_2139_XN_33N093W; (c) N Tharsis (283.36° E, 30.50°), CTX image ID: B17_016475_2099_XI_29N076W; (d) N Tharsis (296.50° E, 6.81°), CTX mosaic: B02_010554_1869_XN_06N063W, G22_026628_1876_XN_07N063W; (e) N Tharsis (288.96° E, 9.83°), CTX image ID: D03_028580_1898_XI_09N071W; (f) S Tharsis (278.54° E, -11.10°), CTX mosaic: P02_001760_1690_XI_11S081W,

B17_016449_1673_XN_12S081W, D01_027631_1682_XN_11S081W,
 F04_037547_1684_XN_11S081W, D22_035991_1684_XN_11S081W..... 63

Figure 2.11: Distribution of DLEs displaying grooves (blue) and those lacking grooves (yellow) over MOLA shaded relief map of Mars (top) and TES colorized dust cover index (bottom). Warmer colors represent areas of higher dust cover; cooler colors represent areas of lower dust cover. Values in Tables 3 and 4 were derived from the map sampling feature in JMARS where the average DCI (after Ruff and Christensen, 2002) was calculated for the total area of a DLE (i.e., area of outer layer) and then averaged with the total DLEs within a specific region..... 64

Figure 2.12: Topographic profiles of representative DLEs from each study region using HRSC DTMs. Dotted lines are planes of reference. All scale bars are 10 km. North is up in all images. (a) 11.7 km diameter crater located in N Tharsis (268.69° E, 55.58°). Vertically exaggerated ~17x. Image ID: H1594_0000. (b) 4.9 km diameter crater located in Elysium (178.26° E, 31.40°). Vertically exaggerated ~17x. Image ID: H1540_0009. (c) 14.7 km diameter crater located in Syrtis Major (75.47° E, 9.61°). Vertically exaggerated ~8x. Image ID: H3025_0000. (d) 5.9 km diameter crater located in S Tharsis (301.04° E, -10.21°). Vertically exaggerated ~6x. Image ID: H1918_0000. (e) 12.8 km diameter crater located in Hesperia Planum (100.44° E, -30.14°). Vertically exaggerated ~9x. Image ID: H0022_0000. 66

Figure 2.13: Examples of the two recently proposed DLE types in the Hesperia region. All scale bars are 10 km. North is up in all images. CTX mosaic: (a) G07_020807_1528_XN_27S258W, B20_017550_1486_XI_31S258W, D13_032345_1512_XN_28S258W; (b) G19_025461_1417_XN_38S237W, F02_036432_1391_XN_40S236W; (c) B20_017312_1564_XN_23S240W, B18_016745_1551_XN_24S240W, B09_013066_1565_XN_23S240W; (d) D21_035417_1540_XN_26S249W, B18_016508_1568_XN_23S250W, G19_025646_1564_XN_23S249W, B17_016297_1565_XN_23S249W, B16_016086_1566_XN_23S249W, F02_036617_1531_XN_26S249W..... 68

Figure 3.1: Examples of non-volcanic (a, b, c) and volcanic (d, e, f) DLEs. (a) 12.2 km diameter crater located at 120.53° E, 34.71°N; CTX mosaic: D04_028863_2145_XN_34N239W, D15_033122_2158_XN_35N239W, P20_008833_2149_XN_34N239W, G22_026964_2131_XN_33N239W, G20_025975_2135_XN_33N288W. (b) 10.7 km diameter crater located at 95.71° E, 57.00° N; CTX mosaic: D21_035549_2381_XN_58N265W, D22_035694_2379_XN_57N263W, G01_018420_2372_XN_57N264W, P16_007344_2382_XN_58N264W. (c) 10.8 km diameter crater located at 308.86° E, 42.54° N; CTX mosaic: B02_010527_2228_XN_42N051W, B17_016118_2250_XN_45N051W. (d) 16.7 km diameter crater located at 296.50° E, 6.81° N; CTX mosaic: B02_010554_1869_XN_06N063W, G22_026628_1876_XN_07N063W. (e) 14.8 km diameter crater located at 119.51° E, 23.24° S; CTX mosaic: B20_017312_1564_XN_23S240W, B18_016745_1551_XN_24S240W, B09_013066_1565_XN_23S240W. (f) 14.7 km diameter crater located at 75.47° E, 9.61° N; HRSC image ID: H0232_0000; H3025_0000. 95

Figure 3.2: Geologic map of Mars modified after Scott and Tanaka (1986), Greeley and Guest (1987), and digitized into ArcGIS by Skinner et al. (2006). Shades of red are interpreted as largely volcanic terrains while blues represent non-volcanic terrains. DLEs are plotted as white circles (non-volcanic) and yellow triangles (volcanic). Though there are some lava flows within Utopia Planitia, we consider it largely a non-volcanic terrain based on the regional interpretation (Table 2). 96

Figure 3.3: Box plots showing the distribution of EM values for the outer (a) and inner (b) layers. Data is binned by 10° latitude. Non-volcanic DLEs are plotted in blue, volcanic DLEs in red. Whiskers represent minimum and maximum values with outliers plotted as circles. The horizontal lines within each box represent the median EM value. 101

Figure 3.4: Box plots showing the distribution of EM values for the outer (a) and inner (b) layers. Data is binned by crater diameter (every 3 km). Non-volcanic DLEs are plotted in blue, volcanic DLEs in red. Whiskers represent minimum and maximum values with outliers plotted as circles. The horizontal lines within each box represent the median EM value. 102

Figure 3.5: Distribution of binned EM data over MOLA shaded relief map of Mars. Top plot (a) shows the outer layer EM, bottom plot (b) shows the inner layer EM. Data is binned by 0.2 values. Non-volcanic DLEs are plotted as circles, volcanic DLEs are triangles. 103

Figure 3.6: Box plots showing the distribution of lobateness values for the outer (a) and inner (b) layers. Data is binned by 10° latitude. Non-volcanic DLEs are plotted in blue, volcanic DLEs in red. Whiskers represent minimum and maximum values with outliers plotted as circles. The horizontal lines within each box represent the median lobateness value. 105

Figure 3.7: Box plots showing the distribution of lobateness values for the outer (a) and inner (b) layers. Data is binned by crater diameter (every 3 km). Non-volcanic DLEs are plotted in blue, volcanic DLEs in red. Whiskers represent minimum and maximum values with outliers plotted as circles. The horizontal lines within each box represent the median lobateness value. 106

Figure 3.8: Distribution of binned lobateness data over MOLA shaded relief map of Mars. Top plot (a) shows the outer layer lobateness, bottom plot (b) shows the inner layer lobateness. Data is binned by 0.2 values. Non-volcanic DLEs are plotted as circles, volcanic DLEs are triangles. 107

Figure 3.9: Topographic profiles of the craters in Fig. 1 derived from MOLA DTMs. Blue profiles are non-volcanic DLEs (a, b, c), red profiles are volcanic DLEs (d, e, f). Dashed lines are planes of reference to emphasize the topography of ejecta. Vertical exaggeration (VE) is included within each profile. IDs for context images are the same as those in Fig. 1 unless otherwise noted. (a) 12.2 km diameter crater located in Utopia Planitia (120.53° E, 34.71°N). (b) 10.7 km diameter crater located in Utopia Planitia (95.71° E, 57.00°N). (c) 10.8 km diameter crater located in Acidalia Planitia (308.86° E, 42.54°N). (d) 16.7 km diameter crater located in Tharsis (296.50° E, 6.81° N). (e) 14.8 km diameter crater located in Hesperia Planum (119.51° E, 23.24° S). (f) 14.7 km diameter crater located in Syrtis Major (75.47° E, 9.61° N). CTX image ID: G01_018698_1896_XN_09N284W. 110

Figure 3.10: Examples of DLE outer layers that resemble the saturated and non-saturated large-scale debris flow experiment morphologies described in Major (1997). The DLEs depicted in a and b resemble the saturated debris flows where multiple surges commonly

overrun earlier emplaced material and form numerous lobes. The DLEs in c and d resemble the non-saturated debris flows where subsequent surges push forward earlier emplaced material and overlapping of lobes is uncommon. All scale bars are 5 km. 116

List of Appendices

Appendix A: Morphometry and location of each crater included in this study	134
--	-----

Chapter 1

1 Introduction

Impact cratering is a geologic process common on every planetary body throughout the solar system. This process involves a projectile (e.g., asteroid, comet) striking the surface of another planetary body at high velocities leaving an initially bowl-shaped depression on the surface called an impact crater. During the impact cratering process, material derived from the subsurface is excavated and emplaced onto the surface outside the crater as a “blanket” (i.e., deposit) referred to as ejecta. By studying impact ejecta, we are also able to study not only the impact process, but the subsurface of planetary bodies. This is especially important for Mars as we currently can only make inferences of the geological makeup of the subsurface from orbit as well as in a few remote locations by current and past rovers. Because Earth is a dynamic geologic body, impact ejecta is quickly modified (e.g., eroded or buried) following emplacement and inevitably becomes recycled, along with the crater itself, into the upper mantle by plate tectonics. In comparison, erosion rates on Mars are extremely low (e.g., Golombek and Bridges, 2000; Golombek et al., 2006) and because the planet lacks plate tectonics, craters and ejecta can be preserved throughout a significant amount of geologic time, making Mars an ideal place to study impact ejecta.

Craters with ejecta that appear layered in appearance are unique to Earth and Mars and, to date, have not been recognized on any other terrestrial body (i.e. the Moon, Mercury and Venus) in the inner Solar System (Carr et al., 1977; Osinski et al., 2011). These morphologies are considered to be emplaced via a ground-hugging flow resulting from the interaction of the ejecta blanket with volatile content likely derived from the target and/or atmosphere (e.g., Carr et al., 1977; Schultz and Gault, 1979). The Ries impact structure in southern Germany is one of the best terrestrial examples of a crater displaying a layered ejecta morphology with substantial amounts of ejecta still preserved. Though it is a very young impact crater (~15 m.y. (Buchner et al., 2010)), the ejecta has already shown signs of significant erosion in places and demonstrates the rapidity of erosion rates on Earth. On Mars, layered ejecta is recognized as the dominant type of

ejecta morphology surrounding craters ≥ 5 km in diameter (Barlow, 1988, 2007). Morphologies include single- (SLE), double- (DLE), and multiple- (MLE) layered ejecta and are defined as displaying one, two, or more than two partial or continuous ejecta layers, respectively (Barlow et al., 2000). While SLEs are abundant globally and MLEs are few in numbers, DLEs are of particular interest because they are heavily concentrated at mid- to high-latitudes, in addition to having two continuous layers of ejecta; one being superposed on top of the other.

The emplacement process of DLEs is not well understood, including as to which layer was emplaced first. This study attempts to answer said question and provide insight into the emplacement process by focusing on the effect target and surface properties have on the morphology and morphometry of DLE craters on Mars. A total of 206 DLE craters were selected for analysis and included two different terrain types: 127 on what is interpreted as volcanic terrains and 79 on what is largely interpreted as sedimentary terrains (Scott and Tanaka, 1986; Greeley and Guest, 1987; Skinner et al., 2006). Analysis included measurement of each ejecta layer (both inner and outer layers) to determine ejecta mobility, the extent an ejecta layer travels from the crater rim, and lobateness, sinuosity of the distal edge of the ejecta layer. This chapter (Chapter 1) provides an overview of Mars, the impact cratering process, and ejecta morphologies on Mars, including current models of the emplacement process of DLE craters. Chapter 2 focuses on the morphology and morphometry of DLEs exclusively in volcanic terrains on Mars while Chapter 3 compares these volcanic DLEs to DLEs situated on largely sedimentary targets. Chapter 4 provides a conclusion of the overall thesis including major results, interpretations, and future work.

1.1 Mars

Mars is the most Earth-like planet in our Solar System (Fig. 1.1). It is roughly half the size of Earth with a radius of ~ 3390 km (compared to Earth's ~ 6371 km) (Table 1.1). Mars orbits the Sun at an average distance of 1.524 AU (2.279×10^8 km) taking nearly two Earth years (686.98 Earth days) to complete one revolution. A day on Mars, termed a "Sol", is 24.623 hours. Like Earth, Mars has seasons due to the tilt of its axis. Currently, its tilt is $\sim 25.2^\circ$ though it has been estimated to have fluctuated from $\sim 15^\circ$ up to as much

as $\sim 60^\circ$ throughout geologic history (Laskar et al., 2004). This fluctuation can cause extreme climate changes, which affects the global distribution of ice. Though the atmosphere is dominantly carbon dioxide, it is relatively thin and dry, making it difficult to absorb and retain solar radiation. Due to this and Mars' distance from the Sun, average diurnal temperatures range from ~ 150 K (-123°C) at the poles to 240 K (-33°C) in the southern hemisphere during midsummer (Kieffer et al., 1977). Regional dust storms are common on Mars, mainly in the southern hemisphere, but can occasional evolve into global ones, such as those observed in 1971, 1977, and 2001 (Fig. 1.2). During these storms, wind speeds average 10 m/s (with gusts up to 40 m/s) as recorded by the Viking landers (Carr, 2006).

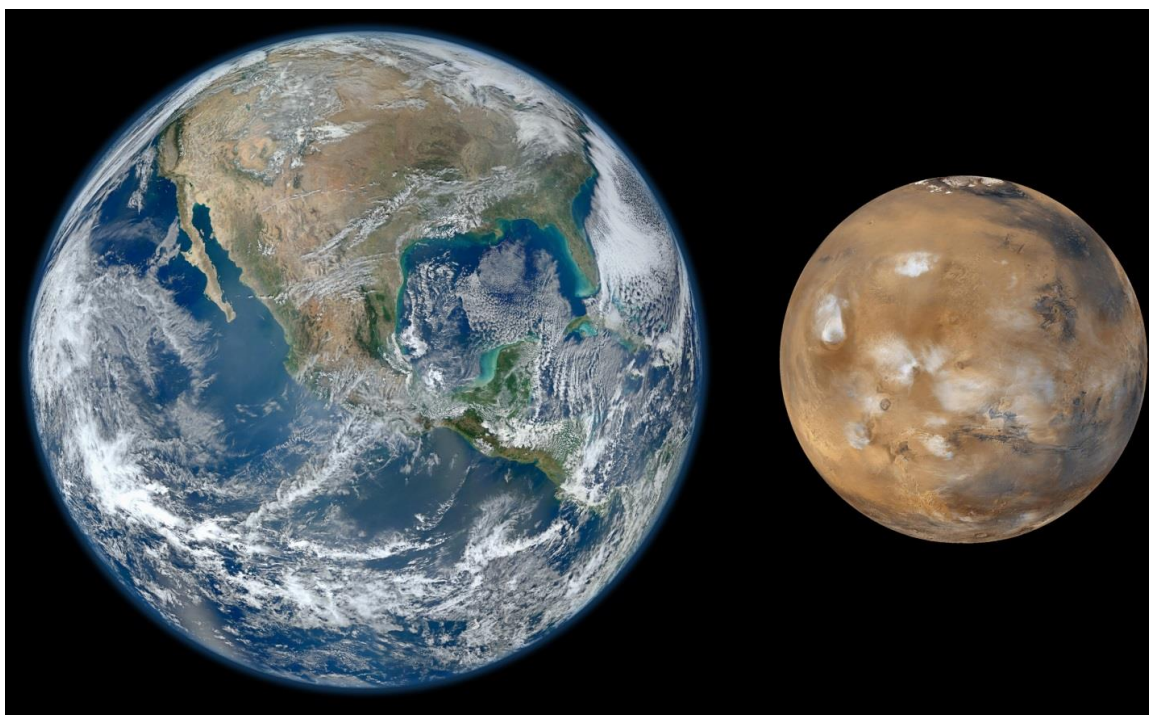


Figure 1.1: A comparison of Earth and Mars. Image of Earth (Jan. 4, 2012) and Mars (April 1999) taken from the VIIRS instrument onboard Suomi NPP (NASA/NOAA/GSFC/Suomi NPP/VIIRS/Norman Kuring) and Mars Orbiter Camera (MOC) onboard Mars Global Surveyor (MGS) (NASA/JPL/MSSS) respectively. Size to scale.

Table 1.1: Fact sheet of Earth and Mars.

	Earth	Mars
Distance from Sun	1.496×10^8 km (1 AU)	2.279×10^8 km (1.524 AU)
Radius	6,371 km	3,390 km
Mass	5.972×10^{24} kg	6.417×10^{23} kg
Density	5.513 g/cm^3	3.934 g/cm^3
Surface gravity	9.807 m/s^2	3.71 m/s^2
Escape velocity	11,190 m/s	5,030 m/s
Axial tilt	23.439°	25.2°
Rotation period	23.934 hours	24.623 hours
Revolution period	365.26 days	686.98 Earth days
Surface temperature	185–331 K	120–293 K
Atmosphere	N ₂ , O ₂ , Ar	CO ₂ , N ₂ , Ar
Surface composition	Basaltic, granitic	Basaltic

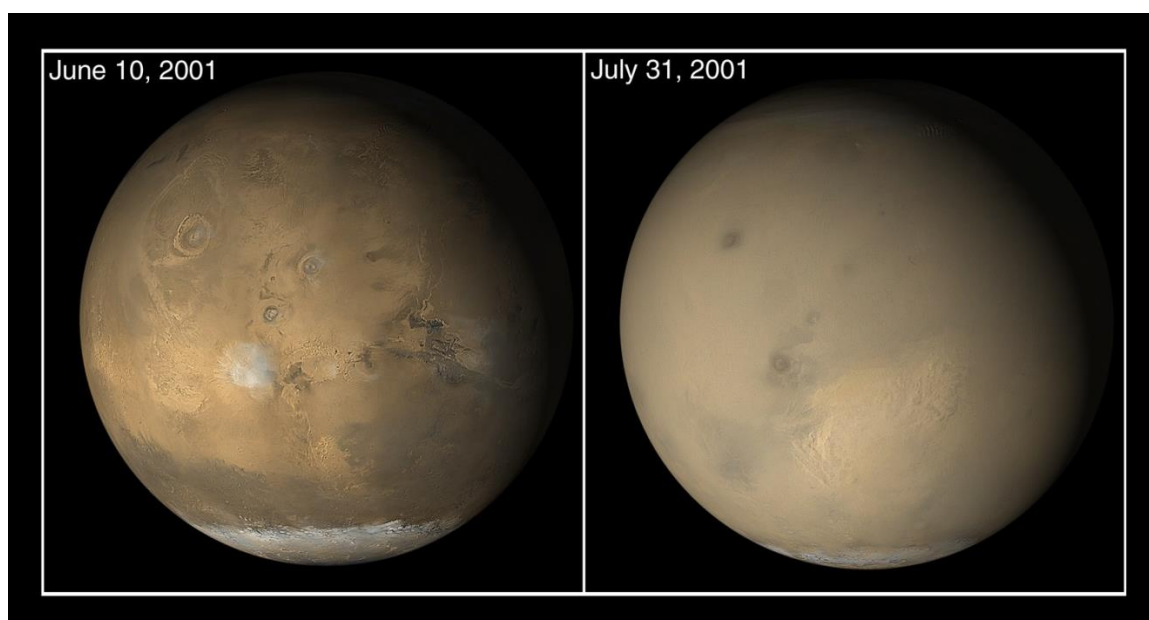


Figure 1.2: The 2001 global dust storm as seen from the Mars Orbiter Camera (MOC). Images centered on the Tharsis volcanic region. These images capture the 2001 global dust storm as southern winter transitions to spring (NASA/JPL/MSSS).

1.2 Global Structure

Mars is differentiated into a core, mantle, and crust. Because Mars has no present-day magnetic field, the core is probably solid (iron-rich). However, there are large remnant

crustal magnetic anomalies in the southern highlands, which may indicate a molten core early on in Mars' history (Acuna et al., 1999). The radius of the core is estimated to be 1300–1500 km (Stevenson, 2001). The Martian crust is largely basaltic and andesitic in composition, as identified by Thermal Emission Spectrometer (TES) data (Bandfield et al., 2000), although the andesitic composition is also interpreted as weathered basaltic surfaces (Wyatt et al., 2004). Crustal thicknesses are extremely varied (estimated to be 5.8–102 km) but is generally much thicker in the southern hemisphere and thinner in the northern hemisphere (Neumann et al., 2004). The upper portion of the crust is also believed to be volatile-rich, as evident by numerous morphological features suggested to result from the interaction of water and/or ice (e.g., gullies, lobate debris aprons, layered ejecta, polygons, hollows, thermokarst) (Carr, 2006). Currently, liquid water is unstable near the surface but may be present beneath a thick cryosphere; volatiles within the cryosphere will be in the solid (e.g., ice) form. It has been suggested that subsurface volatile concentrations are generally more abundant at the poles and decrease equatorward (Rossbacher and Judson, 1981; Clifford and Hillel, 1983; Clifford, 1993; Clifford and Parker, 2001; Clifford et al., 2010), and that poleward of $\pm 40^\circ$ latitude, ground ice is predicted to be stable with the atmosphere (Fanale, 1976; Clifford and Hillel, 1983).

There are many prominent features noticeable on the surface of Mars, including the Tharsis bulge, Valles Marineris, and the Hellas basin, yet the largest and most fundamental feature is the global dichotomy that separates the northern lowlands from the southern highlands (Fig. 1.3). Elevation, crater density, and crustal thicknesses are greatly contrasted between the two provinces, with the northern lowlands being the lower extremity and southern highlands being the upper. The heavily cratered southern highlands represent the oldest surfaces on Mars and are likely from the formation of the planet, while the northern lowlands have been resurfaced and are, therefore, younger and sparsely cratered. The average elevation differences between the two are -4 km below (northern lowlands) and 1.5 km above (southern highlands) the reference datum (Carr, 2006).

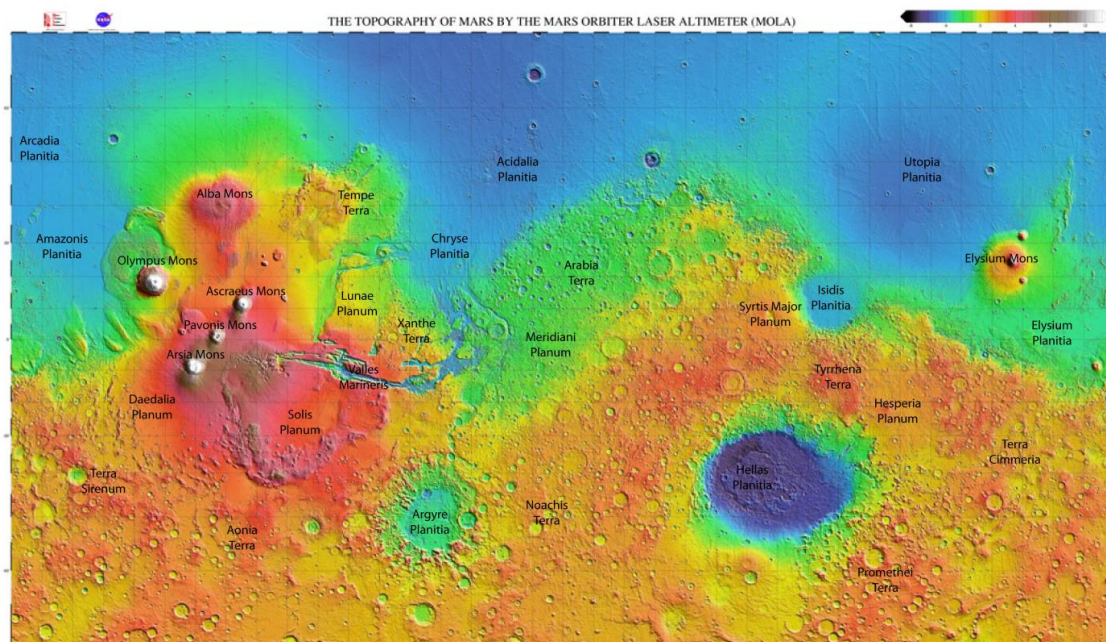


Figure 1.3: The topography of Mars by the Mars Orbiter Laser Altimeter (MOLA). This map shows the general topography of Mars where blues and purples are lowest in elevation (Hellas Basin \sim 7 km) and browns and whites are highest (Olympus Mons \sim 25 km). The global dichotomy is also apparent (mostly greens) and marks the boundary from the northern lowlands (blues) to the southern highlands (yellows and oranges). Image credit: *NASA/MOLA Science Team*.

1.3 Geologic History

The geologic history of Mars is divided into three time-stratigraphic periods based on surface features and the number of superimposed impact craters and are named after type localities representative of each period: Noachian (\sim 4.1–3.7 Gy), Hesperian (\sim 3.7–3.0 Gy), and Amazonian (\sim 3.0 Gy to present) (Fig. 1.4) (Tanaka, 1986; Carr and Head, 2010). A pre-Noachian period is sometimes recognized (e.g., Frey, 2006) but yields many uncertainties regarding the state of the surface, as it has almost certainly been erased. This period of time before the Noachian is considered to characterize the formation of the planet, including accretion and differentiation, and the formation of the global dichotomy, which separates the northern and southern hemispheres (Carr and Head, 2010). The evolution of the dichotomy is uncertain but has been suggested it is either a result of one

or more large impacts (Marinova et al., 2008) or from an internal origin (e.g., mantle convection) (Wise et al., 1979). Tharsis volcanism is also considered to have begun by the end of the period (Carr and Head, 2010).

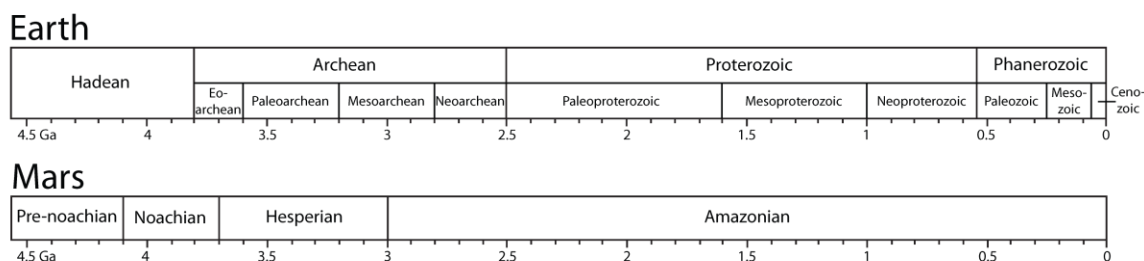


Figure 1.4: Geologic timescale of Mars compared to Earth.

1.3.1 Noachian Period

The Noachian period is bounded by the formation of the Hellas basin and the end of the late heavy bombardment and is characterized by high rates of impact cratering, erosion (compared to successive periods), and valley formation (Carr and Head, 2010). Much of the southern hemisphere is heavily cratered and represents Noachian aged terrain. These terrains appear much more eroded than subsequent Hesperian terrains and suggest that erosion rates dropped significantly after the Noachian. It should be noted that erosion rates on Mars are lower than the average rates on Earth (Golombek and Bridges, 2000; Golombek et al., 2006). Volcanism during the Noachian was likely concentrated around Tharsis, as the majority of the province was emplaced by the end of the period, though volcanic fill from large impacts may have also been prevalent. Outgassing from Tharsis volcanism and the generation of heat from multiple large impact events may have contributed to a warmer, wetter climate by injecting water and other greenhouse gases into the atmosphere (Segura et al., 2002). Subsequent precipitation over “decades” may have initiated valley networks and aqueous alteration of basalts, forming widespread phyllosilicate minerals (Segura et al., 2002; Carr and Head, 2010). These features are all evidence that suggest that the Noachian climate was, at least episodically, warmer and wetter than present-day Mars.

1.3.2 Hesperian Period

The Hesperian period distinguishes post-Noachian plains from the younger Amazonian plains and is dominantly characterized by widespread volcanism and a significant drop in impact cratering and erosion (Carr and Head, 2010). This volcanism is thought to have resurfaced ~30% of the planet mainly in the form of rigid plains and paterae (i.e. volcanic crater with scalloped edges) (Head et al., 2002; Carr and Head, 2010). Large outflow channels seen along the dichotomy are believed to have formed during the Hesperian and were likely carved by the rapid release of large volumes of liquid water from the subsurface (Carr, 1979; Wilson and Head, 2004; Ghatan et al., 2005; Carr and Head, 2010). These flooding events may have led to large bodies of water residing in topographic lows (e.g., the northern plains and large impact basins) and may have deposited sediments that make up the Vastitas Borealis Formation in the northern plains (Kreslavsky and Head, 2002). Excluding these flooding events, erosion rates dropped significantly during the Hesperian and continued through to present-day (Golombek et al., 2006; Carr and Head, 2010). The climate is suggested to have been in a transition stage from a warmer, possibly wetter early Mars into the cold dry planet we know today (Carr and Head, 2010). The formation of sulfates was abundant in the Hesperian and may have resulted from a decline in volcanic activity which led to the removal of SO₂ from the atmosphere and a drop in temperatures moving toward a colder climate (Head et al., 2002; Bibring et al., 2006; Halevy et al., 2007; Carr and Head, 2010). Accumulation of a global cryosphere may have begun as well (Carr and Head, 2010).

1.3.3 Amazonian Period

The Amazonian period represents roughly two-thirds of Martian geologic history and is characterized largely by the presence of ice (Carr and Head, 2010). Modification of the Martian surface by ice likely occurred throughout much of the Amazonian at mid- to high-latitudes (Head and Marchant, 2006; Head et al., 2006, 2010; Madeleine et al., 2009; Souness and Hubbard, 2012) and is also suggested to have occurred at tropical latitudes, likely restricted to higher altitudes (e.g., Tharsis Montes), during periods of higher obliquity (Head and Marchant, 2003; Head et al., 2005; Shean et al., 2005; Fastook et al., 2008; Carr and Head, 2010). Melting of this ice likely formed many of the

small gullies observed on steep slopes at mid- to high-latitudes and represents the main form of fluvial activity during the Amazonian (Costard et al., 2002; Williams et al., 2009). Though the origin of gullies are still debated, their morphologic similarity to terrestrial gullies suggests that liquid water is the dominant formation agent (Malin et al., 2006). Volcanism likely occurred episodically and is characterized by much lower eruption rates concentrated mainly around the Tharsis and Elysium provinces (Werner, 2009; Carr and Head, 2010). Erosion rates are similar to those of the Hesperian period and is largely aeolian in nature as made evident by the numerous dunes distributed globally (Golombek et al., 2006; Carr and Head, 2010).

1.4 Cratering Rates and the Cratering Record on Mars

Cratering rates within the inner Solar System are thought to vary and are believed to be a function of the population of projectiles around a specific planetary body (Michel and Morbidelli, 2013). The cratering rate for the Moon has been determined by age-dating lunar samples returned from the Apollo missions. Because the location of each sample is known, an absolute age for a particular surface can be determined and subsequently, a cratering rate for the Moon can be calculated. Unfortunately for Mars, we currently have no samples collected in situ so the cratering rate can only be derived from the Moon's. The current cratering rate on Mars is much lower than it was in the early history of the planet (e.g., Daubar et al., 2013). In fact, it is generally recognized that a spike in the impact cratering record occurred ~ 3.9 Ga for the entire inner Solar System and is usually referred to as the Late Heavy Bombardment (LHB) (e.g., Gomes et al., 2005; Michel and Morbidelli, 2013; Tsiganis et al., 2005). The NICE model proposes the LHB is a result from the outward migration of the giant planets to their current orbits (Gomes et al., 2005; Tsiganis et al., 2005). This in turn disrupted the whole Solar System and sent left over planetesimals towards the inner Solar System (Gomes et al., 2005).

The three Martian periods described above are derived from the impact cratering record throughout the planets geologic history (Scott and Carr, 1978; Tanaka, 1986). By counting the number of craters in a given area, the age of a particular surface can be estimated. For example, a heavily cratered surface is much older than a surface with fewer craters simply because it has been exposed to the cratering rate for a longer period

of time. Lava flows and other geologic processes can bury or erase (i.e., resurface) older surfaces thereby providing a “clean slate” for the cratering record. Many of the craters in the southern highlands of Mars are remnants from the LHB. In addition, the largest impact basins (e.g., Hellas, Argyre, Isidis, Utopia) were formed during this time (e.g., Carr and Head, 2010; Frey, 2006). Comparatively, the northern plains are sparsely cratered and have since been resurfaced.

1.5 The Impact Cratering Process

Hypervelocity impact events produce many of the craters observed on solid surface bodies within the Solar System such as the terrestrial planets and icy satellites. These events occur when a projectile (e.g., asteroid or comet) is large enough to pass through an atmosphere (if present) without losing its original velocity (or very little), producing shock waves upon striking the surface. Smaller objects lose most of their initial velocity as they pass through the atmosphere; therefore they do not generate shock waves and produce small “penetration craters”. Gault et al. (1968) was the first to propose a multi-stage process during an impact event: contact and compression, excavation, and modification (Fig. 1.5). Each is described below.

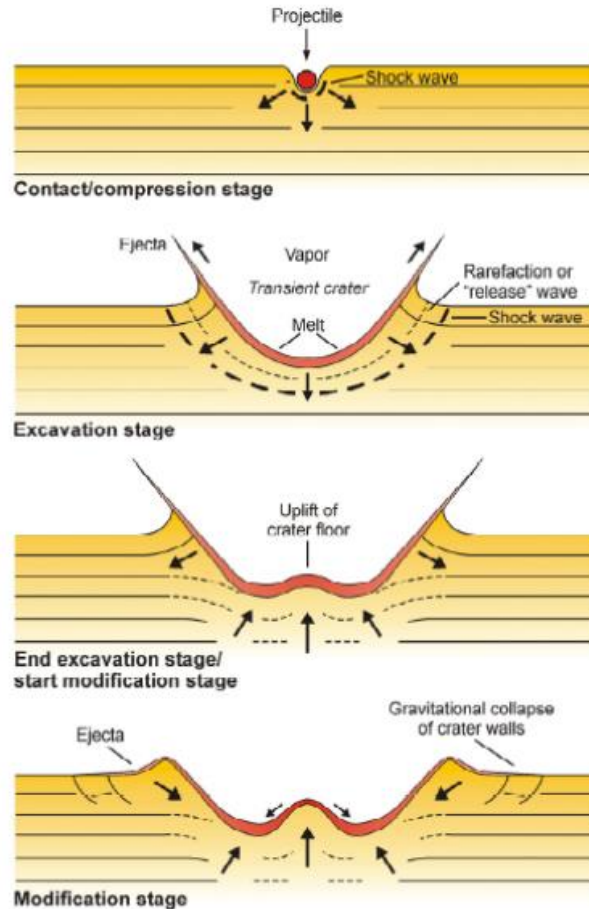


Figure 1.5: The impact cratering process as illustrated by Osinski, 2004.

1.5.1 Contact and Compression

The contact and compression stage is the briefest of the three stages lasting only a fraction of a second, beginning when the projectile makes contact with the target and ends once the projectile unloads. At the point of impact, shock waves form at the projectile-target interface and propagate down and outward through the target as well as up through the projectile; both the target and projectile compress and become highly distorted (Melosh, 1989). High pressure regions develop near the sides of the projectile and create a phenomenon known as jetting where highly shocked material is thrown, or squeezed, out laterally at speeds several times faster than the projectile (Melosh, 1989). The downward motion of the projectile compresses itself and the target even further, as

the shock wave travels through the projectile to its rear surface at which point it is reflected back as a rarefaction wave directed back down toward the target. Once the rarefaction wave reaches the projectile-target interface, unloading occurs and pressures are reduced to near-zero (Melosh, 1989). The projectile is completely distorted as much of it is now vaporized and lines the opening crater cavity. The shock wave propagating down and outward through the target is ongoing throughout the contact and compression stage. It should be noted that the preceding processes describe a projectile striking the surface at a 90° angle (perpendicular) to the surface, though it is extremely rare for a meteorite to strike at such an angle. Most impacts come in at an oblique angle, probably $\sim 45^\circ$, yet the processes are very similar. The main difference is the shock wave generated is asymmetric and weakens with decreasing impact angle (Pierazzo and Melosh, 2000). Therefore, the preceding processes are applicable for all but the most oblique ($< 10^\circ$) impact events.

1.5.2 Excavation

During the excavation stage, a bowl-shaped cavity begins to take form and grow into what is called the “transient cavity” or “transient crater”. This cavity is temporary and is usually enlarged to some degree during the modification stage depending on the crater type (i.e., simple or complex). The contact and compression stage transitions into the excavation stage and is characterized by the ejection of material out of the transient cavity. The initial shock wave produced during contact and compression continues to expand, roughly hemispherically, eventually decaying in strength into a plastic wave followed by an elastic wave. Shock waves that travel upwards reach the surface and are then reflected back down through the target as rarefaction waves. The combination of the shock and rarefaction waves set material in motion outward and downward, radially, producing the excavation flow which then opens up the transient cavity. The transient cavity can be divided into two “zones” resulting from the varying trajectories the material takes; an upper “excavated zone” and lower “displaced zone”. Material within the excavated zone is thrown out and beyond the transient cavity rim to form the continuous ejecta blanket(s) while material within the displaced zone is pushed further down and outward forming the base of the expanding cavity. A vapor plume, or impact plume, is

formed immediately after unloading of the projectile which results from vaporization of most of the projectile and some portion of the target. This gas expands outwards at extremely high speeds and is important for distal ejecta emplacement (see later section), hence its inclusion in the excavation stage.

1.5.3 Modification

The final stage in the impact cratering process is characterized by the modification, or collapse, of the transient cavity and is driven dominantly by gravitational forces. This generally occurs after the crater has been fully excavated. Modification of the transient cavity can produce two main crater types based on morphology: simple or complex (Fig. 1.6) The transition from simple to complex craters differs on each planetary body and is mainly dependent on gravity and the target. On Mars, this transition occurs between ~5 – 10 km in diameter (Pike, 1980), where simple craters are smaller and complex craters are larger. Craters with diameters in this range can have morphologies of both simple and complex craters (discussed below) and are therefore termed “transitional craters” (Fig. 1.6). Simple craters are nearly circular, bowl-shaped depressions that have undergone only minor modification of the transient cavity (Fig. 1.6). The cavity walls are generally more stable, resisting gravitational collapse, thus the final observed crater resembles that of the original transient cavity. The floors of simple craters usually contain a lens of breccia mixed with melt and shocked material. Complex craters, as the name implies, are more complex and undergo major modification of the transient cavity. As transient diameters increase, cavity walls become less stable and collapse under gravity usually forming a terraced crater rim by listric faulting (Fig. 1.6). Central peaks, or central uplifts, are a common feature on the floors of complex craters, where material is brought to the surface as a mound. Though the formation and origin is still debated, it is analogous to the physics of a droplet impacting water.

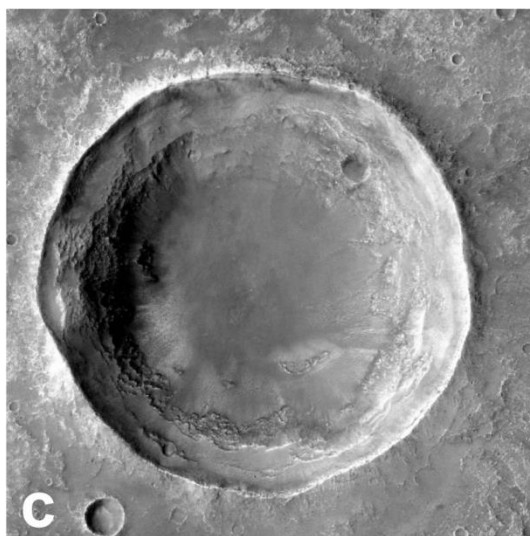
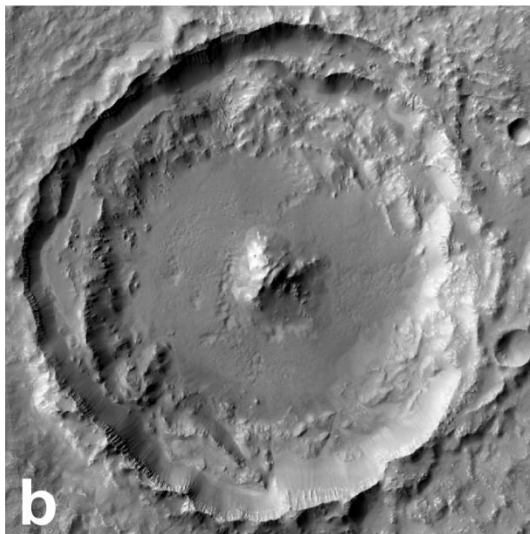
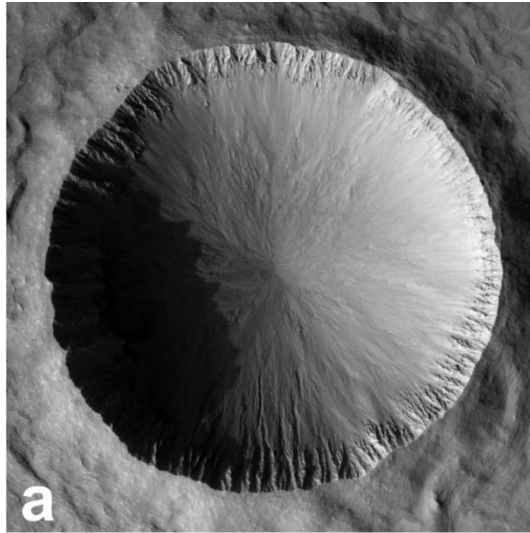


Figure 1.6: Examples of the three crater morphology types: (a) 4 km diameter simple crater located 316.10° E, 38.69° N (HiRISE image ID: ESP_020245_2190_RED); (b) 24 km diameter complex crater located 122.97° E, 4.06° N (CTX mosaic: P17_007752_1832_XN_03N237W; B19_016903_1828_XN_02N237W; P21_009189_1827_XN_02N236W); (c) 7.6 km diameter transitional crater located 277.77° E, 23.81° S (CTX image ID: G12_022818_1564_XN_23S082W).

1.6 Ejecta Morphologies on Mars

Relatively fresh impact craters on terrestrial bodies usually exhibit continuous ejecta blankets that extend $> \sim 1$ crater radii from the crater rim (Melosh, 1989). Several types of ejecta morphologies surrounding Martian craters have been recognized and are markedly different from those observed on the Moon and Mercury (discussed below).

1.6.1 Radial Ejecta

On airless bodies such as the Moon and Mercury, ejecta commonly appears “rayed” and is generally accepted to have been emplaced ballistically (e.g., Oberbeck, 1975; Melosh, 1989) (Figs. 1.7 and 1.8). This type of ejecta has been referred to as ballistic or “radial” ejecta. These morphologies have also been observed on Mars, but are much less common (e.g., Barlow 1988; Barlow 2007). Initial emplacement of radial ejecta is via a process of ballistic sedimentation, where material (termed primary ejecta) is ejected out of the transient cavity at different angles, following parabolic flight paths that strike the ground at different distances away from the crater rim (Oberbeck, 1975; Melosh, 1989; Osinski et al., 2011) (Fig. 1.8). Material ejected at higher velocities can form secondary craters, upon impact, which excavates and incorporates local target material (secondary ejecta) into the ejecta blanket (e.g., Oberbeck, 1975; Hörz et al., 1983; Melosh, 1989; Osinski et al., 2013). Incorporation of local material also allows ejecta to move across the surface (e.g., Hörz et al., 1983; Osinski et al., 2013). Studies of impact craters on Earth, such as the Ries impact structure in western Germany, support this theory and provide evidence that a substantial amount of local target material can become incorporated into an ejecta layer (~ 69 vol. % average of local target is included in the Bunte Breccia at Ries)

(Oberbeck, 1975; Hörz et al., 1983; Melosh, 1989; Osinski et al., 2013). A typical topographic profile of radial ejecta morphologies usually show thicker deposits near the rim that rapidly thin outwards (e.g., McGetchin et al., 1973; Melosh, 1989).

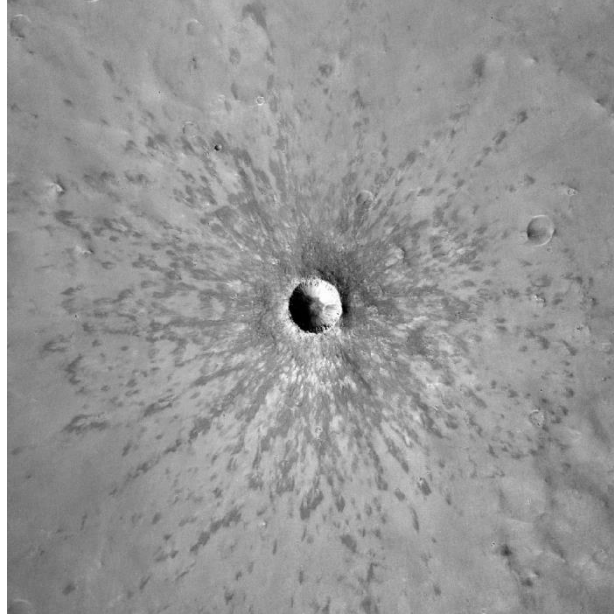


Figure 1.7: Winslow crater (1.1 km diameter) on Mars (59.16° E, 3.74° S) displaying a radial ejecta morphology (CTX image ID: P08_004313_1780_XI_02S301W).

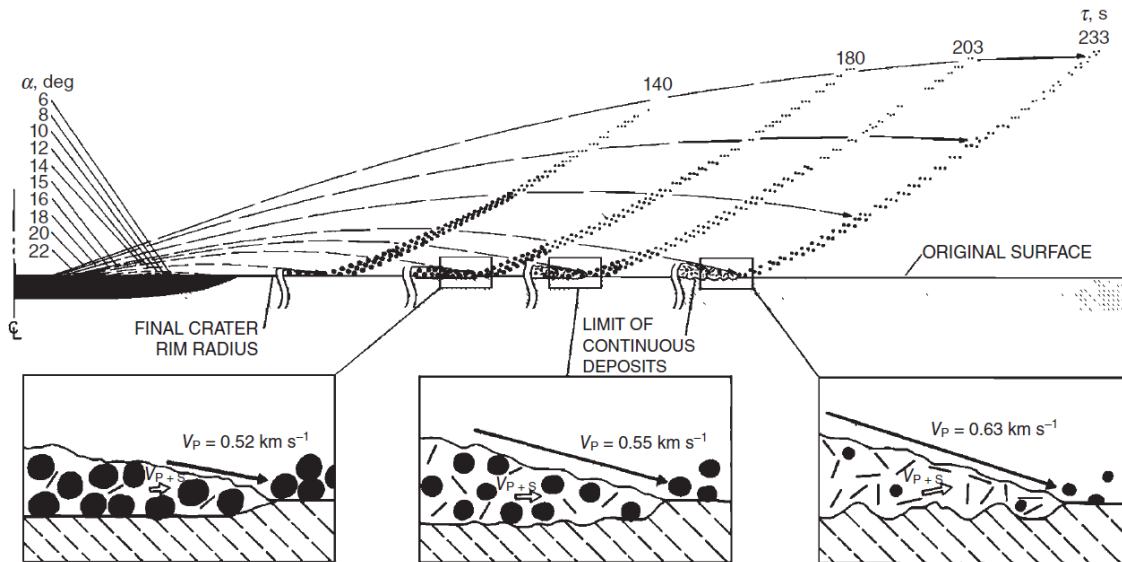


Figure 1.8: Ballistic sedimentation model (after Oberbeck, 1975). Material ejected out of the transient cavity follow ballistic trajectories where the innermost ejecta is ejected first (at the steepest angles and highest velocities) and material closest to the rim is ejected later (at lower angles and velocities). The largest particles fall closer to the rim while smaller particles travel further. Airborne (primary) ejecta re-impacts the target and incorporates local material (secondary ejecta) into the developing ejecta blanket which then moves as a ground-hugging flow behind the primary ejecta curtain. The interaction of airborne (primary) ejecta (black circles) with the surface (dashed lines) are depicted in the three lower boxes.

1.6.2 Layered Ejecta Morphologies

In addition to radial ejecta morphologies, Mars has a distinctly different type of ejecta morphology that is layered in appearance (Fig. 1.9). Ejecta displaying this type of morphology were first recognized from Mariner 9 images and were aptly named “rampart” craters as the distal edge of the ejecta typically terminates as a ridge or rampart (McCauley, 1973). They have since been termed “layered ejecta” craters (Barlow et al., 2000). These types of ejecta morphologies are interpreted to have been fluidized during the emplacement process and travel away from the crater rim as a ground hugging flow (Carr et al., 1977; Mouginiis-Mark, 1979, 1981; Baloga et al., 2005; Komatsu et al., 2007). Average travel distances range from ~ 1.5 – 3.3 crater radii from the rim (Barlow,

2006). It is generally accepted that volatile content within the target (Carr et al., 1977; Mouginiis-Mark, 1981, 1987; Wohletz and Sheridant, 1983; Costard, 1989; Barlow and Bradley, 1990; Barlow and Perez, 2003; Barlow, 2005; Osinski, 2006; Boyce and Mouginiis-Mark, 2006; Komatsu et al., 2007; Oberbeck, 2009), atmosphere (Schultz and Gault, 1979; Schultz, 1992; Barnouin-Jha and Schultz, 1998; Barnouin-Jha et al., 1999a, 1999b), or a combination of the two (Barlow, 2005; Komatsu et al., 2007) is largely responsible for the mobilization of ejecta, though emplacement as a granular flow has also been proposed (Barnouin-Jha et al., 2005; Wada and Barnouin-Jha, 2006). Of the 10,651 cataloged Martian craters ≥ 5 km in diameter that display some sort of discernible ejecta blanket (e.g., radial, layered), layered morphologies make up over 90% (Barlow, 1988, 2005, 2007).

1.6.2.1 Layered Ejecta Morphology Types

Several types of layered ejecta morphologies have been recognized on Mars including single- (SLE), double- (DLE), and multi- (MLE) layered ejecta that are characterized by having one continuous layer of ejecta, two layers, or more than two partial or continuous layers of ejecta respectively (Barlow et al., 2000) (Fig. 1.9). SLEs are the most abundant type of the three and account for ~86% of all layered ejecta morphologies on Mars while DLEs (~9%) and MLEs (~5%) only make up a fraction of this population (Barlow, 2005). Although these three morphologies can be found globally, DLEs are heavily concentrated at northern mid-latitudes (Barlow and Perez, 2003). Topographic profiles of DLEs and MLEs typically show the innermost layers as being topographically higher than outermost ones. Some SLE, DLE, and MLE morphologies include a very thin (~10 m thick) extensive (at least 6 crater radii) additional layer and have recently been recognized as low-aspect ratio layered ejecta (LARLE) craters (Barlow et al., 2014; Boyce et al., 2015b) (Fig. 1.10). These craters displaying a LARLE morphology are interpreted to be relatively fresh and are emplaced as a base surge resulting from impact into ice-rich, fine grained deposits (Barlow et al., 2014; Boyce et al., 2015b). Distributions are predominantly at mid- to high-latitudes though some are found near the equator (Barlow et al., 2014). Pedestal craters are also recognized on Mars and are characterized by being plateaued above the surrounding terrain (McCauley, 1973; Barlow

et al., 2000; Kadish et al., 2009) (Fig. 1.10). These craters share many similarities with LARLE craters (e.g., size, distribution, morphology) and have recently been suggested to be eroded versions of their counterparts (Barlow et al., 2014; Boyce et al., 2015b). It is believed that the emplacement process of the LARLE layer armors the ground surrounding the crater, leaving it more resistant to erosion (Kadish et al., 2009; Barlow et al., 2014). The evolution of a pedestal crater results from subsequent sublimation and erosion of the less resistant surrounding terrain leaving the crater and armored ejecta “perched” (Kadish et al., 2009).

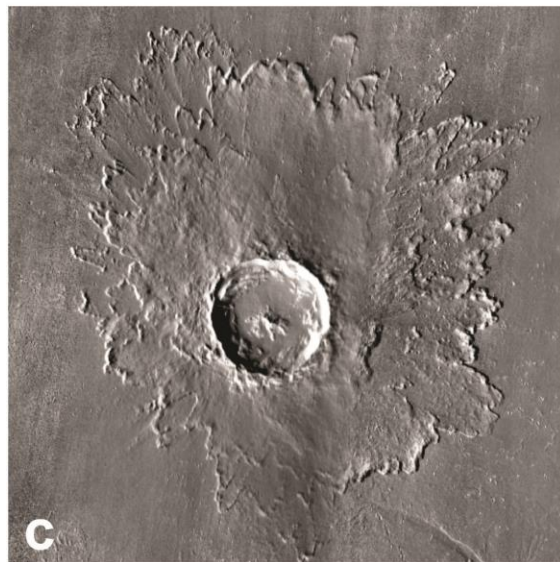
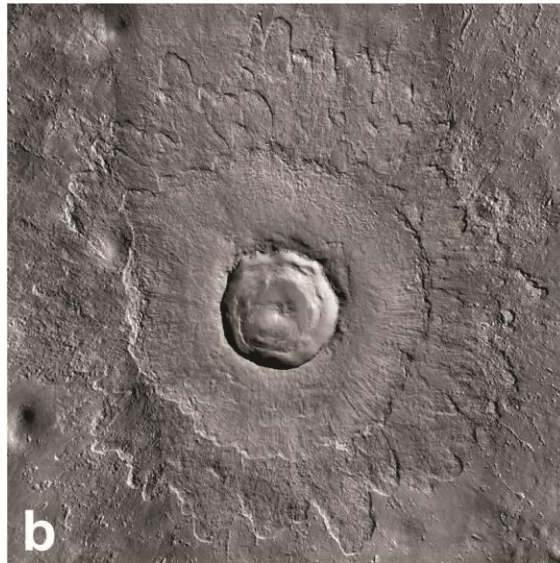
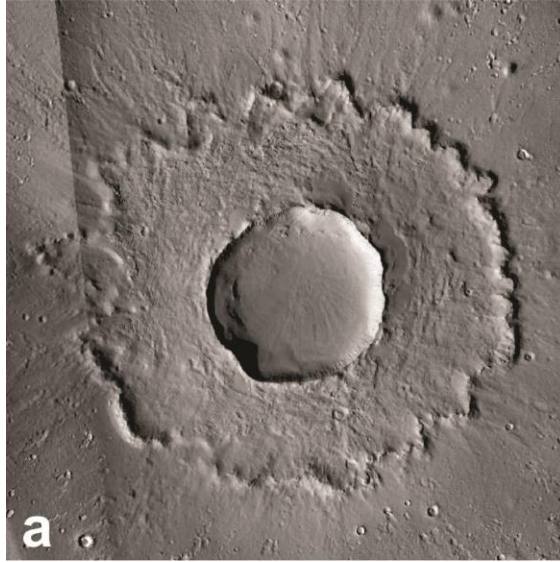


Figure 1.9: The 3 common types of layered ejecta morphologies: (a) 12 km diameter single layered ejecta (SLE) crater located 80.47° E, 36.02° N (CTX mosaic: B05_011564_2163_XN_36N279W; P18_008083_2177_XN_37N280W); (b) Steinheim Crater, an 11 km diameter double layered ejecta (DLE) crater located 190.65° E, 54.57° N (CTX mosaic: G21_026302_2344_XN_54N169W; G02_018944_2348_XI_54N168W; P15_006945_2349_XN_54N169W; P17_007736_2349_XI_54N169W); (c) Tooting Crater, a 28 km diameter multiple layered ejecta (MLE) crater located 207.76° E, 23.21° N (THEMIS day IR 100m global mosaic).

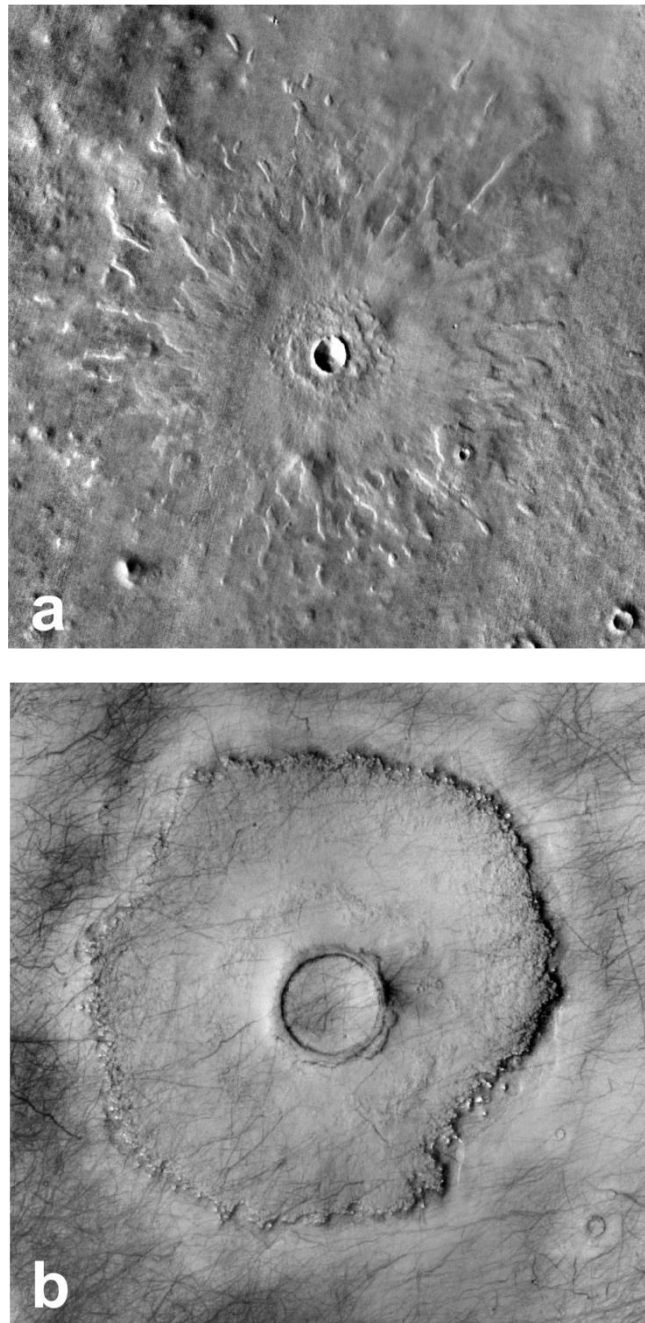


Figure 1.10: Example of a LARLE (a) and pedestal (b) crater on Mars. (a) 5 km diameter crater located 266.37° E, 68.29° N (THEMIS day IR 100m global mosaic); (b) 3 km diameter crater located 91.78° E, 55.28° N (CTX mosaic: G23_027110_2354_XN_55N268W; G21_026477_2355_XN_55N267W).

1.7 Double Layered Ejecta Emplacement Models

Early emplacement models originated prior to the higher resolution data readily available today and were developed almost exclusively using Viking orbiter data. Carr et al., (1977) is usually credited as the first to propose that the emplacement of layered ejecta is via a ground hugging flow. This model is still widely used as the foundation for the more recent models discussed below.

It is generally acknowledged that the layers of DLE morphologies are emplaced in two (or more) separate stages, where fluidity of the ejected material is thought to vary (Mouginis-Mark 1981; Boyce and Mouginis-Mark 2006; Barlow 1994; Osinski et al. 2011). Several models have been proposed involving the formation process of DLE morphologies, yet an ongoing debate remains for the emplacement chronology of the inner and outer ejecta layers. Based solely on appearance, the inner layer appears superposed on the outer layer. Applying Steno's Law of Superposition, the inner layer would, therefore, be younger than the outer implying emplacement after. However, the outer layer is much thinner, therefore finer-grained, than the inner layer, thus some workers have proposed that it could be draped over the inner layer and still appear below (e.g., Mouginis-Mark, 1981; Boyce and Mouginis-Mark, 2006). Despite this dispute, all agree that the incorporation of volatiles in the ejecta blanket, either derived from the subsurface (Carr et al., 1977; Mouginis-Mark, 1981, 1987; Wohletz and Sheridan, 1983; Costard, 1989; Barlow and Bradley, 1990; Barlow and Perez, 2003; Barlow, 2005; Osinski, 2006; Boyce and Mouginis-Mark, 2006; Komatsu et al., 2007; Oberbeck, 2009), atmosphere (Schultz and Gault, 1979; Schultz, 1992; Barnouin-Jha and Schultz, 1998; Barnouin-Jha et al., 1999a, 1999b), or some combination of the two (Barlow, 2005; Komatsu et al., 2007) allow enhanced mobility of ejecta during emplacement.

1.7.1 Schultz and Gault (1979) and Schultz (1992) Atmospheric Model

This model proposes that atmospheric drag effects are largely responsible for the emplacement of layered ejecta morphologies. In this model, finer particles are winnowed out of the initial ejecta curtain due to atmospheric drag as the larger particles continue on

their ballistic trajectories. Finer particles suspended in this “distorted” curtain eventually fall back down producing a turbulent cloud (or base surge) over the already emplaced ejecta. This density current can remobilize emplaced ejecta as well as deposit finer grained material on top. Vapor explosions produced by melt-water interactions are also suggested to modify the ballistic flow field (Wohletz and Sheridan, 1983).

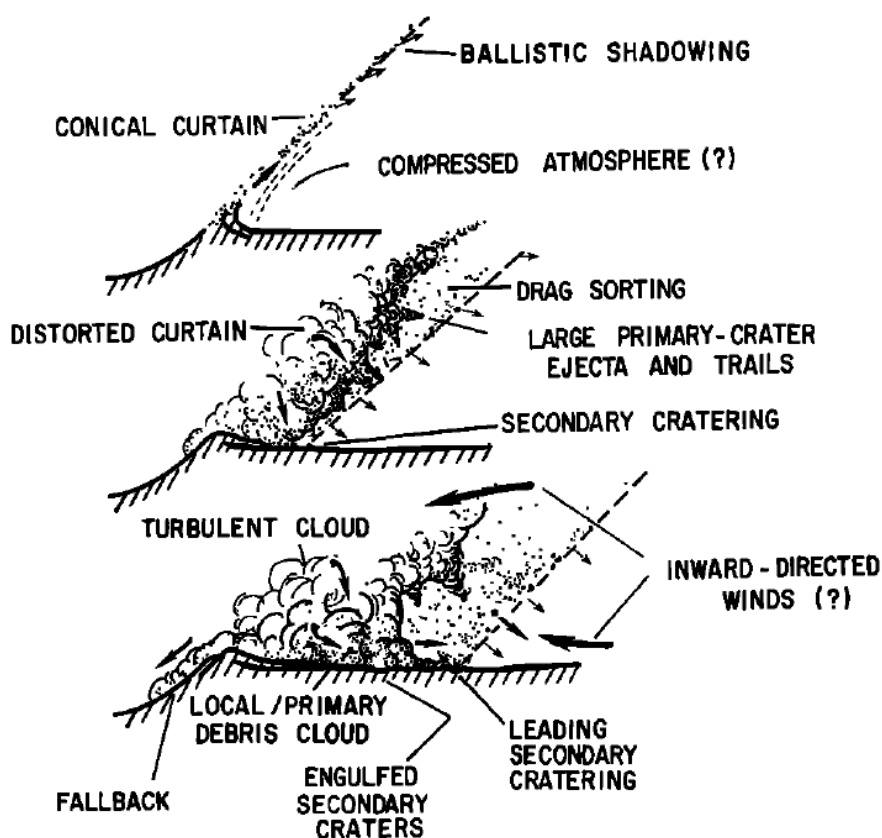


Figure 1.11: Schematic diagram of the atmospheric model. Ejecta is emplaced ballistically in which finer particles are winnowed out of the advancing curtain from atmospheric drag. A vortex ring is produced by atmospheric turbulence which can then remobilize emplaced ejecta and deposit smaller material over initial ejecta.

1.7.2 Mouginis-Mark (1981) and Boyce and Mouginis-Mark (2006) Model

The original model developed by Mouginis-Mark (1981) suggests a two stage emplacement process that results from the change in ejection angle produced by a layered

target of volatile-poor and volatile-rich layers. In this model, impact into a “dry” upper layer throws ejecta out at a lower angle and makes up the inner layer of ejecta. As the transient cavity grows, it excavates into the deeper “wet” layer which initiates an ejecta angle change from wider to more narrow (steeper) and produces a volatile-rich ejecta cloud. The inner layer is already emplaced at this point as the ejecta cloud starts to fall back down to the surface and comprises the material for the outer layer. Because this material is volatile-rich, it is less viscous and flows over and beyond the inner layer. As higher resolution imagery has allowed for the recognition of radial grooves on some DLE craters, Boyce and Mouginiis-Mark (2006) have made slight modifications to this original model proposing that the collapse of an explosion column produces a base surge that etches grooves into the inner layer and deposits the outer layer of ejecta over the inner layer.

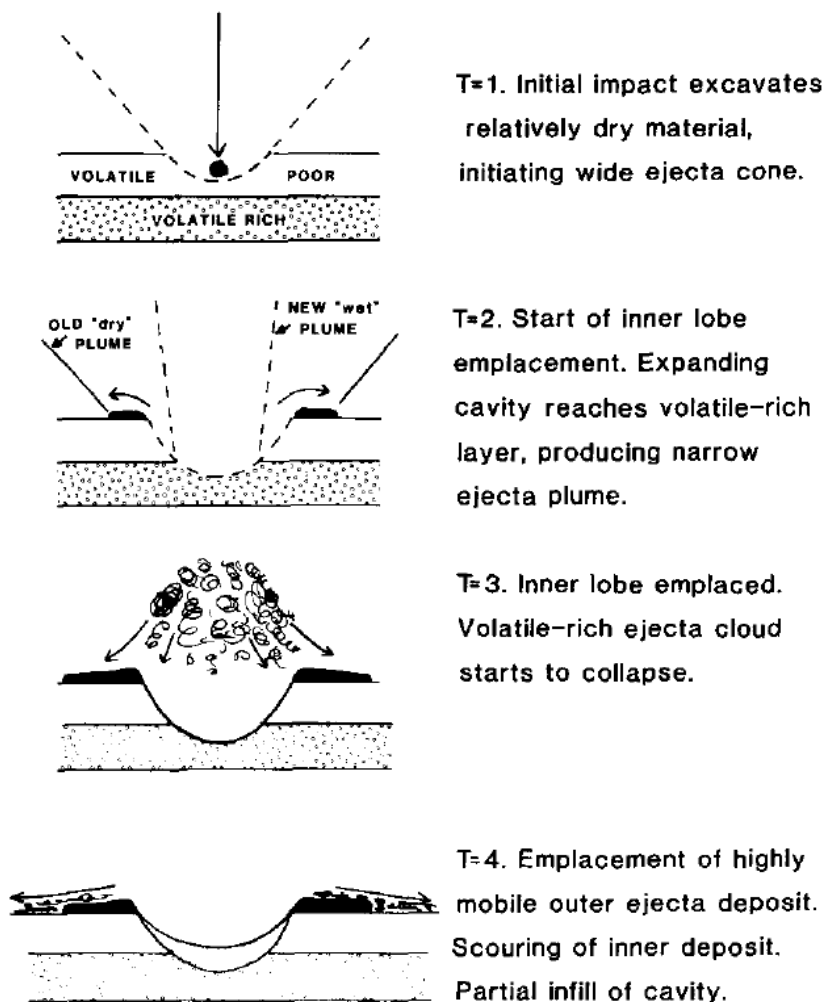


Figure 1.12: Schematic diagram showing the inner layer being emplaced before the outer layer. Outer layer is emplaced as a base surge-like process, flowing over and beyond the inner layer and etching grooves into the inner layer.

1.7.3 Komatsu et al. (2007) Model

This model suggests some combination of near-surface and atmospheric volatiles are responsible for layered morphologies. They propose an impact into a water-rich near-surface layer causes liquefaction of the surrounding terrain by the expanding shock wave. Liquefaction forms the extent of a non-conventionally emplaced outer layer. Ballistically emplaced ejecta comprises the inner layer, is water-rich, and, therefore, moved as a ground-hugging flow outward initiated by gravity and the uplifted rim. A vortex, or base

surge, assists mobility of the inner layer and contains fine-particles winnowed from the initial ejecta curtain. This material scours grooves into both ejecta layers and deposits the remainder of the outer layer. In this model, the outer layer can contain material prior to, and after the emplacement of the inner layer.

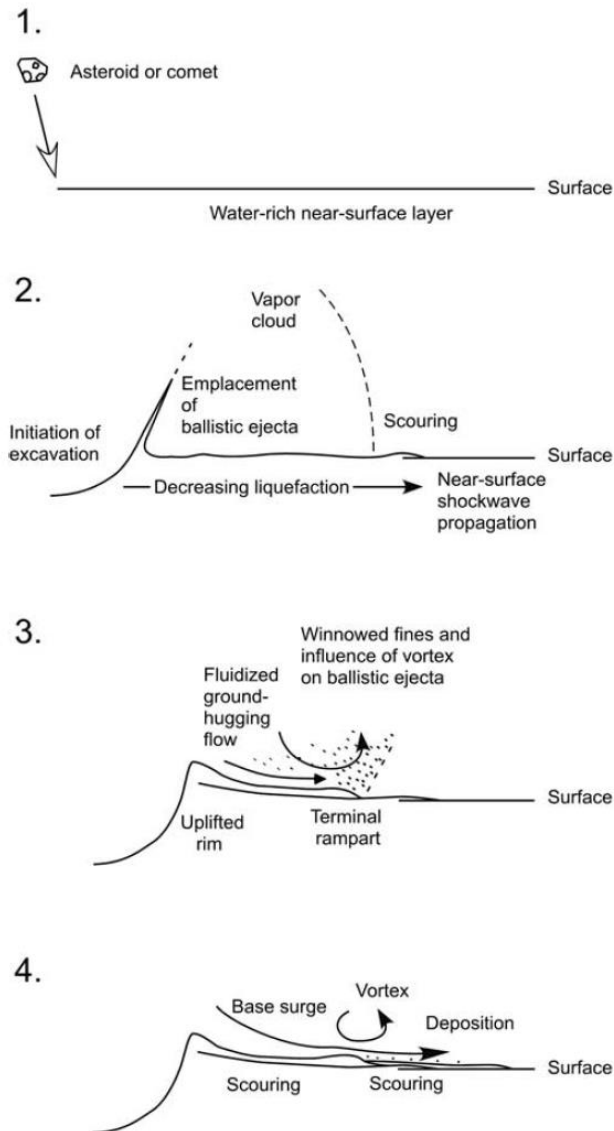
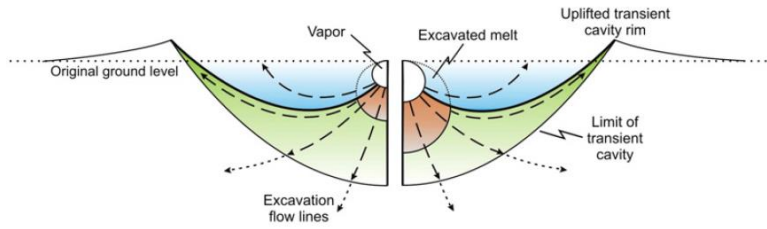


Figure 1.13: Schematic diagram showing the interaction of near-surface and atmospheric volatiles to produce a layered ejecta morphology.

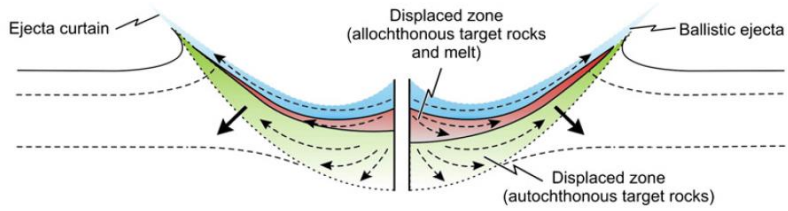
1.7.4 Osinski et al. (2011) Model

This model suggests a two stage emplacement process where the outer layer is emplaced first via ballistic sedimentation and radial flow. Melt-rich material lining the transient cavity is subsequently uplifted during modification, generating an outward momentum which allows a portion of the melt to flow up and over the crater rim and emplace a second layer of ejecta (i.e., inner layer). The first layer emplaced contains material from the uppermost target (excavated zone), while the second layer is derived from deeper material (displaced zone) that has been highly shocked, and because, it is predominately melt-rich. Volatile content will also increase the melt produced if present at depth, allowing the inner layer to become more fluidized as well.

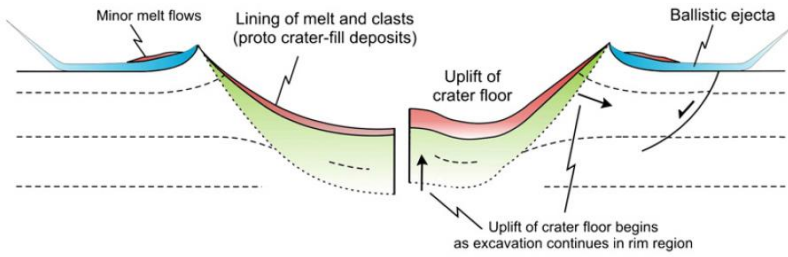
SUMMARY: EXCAVATION AND DISPLACED ZONES:



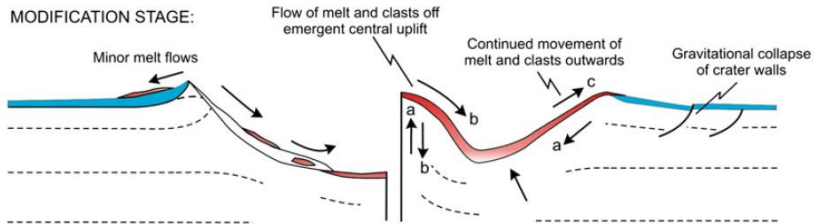
DURING EXCAVATION:



END EXCAVATION STAGE/
START MODIFICATION STAGE:



MODIFICATION STAGE:



- Excavated Zone
- Displaced Zone (allochthonous target rocks)
- Displaced Zone (clasts of allochthonous target rocks and melt)

END OF MODIFICATION STAGE:

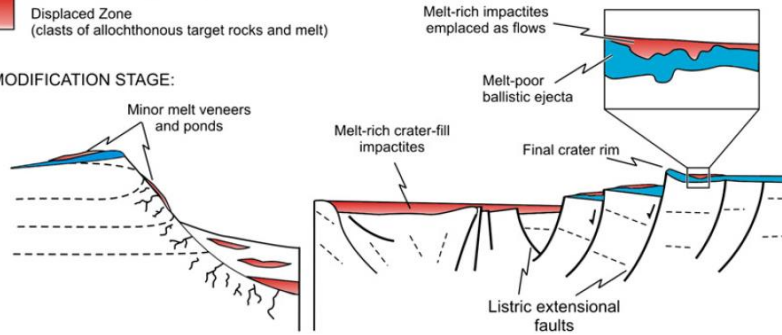


Figure 1.14: Schematic diagram showing emplacement of the outer layer first via ballistic sedimentation and radial flow. The inner layer is emplaced after as melt-rich material (within transient cavity) that flows out and over crater rim via uplift during the crater modification stage.

1.7.5 Weiss and Head (2013) Glacial Substrate Model

This model requires an upper glacial substrate layer be present in order to form a DLE morphology, where the impact penetrates through the icy layer down into an underlying regolith layer. The outer layer of ejecta is emplaced as the crater rim is structurally uplifted. Ejecta proximal to the rim is lubricated by the underlying glacial substrate and is emplaced via landslide mode over the initial ejecta as the inner layer.

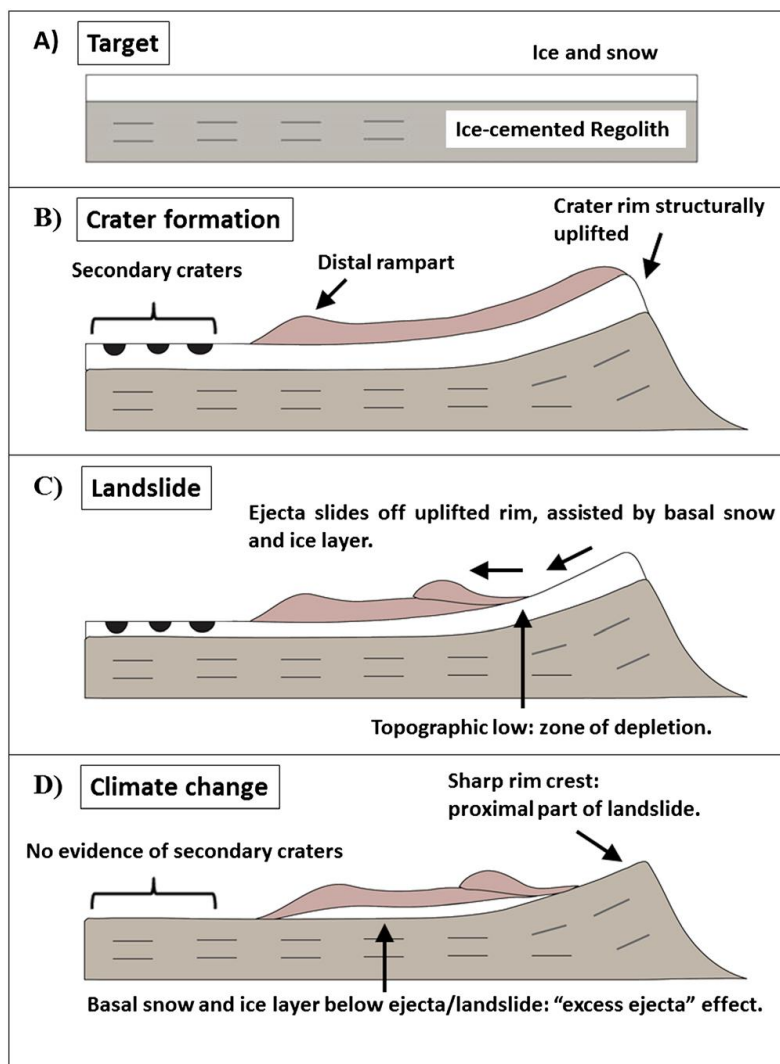


Figure 1.15: Schematic diagram of the glacial substrate model. The outer layer is emplaced ballistically while the inner layer is emplaced via landslide mode off of the uplifted crater rim. Impact into a glacial substrate provides ample volatile concentrations to initiate slide mechanism of the inner layer.

1.7.6 Wulf and Kenkmann (2015) Model

This model is similar to the glacial substrate model described above minus the requirement of an icy surface layer. In this model, impact into volatile-rich target results in high ejection angles, which leads to the formation of a steep ejecta curtain. Distal ejecta have higher initial velocities and a greater component of volatiles that initiates movement as a debris flow. Proximal ejecta, in comparison, is “dryer” and accumulates

near the transient cavity rim because of low ejection velocities. As the loading pressure builds on proximal ejecta, basal frictional heating melts the ice component of ejecta and promotes a transitional slide mode of the inner layer on top of the outer layer.

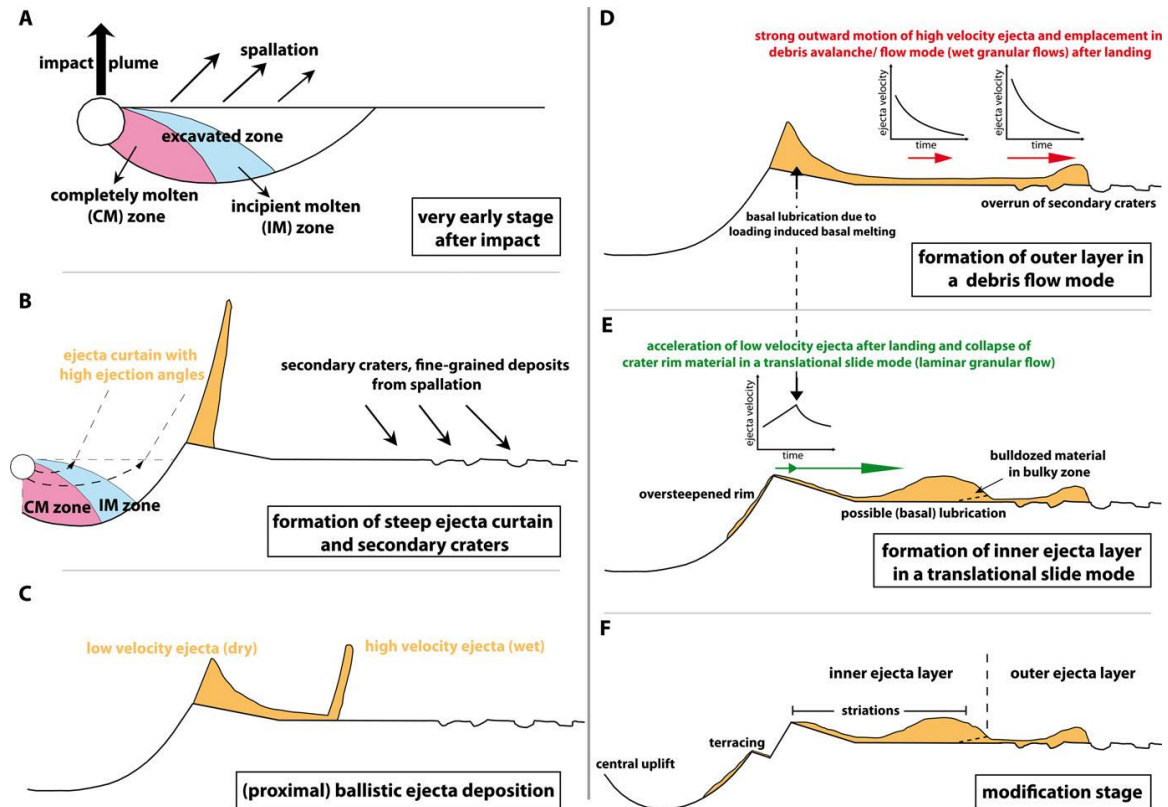


Figure 1.16: Schematic diagram showing the outer layer being emplaced first as a debris flow mode and the inner layer being emplaced as a translational slide model.

1.8 References

- Acuna, M.H., Connerney, J.E.P., Ness, N.F., Lin, R.P., Mitchell, D., Carlson, C.W., McFadden, J., Anderson, K.A., Reme, H., Mazelle, C., Vignes, D., Wasilewski, P., Cloutier, P., 1999. Global Distribution of Crustal Magnetization Discovered by the Mars Global Surveyor MAG/ER Experiment. *Science* (80-.). 284, 790–793. doi:10.1126/science.284.5415.790.
- Baloga, S.M., Fagents, S.A., Mouginis-Mark, P.J., 2005. Emplacement of Martian rampart crater deposits. *J. Geophys. Res.* 110. doi:10.1029/2004JE002338.

- Bandfield, J.L., Hamilton, V.E., Christensen, P.R., 2000. A global view of martian surface compositions from MGS-TES. *Science* (80-.). 287, 1626 – 1630.
- Barlow, N.G., 1988. Crater size-frequency distributions and a revised Martian relative chronology. *Icarus* 75, 285–305. doi:10.1016/0019-1035(88)90006-1.
- Barlow, N.G., 2005. A review of Martian impact crater ejecta structures and their implications for target properties, in: Kenkmann, T., Hörz, F., Deutsch, A. (Eds.), *Large Meteorite Impacts III*, Geol. Soc. Am. Spec. Pap. 384. pp. 433 – 442.
- Barlow, N.G., 2006. Impact craters in the northern hemisphere of Mars: Layered ejecta and central pit characteristics. *Meteorit. Planet. Sci.* 41, 1425–1436. doi:10.1111/j.1945-5100.2006.tb00427.x.
- Barlow, N.G., 2007. New insights into impact crater morphologies from the revised Catalog of Large Martian Impact Craters. *Seventh Int. Conf. Mars Abstract #3347*.
- Barlow, N.G., Bradley, T.L., 1990. Martian impact craters: Correlations of ejecta and interior morphologies with diameter, latitude, and terrain. *Icarus* 87, 156–179.
- Barlow, N.G., Perez, C.B., 2003. Martian impact crater ejecta morphologies as indicators of the distribution of subsurface volatiles. *J. Geophys. Res.* 108, 5085. doi:10.1029/2002JE002036.
- Barlow, N.G., Boyce, J.M., Costard, F.M., Craddock, R.A., Garvin, J.B., Sakimoto, S.E.H., Kuzmin, R.O., Roddy, D.J., Soderblom, L.A., 2000. Standardizing the nomenclature of Martian impact crater ejecta morphologies. *J. Geophys. Res.* 105, 26733 – 26738.
- Barlow, N.G., Boyce, J.M., Cornwall, C., 2014. Martian Low-Aspect-Ratio Layered Ejecta (LARLE) craters: Distribution, characteristics, and relationship to pedestal craters. *Icarus* 239, 186–200. doi:10.1016/j.icarus.2014.05.037.
- Barnouin-Jha, O.S., Schultz, P.H., 1998. Lobateness of impact ejecta deposits from atmospheric interactions. *J. Geophys. Res.* 103, 25739 – 25756.

- Barnouin-Jha, O.S., Schultz, P.H., Lever, J.H., 1999a. Investigating the interactions between an atmosphere and an ejecta curtain 1. Wind tunnel tests. *J. Geophys. Res.* 104, 27105–27115.
- Barnouin-Jha, O.S., Schultz, P.H., Lever, J.H., 1999b. Investigating the interactions between an atmosphere and an ejecta curtain 2. Numerical experiments. *J. Geophys. Res.* 104, 27117–27131.
- Barnouin-Jha, O.S., Baloga, S., Glaze, L., 2005. Comparing landslides to fluidized crater ejecta on Mars. *J. Geophys. Res.* 110. doi:10.1029/2003JE002214.
- Bibring, J.-P., Langevin, Y., Mustard, J.F., Poulet, F., Arvidson, R., Gendrin, A., Gondet, B., Mangold, N., Pinet, P., Forget, F., Team, the O., 2006. Global mineralogical and aqueous Mars history derived from OMEGA/Mars Express data. *Science* (80-.). 312, 400–404. doi:10.1126/science.1122659.
- Boyce, J.M., Mouginiis-Mark, P.J., 2006. Martian craters viewed by the Thermal Emission Imaging System instrument: Double-layered ejecta craters. *J. Geophys. Res.* 111. doi:10.1029/2005JE002638.
- Boyce, J.M., Wilson, L., Barlow, N.G., 2015. Origin of the outer layer of martian low-aspect ratio layered ejecta craters. *Icarus* 245, 263–272. doi:10.1016/j.icarus.2014.07.032.
- Buchner, E., Schwarz, W.H., Schmieder, M., Tieloff, M., 2010. Establishing a 14.6 ± 0.2 Ma age for the Nördlinger Ries impact (Germany) – A prime example for concordant isotopic ages from various dating materials. *Meteorit. Planet. Sci.* 45, 662–674. doi:10.1111/j.1945-5100.2010.01046.x.
- Carr, M.H., 1979. Formation of Martian flood features by release of water from confined aquifers. *J. Geophys. Res.* 84, 2995–3007. doi:10.1029/JB084iB06p02995.
- Carr, M.H., 2006. *The Surface of Mars*. Cambridge University Press, 307 p.

- Carr, M.H., Head, J.W., 2010. Geologic history of Mars. *Earth Planet. Sci. Lett.* 294, 185–203. doi:10.1016/j.epsl.2009.06.042.
- Carr, M.H., Crumpler, L.S., Cutts, J.A., Greeley, R., Guest, J.E., Masursky, H., 1977. Martian impact craters and emplacement of ejecta by surface flow. *J. Geophys. Res.* 82, 4055–4065. doi:10.1029/JS082i028p04055.
- Clifford, S.M., 1993. A model for the hydrologic and climatic behavior of water on Mars. *J. Geophys. Res.* 98, 10973–11016. doi:10.1029/93JE00225.
- Clifford, S.M., Hillel, D., 1983. The stability of ground ice in the equatorial region of Mars. *J. Geophys. Res.* 88, 2456–2474. doi:10.1029/JB088iB03p02456.
- Clifford, S.M., Parker, T.J., 2001. The evolution of the Martian hydrosphere: Implications for the fate of a primordial ocean and the current state of the northern plains. *Icarus* 154, 40–79. doi:10.1006/icar.2001.6671.
- Clifford, S.M., Lasue, J., Heggy, E., Boisson, J., McGovern, P., Max, M.D., 2010. Depth of the Martian cryosphere: Revised estimates and implications for the existence and detection of subpermafrost groundwater. *J. Geophys. Res.* 115. doi:10.1029/2009JE003462.
- Costard, F.M., 1989. The spatial distribution of volatiles in the Martian hydrolithosphere. *Earth. Moon. Planets* 45, 265–290.
- Costard, F., Forget, F., Mangold, N., Peulvast, J.P., 2002. Formation of recent Martian debris flows by melting of near-surface ground ice at high obliquity. *Science* (80-.). 295, 110–113. doi:10.1126/science.1066698.
- Daubar, I.J., McEwen, A.S., Byrne, S., Kennedy, M.R., Ivanov, B., 2013. The current martian cratering rate. *Icarus* 225, 506–516. doi:10.1016/j.icarus.2013.04.009.
- Fanale, F.P., 1976. Martian volatiles : Their degassing history and geochemical fate. *Icarus* 28, 179–202.

- Fastook, J.L., Head, J.W., Marchant, D.R., Forget, F., 2008. Tropical mountain glaciers on Mars: Altitude-dependence of ice accumulation, accumulation conditions, formation times, glacier dynamics, and implications for planetary spin-axis/orbital history. *Icarus* 198, 305–317. doi:10.1016/j.icarus.2008.08.008.
- Frey, H. V., 2006. Impact constraints on, and a chronology for, major events in early Mars history. *J. Geophys. Res. Planets* 111, E08S91. doi:10.1029/2005JE002449.
- Gault, D.E., Quaide, W.L., Oberbeck, V.R., 1968. Impact cratering mechanics and structures, in: French, B.M., Short, N.M. (Eds.), *Shock Metamorphism of Natural Materials*. Baltimore: Mono Book Corp.
- Gentner, W., Wagner, A.W., 1969. Altersbestimmungen an Riesglfisern und Moldaviten. *Geol. Bavarica* 61, 296–303.
- Ghatan, G.J., Head, J.W., Wilson, L., 2005. Mangala Valles, Mars: Assessment of early stages of flooding and downstream flood evolution. *Earth, Moon Planets* 96, 1–57. doi:10.1007/s11038-005-9009-y.
- Golombek, M.P., Bridges, N.T., 2000. Erosion rates on Mars and implications for climate change: Constraints from the Pathfinder landing site. *J. Geophys. Res.* 105, 1841–1853.
- Golombek, M.P., Grant, J.A., Crumpler, L.S., Greeley, R., Arvidson, R.E., Bell, J.F., Weitz, C.M., Sullivan, R., Christensen, P.R., Soderblom, L.A., Squyres, S.W., 2006. Erosion rates at the Mars Exploration Rover landing sites and long-term climate change on Mars. *J. Geophys. Res.* 111. doi:10.1029/2006JE002754.
- Gomes, R., Levison, H.F., Tsiganis, K., Morbidelli, A., 2005. Origin of the cataclysmic Late Heavy Bombardment period of the terrestrial planets. *Nature* 435, 466–469. doi:10.1038/nature03676.
- Greeley, R., Guest, J.E., 1987. Geologic map of the eastern equatorial region of Mars (1:15,000,000). USGS Misc. Inv. Ser. Map I-1802-B.

- Halevy, I., Zuber, M.T., Schrag, D.P., 2007. A sulfur dioxide climate feedback on early Mars. *Science* (80-.). 318, 1903–1907.
- Head, J.W., Marchant, D.R., 2003. Cold-based mountain glaciers on Mars : Western Arsia Mons. *Geology* 31, 641–644.
- Head, J.W., Marchant, D.R., 2006. Evidence for global-scale northern mid-latitude glaciation in the Amazonian period of Mars: Debris-covered glacier and valley glacier deposits in the 30 - 50 N latitude band. *Lunar Planet. Sci. Conf. XXXVII*. doi:10.1029/2004.
- Head, J.W., Kreslavsky, M.A., Pratt, S., 2002. Northern lowlands of Mars: Evidence for widespread volcanic flooding and tectonic deformation in the Hesperian Period. *J. Geophys. Res.* 107, 5003.
- Head, J.W., Neukum, G., Jaumann, R., Hiesinger, H., Hauber, E., Carr, M.H., Masson, P., Foing, B., Hoffmann, H., Kreslavsky, M., Werner, S., Milkovich, S., van Gasselt, S., 2005. Tropical to mid-latitude snow and ice accumulation, flow and glaciation on Mars. *Nature* 434, 346–351.
- Head, J.W., Marchant, D.R., Agnew, M.C., Fassett, C.I., Kreslavsky, M.A., 2006. Extensive valley glacier deposits in the northern mid-latitudes of Mars: Evidence for Late Amazonian obliquity-driven climate change. *Earth Planet. Sci. Lett.* 241, 663–671. doi:10.1016/j.epsl.2005.11.016.
- Head, J.W., Marchant, D.R., Dickson, J.L., Kress, A.M., Baker, D.M., 2010. Northern mid-latitude glaciation in the Late Amazonian period of Mars: Criteria for the recognition of debris-covered glacier and valley glacier landsystem deposits. *Earth Planet. Sci. Lett.* 294, 306–320. doi:10.1016/j.epsl.2009.06.041.
- Hörz, F., Ostertag, R., Rainey, D.A., 1983. Bunte Breccia of the Ries: Continuous deposits of large impact craters. *Rev. Geophys. Sp. Phys.* 21, 1667–1725.

- Kadish, S.J., Barlow, N.G., Head, J.W., 2009. Latitude dependence of Martian pedestal craters: Evidence for a sublimation-driven formation mechanism. *J. Geophys. Res. Planets* 114, E10001. doi:10.1029/2008JE003318.
- Kieffer, H.H., Martin, T.Z., Peterfreund, A.R., Jakosky, B.M., Miner, E.D., Palluconi, F.D., 1977. Thermal and albedo mapping of Mars during the Viking primary mission. *J. Geophys. Res.* 82, 4249–4291. doi:10.1029/JS082i028p04249.
- Komatsu, G., Ori, G.G., Di Lorenzo, S., Rossi, A.P., Neukum, G., 2007. Combinations of processes responsible for Martian impact crater “layered ejecta structures” emplacement. *J. Geophys. Res.* 112. doi:10.1029/2006JE002787.
- Kreslavsky, M.A., Head, J.W., 2002. Fate of outflow channel effluents in the northern lowlands of Mars: The Vastitas Borealis Formation as a sublimation residue from frozen ponded bodies of water. *J. Geophys. Res.* 107, 5121. doi:10.1029/2001JE001831
- Laskar, J., Correia, A.C.M., Gastineau, M., Joutel, F., Levrard, B., Robutel, P., 2004. Long term evolution and chaotic diffusion of the insolation quantities of Mars. *Icarus* 170, 343–364. doi:10.1016/j.icarus.2004.04.005.
- Madeleine, J.-B., Forget, F., Head, J.W., Levrard, B., Montmessin, F., Millour, E., 2009. Amazonian northern mid-latitude glaciation on Mars: A proposed climate scenario. *Icarus* 203, 390–405. doi:10.1016/j.icarus.2009.04.037.
- Malin, M.C., Edgett, K.S., Posiolova, L. V., McColley, S.M., Dobrea, E.Z.N., 2006. Present-day impact cratering rate and contemporary gully activity on Mars. *Science* (80-.). 314, 1573–1577.
- Marinova, M.M., Aharonson, O., Asphaug, E., 2008. Mega-impact formation of the Mars hemispheric dichotomy. *Nature* 453, 1216–1219. doi:10.1038/nature07070.
- McCauley, J.F., 1973. Mariner 9 evidence for wind erosion in the equatorial and mid-latitude regions of Mars. *J. Geophys. Res.* 78, 4123–4137. doi:10.1029/JB078i020p04123.

- McGetchin, T.R., Settle, M., Head, J.W., 1973. Radial thickness variation in impact crater ejecta: Implications for Lunar basin deposits. *Earth Planet. Sci. Lett.* 20, 226–236.
- Melosh, H.J., 1989. *Impact Cratering: A Geologic Process*. Oxford University Press, 245 p.
- Michel, P., Morbidelli, A., 2013. Population of impactors and the impact cratering rate in the inner Solar System, in: *Impact Cratering: Processes and Products*. pp. 21–31. doi:10.1002/9781118447307.ch2.
- Mouginis-Mark, P.J., 1979. Martian fluidized crater morphology: Variations with crater size, latitude, altitude, and target material. *J. Geophys. Res.* 84, 8011 – 8022. doi:10.1029/JB084iB14p08011.
- Mouginis-Mark, P.J., 1981. Ejecta emplacement and modes of formation of Martian fluidized ejecta craters. *Icarus* 45, 60–76. doi:10.1016/0019-1035(81)90006-3.
- Mouginis-Mark, P.J., 1987. Water or ice in the Martian regolith?: Clues from rampart craters seen at very high resolution. *Icarus* 71, 268–286. doi:10.1016/0019-1035(87)90152-7.
- Neumann, G.A., Zuber, M.T., Wieczorek, M.A., McGovern, P.J., Lemoine, F.G., Smith, D.E., 2004. Crustal structure of Mars from gravity and topography. *J. Geophys. Res.* 109, E08002. doi:10.1029/2004JE002262.
- Oberbeck, V.R., 1975. The role of ballistic erosion and sedimentation in Lunar stratigraphy. *Rev. Geophys. Sp. Phys.* 13, 337–362.
- Oberbeck, V.R., 2009. Layered ejecta craters and the early water/ice aquifer on Mars. *Meteorit. Planet. Sci.* 44, 43–54. doi:10.1111/j.1945-5100.2009.tb00716.x.
- Osinski, G.R., 2004. Hypervelocity impact into sedimentary targets: Processes and products (PhD Thesis). University of New Brunswick.

- Osinski, G.R., 2006. Effect of volatiles and target lithology on the generation and emplacement of impact crater fill and ejecta deposits on Mars. *Meteorit. Planet. Sci.* 41, 1571–1586. doi:10.1111/j.1945-5100.2006.tb00436.x.
- Osinski, G.R., Tornabene, L.L., Grieve, R.A.F., 2011. Impact ejecta emplacement on terrestrial planets. *Earth Planet. Sci. Lett.* 310, 167–181. doi:10.1016/j.epsl.2011.08.012.
- Osinski, G.R., Grieve, R.A.F., Tornabene, L.L., 2013. Excavation and impact ejecta emplacement, in: Osinski, G.R., Pierazzo, E. (Eds.), *Impact Cratering: Processes and Products*. pp. 43–59.
- Pierazzo, E., Melosh, H.J., 2000. Understanding oblique impacts from experiments, observations, and modeling. *Annu. Rev. Earth Planet. Sci.* 28, 141–167.
- Pike, R.J., 1980. Control of crater morphology by gravity and target type: Mars, Earth, Moon. *Proc. Lunar Planet. Sci. Conf.* 11, 2159–2189.
- Rossbacher, L.A., Judson, S., 1981. Ground ice on Mars: Inventory, distribution, and resulting landforms. *Icarus* 45, 39–59. doi:10.1016/0019-1035(81)90005-1.
- Schultz, P.H., 1992. Atmospheric effects on ejecta emplacement. *J. Geophys. Res.* 97, 11623–11662. doi:10.1029/92JE00613.
- Schultz, P.H., Gault, D.E., 1979. Atmospheric effects on martian ejecta emplacement. *J. Geophys. Res.* 84, 7669–7687.
- Scott, D.H., Carr, M.H., 1978. Geologic map of Mars. U. S. Geol. Surv. Misc. Inv. Map I-1083.
- Scott, D.H., Tanaka, K.L., 1986. Geologic map of the western equatorial region of Mars (1:15,000,000). USGS Misc. Inv. Ser. Map I-1802-A.
- Segura, T.L., Toon, O.B., Colaprete, A., Zahnle, K., 2002. Environmental effects of large impacts on Mars. *Science* (80-.). 298, 1977–1980. doi:10.1126/science.1073586.

- Shean, D.E., Head, J.W., Marchant, D.R., 2005. Origin and evolution of a cold-based tropical mountain glacier on Mars: The Pavonis Mons fan-shaped deposit. *J. Geophys. Res.* 110, E05001. doi:10.1029/2004JE002360.
- Skinner, J.A., Hare, T.M., Tanaka, K.L., 2006. Digital renovation of the atlas of Mars 1:15,000,000-scale global geologic series maps. *Lunar Planet. Sci.* XXXVII Abstract #2331.
- Souness, C., Hubbard, B., 2012. Mid-latitude glaciation on Mars. *Prog. Phys. Geogr.* 36, 238–261. doi:10.1177/0309133312436570.
- Stevenson, D.J., 2001. Mars' core and magnetism. *Nature* 412, 214–219. doi:10.1038/35084155.
- Tanaka, K.L., 1986. The stratigraphy of Mars. *J. Geophys. Res.* 91, E139–E158. doi:10.1029/JB091iB13p0E139.
- Tsiganis, K., Gomes, R., Morbidelli, A., Levison, H.F., 2005. Origin of the orbital architecture of the giant planets of the Solar System. *Nature* 435, 459–461. doi:10.1038/nature03539.
- Wada, K., Barnouin-Jha, O.S., 2006. The formation of fluidized ejecta on Mars by granular flows. *Meteorit. Planet. Sci.* 41, 1551–1569. doi:10.1111/j.1945-5100.2006.tb00435.x.
- Werner, S.C., 2009. The global martian volcanic evolutionary history. *Icarus* 201, 44–68. doi:10.1016/j.icarus.2008.12.019.
- Williams, K.E., Toon, O.B., Heldmann, J.L., Mellon, M.T., 2009. Ancient melting of mid-latitude snowpacks on Mars as a water source for gullies. *Icarus* 200, 418–425. doi:10.1016/j.icarus.2008.12.013.
- Wilson, L., Head, J.W., 2004. Evidence for a massive phreatomagmatic eruption in the initial stages of formation of the Mangala Valles outflow channel, Mars. *Geophys. Res. Lett.* 31, L15701. doi:10.1029/2004GL020322.

- Wise, D.U., Golombek, M.P., McGill, G.E., 1979. Tectonic evolution of Mars. *J. Geophys. Res.* 84, 7934–7939.
- Wohletz, K.H., Sheridant, M.F., 1983. Martian Rampart Crater Ejecta: Experiments and Analysis of Melt-Water Interaction. *Icarus* 37, 15–37.
- Wyatt, M.B., Mcsween, H.Y., Tanaka, K.L., Head, J.W., 2004. Global geologic context for rock types and surface alteration on Mars. *Geology* 32, 263–266.

Chapter 2

2 A Comparative Morphologic and Morphometric Study of Double Layered Ejecta Craters in Volcanic Terrains on Mars

2.1 Introduction

The majority of Martian impact craters with observable ejecta have continuous ejecta blankets that have been referred to as “layered”, “fluidized”, “lobed”, or “rampart” ejecta craters (Barlow, 1988; Barlow and Bradley, 1990; Barlow et al., 2000). These morphologies differ from the ballistically emplaced “radial” ejecta observed on airless, volatile-poor bodies like the Moon and Mercury in that they are distinctively layered in appearance and appear to have been more mobile during emplacement. Ejecta interacting with volatiles within the target (Carr et al., 1977; Gault and Greeley, 1978; Mougini-Mark, 1981, 1987; Wohletz and Sheridan, 1983; Costard, 1989; Barlow and Bradley, 1990; Barlow and Perez, 2003; Barlow, 2005; Osinski, 2006; Boyce and Mougini-Mark, 2006; Komatsu et al., 2007; Oberbeck, 2009), atmosphere (Schultz and Gault, 1979; Schultz, 1992; Barnouin-Jha and Schultz, 1998; Barnouin-Jha et al., 1999a, 1999b), or a combination of both (Barlow, 2005; Komatsu et al., 2007) is generally recognized as a major variable aiding mobility during emplacement, though emplacement as a dry granular flow has also been proposed (Barnouin-Jha et al., 2005; Wada and Barnouin-Jha, 2006). Because layered ejecta craters have been observed on other airless bodies (e.g., Ganymede and Europa), it has been suggested that an atmosphere is not required to form these types of morphologies (e.g., Horner and Greeley 1982; Boyce et al. 2010). Therefore, volatile content within, or on, the target is thought to be the major factor in the emplacement of layered ejecta (Carr et al., 1977; Gault and Greeley, 1978; Wohletz and Sheridan, 1983; Mougini-Mark, 1987; Barlow and Perez, 2003; Komatsu et al., 2007). If indeed layered ejecta formation is mainly dependent on volatile content, then the extent an ejecta blanket travels (i.e., ejecta mobility) should be a function of volatile concentration. Preexisting topography is also suggested to affect ejecta mobility (Carr et al., 1977; Wohletz and Sheridan, 1983; Baloga et al., 2005; Komatsu et al., 2007;

Osinski et al., 2011; Jones and Osinski, 2015), but to what extent remains largely unconstrained.

Three major types of layered ejecta morphologies are recognized on Mars: single- (SLE), double- (DLE), and multiple- (MLE) layered ejecta (see Barlow et al., 2000). The current definition for “layered ejecta”, as defined by Barlow et al. (2000), is “an ejecta blanket that is composed of one or more complete layers of material surrounding the crater, which also appears to have been emplaced by fluidization processes”. This includes so-called “pedestal” craters that are interpreted to have undergone substantial erosion to where the layered ejecta becomes elevated, or perched, above the surrounding terrain. In addition to the definition above, most “well-preserved” layered ejecta craters have a distal ridge, or rampart, at the terminus of the ejecta blanket (McCauley, 1973; Barlow et al., 2000). Recently, some workers have proposed that there are two distinct types of DLE craters based on morphology (Barlow, 2015b). Type 1 DLEs are described as possessing a thick, low sinuous inner layer that terminates into a broad distal rampart and a thinner, more sinuous outer layer with a narrow rampart (Barlow, 2015a). In type 2 DLEs, both layers are proposed to be relatively uniform in thickness, terminate into narrow ramparts, and are more sinuous than type 1 DLEs (Barlow, 2015a). In this contribution, we use the original definition of a DLE crater, as defined by Barlow et al. (2000), which is “two layers of (ejecta) material, where the inner layer is smaller in diameter than the outer layer” (Fig. 1).

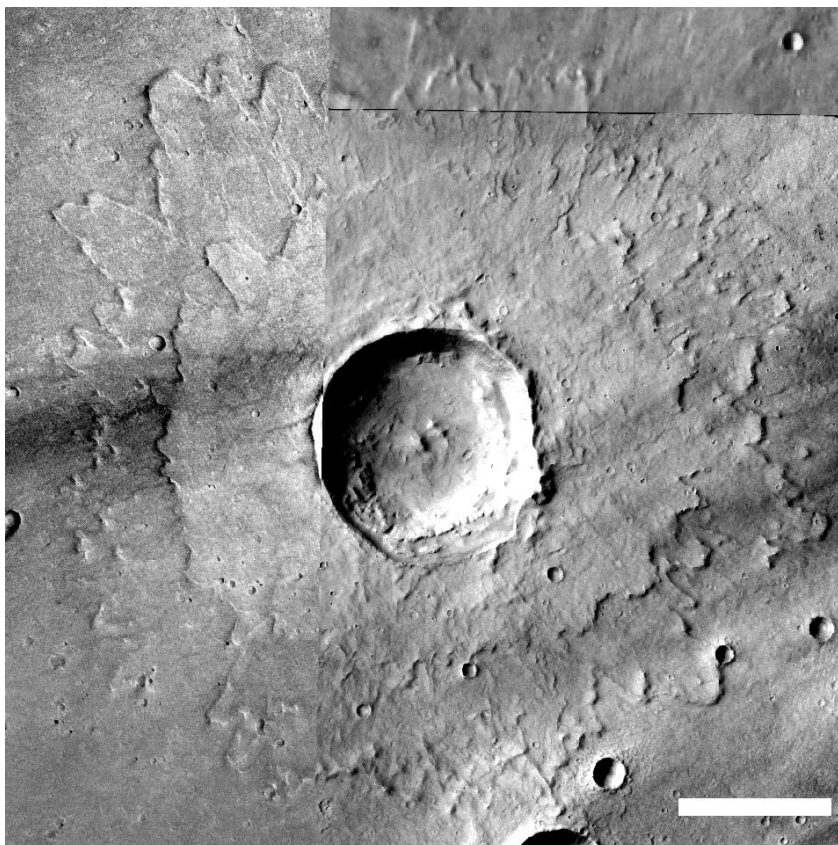


Figure 2.1: Example of a double layered ejecta crater in the Syrtis Major region (75.46° E, 9.61° N). HRSC (IDs: H0230_0000_ND4 and H3025_0000_ND4) and THEMIS Day IR 100m mosaic. Scale bar 10 km. North is up.

While SLE and MLE morphologies are distributed globally, DLEs are of particular interest because they occur predominately at northern latitudes (but not exclusively), where geomorphological evidence for an abundance of near-surface ice is common (Barlow and Perez, 2003). However, the very fact that some DLE craters occur near the equator must be taken into account in any model for their formation, but this fact is often overlooked. Previous observations of DLEs have suggested that ejecta mobility is greater at higher latitudes than at lower latitudes, consistent with increasing ice concentration near-surface as a function of increasing latitude (Rossbacher and Judson, 1981; Clifford, 1993; Clifford and Parker, 2001; Clifford et al., 2010); however, this has not been well quantified. The goal of this study is to constrain the affect(s) of the target material to determine whether morphometry of DLEs specifically into plains units interpreted to be

volcanic targets varies as a function of latitude. Since target material will be grossly similar on all these volcanic terrains (e.g., basaltic lavas [Scott and Tanaka, 1986; Greeley and Guest, 1987; Skinner et al., 2006; Tanaka et al., 2014]) (Table 1), any differences in morphometry (i.e. ejecta mobility and lobateness) between regions must predominately reflect other factors, such as the volatile content in the target, whether surficial or at depth, and/or the cohesiveness of the target surface.

2.2 Methodology

Robbins and Hynek (2012) classified 3413 DLE craters ≥ 1 km (up to ~ 50 km) in diameter. We have reevaluated each DLE crater from the Robbins Crater Database using Mars Reconnaissance Orbiter (MRO) Context Camera (CTX) (resolution 6 m/pixel) (Malin et al., 2007) and Thermal Emission Imaging System (THEMIS) visible (VIS) images (resolution 18 m/pixel) (Christensen et al., 2004), where available, as well as THEMIS daytime thermal infrared (IR) band 9 global mosaic (resolution 100 m/pixel) (Edwards et al., 2011; Hill et al., 2014) to compile a revised global database of 1351 DLE craters 1–27 km in diameter. Our revised database comprises 40% of the DLEs in Robbins database having the same diameter range. Classification was based on the original definition of Barlow et al. (2000) that a DLE possesses a distinct two-layered ejecta morphology. Using craters from our revised DLE database, we have downselected to 127 craters that specifically fall within volcanic regions. These craters range from ~ 3 to 25 km in diameter, retain a continuous inner and outer layer, and possess good enough image coverage to permit morphological (e.g., radial grooves) and morphometric investigations. Regions include: Tharsis, Elysium, Syrtis Major, and Hesperia (Fig. 2).

The Java Mission-planning and Analysis for Remote Sensing (JMARS) software was used for our morphologic and morphometric analyses of DLE craters, and is based largely on THEMIS visible (VIS) and CTX images, which provide resolutions of 18 m/pixel and 6 m/pixel respectively (Christensen et al., 2004, 2009; Malin et al., 2007). Individual shape files were drawn outlining each ejecta layer (e.g., inner and outer), as well as the crater rim. Area and perimeter of an individual shape file can be calculated automatically in JMARS. Because we have measured the total enclosed area of the outer and inner layers for each crater, the area of the crater itself is subtracted to determine the

true area of an ejecta layer. The analysis includes the documentation of radial grooves (if any), as well as the measurement of the inner and outer layers to determine Ejecta Mobility (EM):

$$EM = \frac{\text{average extent of ejecta layer from crater rim}}{\text{crater radius}}$$

and lobateness (Γ):

$$\Gamma = \frac{\text{perimeter of ejecta layer}}{[4\pi(\text{area of ejecta layer})]^{\frac{1}{2}}}$$

Ejecta mobility measures the extent an ejecta layer travels from the crater rim normalized by the crater diameter (Mouginis-Mark, 1979; Costard, 1989; Barlow, 2004; Boyce et al., 2010), while lobateness (Γ) is generally characterized by the number of ejecta “lobes” or distal ramparts (Johansen, 1979; Kargel, 1986, 1989; Barlow, 1994); more specifically, lobateness mathematically represents the sinuosity of the perimeter of an ejecta blanket. For purposes of this study, we have modified the EM equation to determine an “effective” radius of an ejecta layer using the area of a circle (see also Barlow et al., 2014; Li et al., 2015):

$$EM = \frac{\sqrt{\frac{A}{\pi}} - r}{r}$$

where A is the total enclosed area inside an ejecta layer (including the crater itself), and r is the radius of the crater. This gives a more precise average radius of an individual ejecta layer by essentially averaging every radii along the circumference of a layer.

Profiles of a representative crater from each region are also included. These were derived from High Resolution Stereo Camera (HRSC) Digital Terrain Models (DTM) and analyzed in ENVI (ENvironment for Visualizing Images) v5.1 software produced by Exelis. The HRSC DTMs are co-registered with MOLA DTM data and provide spatial resolutions of 10m/px and 463m/px respectively (Neukum et al., 2004; Gwinner et al., 2009). Vertical resolutions of HRSC data are expected to be equal to or higher than that

of MOLA (1 m) (Gwinner et al., 2009). In places where there are data gaps with MOLA, elevation is interpolated from adjacent shots, which may result in an inaccurate representation of the topographic profile for a specific surface and/or failure to detect small-scale features, such as crater ramparts. HRSC DTMs are based on stereo images; therefore, HRSC elevation data are more complete than MOLA because they do not suffer from areas of interpolation due to data gaps from insufficient orbits or MOLA laser-shot coverage.

2.2.1 Study Areas

Four volcanic provinces were chosen based on location (i.e., low, mid, and high latitudes within each hemisphere) and abundance of DLE craters within each region: Elysium, Syrtis Major, Hesperia Planum, and Tharsis (Fig. 2). Due to its size and geographic location Tharsis was subsequently divided into northern (circa Alba Patera) and southern (Solis, Syria, Sinai, Thaumasia, and Ophir Planums) regions. All of these craters are located from $\sim 60^\circ$ N to $\sim 40^\circ$ S latitude, with elevations ranging from 6 to -6 km. Representative examples from each region are shown in Figures 1 and 3. Bulk terrain types are interpreted as being basaltic lavas and are Hesperian to Amazonian in age (Scott and Tanaka, 1986; Greeley and Guest, 1987; Skinner et al., 2006; Tanaka et al., 2014). Table 1 summarizes the major parameters for each region and lists the units each DLE is situated in. It should be noted that we inspected both the old and new geologic maps of Mars (i.e., USGS I-1802-A and -B, 1:15M scale; USGS SIM 3292, 1:20M scale) for interpretations, but have used the older, more detailed map for assigning geologic units for this study. Currently, much of the northern hemisphere is mantled with a young layer of dust ($\sim 10^6$ – 10^5 years) (including northern Tharsis and Elysium) that could be up to 2 m thick in areas and likely represents the most recent cycle of dust deposition and removal that has occurred throughout Mars' geologic history (Christensen, 1986).

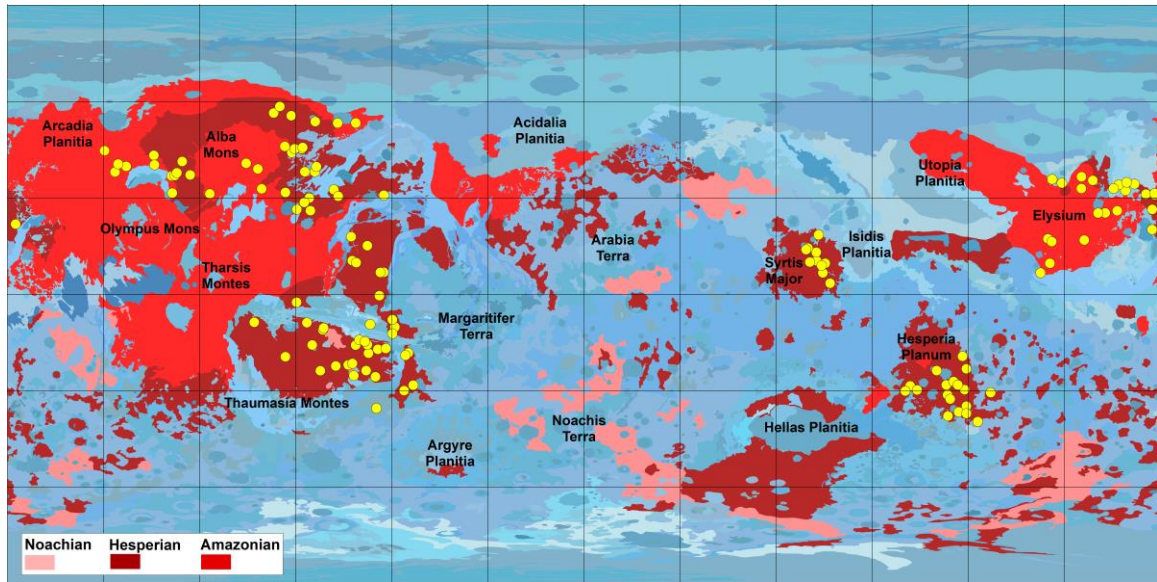


Figure 2.2: Geologic map of Mars highlighting volcanic geologic units (shades of red) (modified after Skinner et al., 2006). DLEs are plotted in yellow.

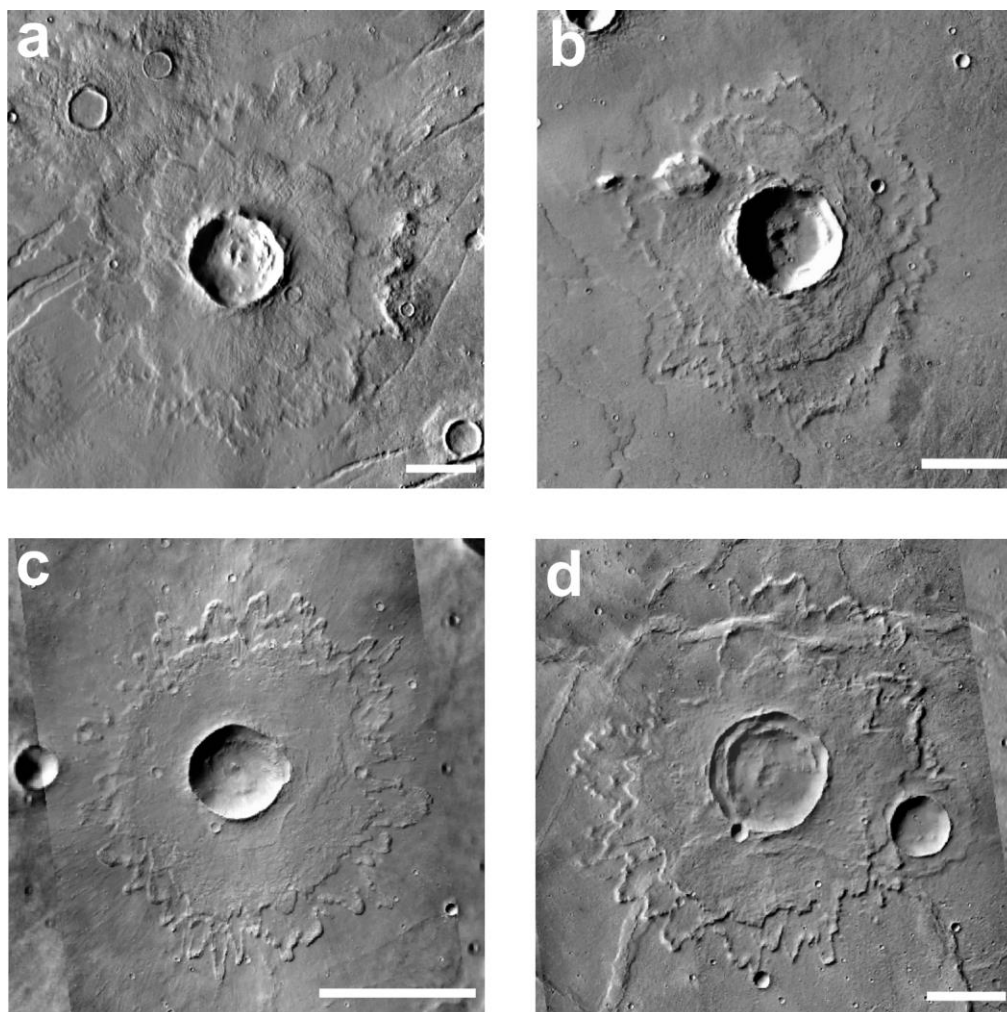


Figure 2.3: Representative DLEs from each study region. Scale bars 10 km. North is up in all images. (a) N Tharsis (276.54° E, 39.73°), THEMIS Day IR 100m global mosaic. (b) Elysium (145.63° E, 9.63°), HRSC image ID: H2973_0000_ND4. (c) S Tharsis (301.04° E, -10.21°), CTX image ID: G22_026773_1700_XN_10S059W. (d) Hesperia Planum (119.51° E, -23.24°), CTX mosaic: B20_017312_1564_XN_23S240W, B18_016745_1551_XN_24S240W, B09_013066_1565_XN_23S240W.

Table 2.1: Study regions showing the number of DLEs corresponding to each geologic unit (See Scott and Tanaka, 1986 and Greeley and Guest, 1987 for full unit descriptions). The first letter of each unit represents each geologic period: A = Amazonian; H = Hesperian; N = Noachian.

Region	# DLEs	Unit	Interpretation	Regional interpretation
Northern Tharsis	4	Aa ₁	Lava flows	Generally around the Alba Patera region. Emplacement began in the early Hesperian and continues throughout the Amazonian Period (Cattermole, 1990; Schneeberger and Pieri, 1991). Four main eruptive phases: (1) fissure erupted extensive floodlike flows; (2) emplacement of pyroclastic materials; (3) voluminous lava flows erupted from a central vent; (4) effusive flows followed by collapse of summit caldera (Schneeberger and Pieri, 1991). Estimated to be hundreds of meters thick (Tanaka et al., 2014).
	3	Aa ₃	Lava flows	
	3	Aam	Lava flows	
	2	AHcf	Lava flows	
	13	Hal	Lava flows	
	1	Hf	Interlayered lava flows and impact breccias	
	3	Ht ₂	Lava flows	
	3	Htl	Lava flows	
	3	Htm	Lava flows	
Elysium	9	Hr	Lava flows	Bulk of edifice constructed during Noachian with episodic activity through to the Amazonian (Platz and Michael, 2011). Primarily effusive lava flows overlying heavily cratered terrain (Hartmann and Berman, 2000; Platz and Michael, 2011). Sedimentary layers possible between flows (Hartmann and Berman, 2000). Thickness estimated to be on the order of hundreds of meters (Tanaka et al., 2014).
	10	Ael ₁	Lava flows	
	1	Apk	Diverse origins	
	4	Aps	Diverse origins	
	1	AHpe	Eroded material	
	5	Hr	Lava flows	
	2	HNu	Undivided material	
Syrtris Major	1	Npld	Lava flows, pyroclastic material, and impact breccias	First episode of eruption in late Noachian or early Hesperian as extensive ridge-plains unit followed by flows from calderas (Schaber, 1982). Surface heterogeneous, but basaltic in composition (Mustard et al., 1993; Hiesinger and Head, 2004). Overall thickness ~0.5 – 1 km (Hiesinger and Head, 2004).
	10	Hs	Lava flows	

Southern Tharsis	1	Hf	Interlayered lava flows and impact breccias	Heavily fractured basement from heavy bombardment overlain by a 2 – 3 km thick friable impact generated megaregolith layer (Carr, 1986; MacKinnon and Tanaka, 1988; Davis and Golombek, 1990). Multiple lava flows superposed at surface and are estimated to be a few hundred meters thick (Davis and Golombek, 1990; Tanaka et al., 2014). Emplacement continuous since Noachian (Carr and Head, 2010).
	1	Hpl ₃	Interbedded lava flows and sedimentary deposits	
	21	Hr	Lava flows	
	6	Hsu	Lava flows	
	2	Npl ₂	Interbedded lava flows and aeolian deposits	
Hesperia	18	Hr	Lava flows	Pyroclastic deposits from Tyrrhena Patera overlain by lava flows originating from same vent (Greeley and Crown, 1990; Crown et al., 1992; Gregg and Farley, 2006). Region estimated to be few hundred meters thick (Tanaka et al., 2014). Emplacement began in the late Noachian or early Hesperian and ceased in late Hesperian to early Amazonian (Gregg and Farley, 2006).

2.3 Results

2.3.1 Ejecta Mobility (EM)

Our results indicate that EM varies across the globe depending on latitude and is broadly consistent with previous studies (Mouginis-Mark, 1979; Costard, 1989; Barlow, 2006; Barlow et al., 2014; Jones and Osinski, 2015). However, our results show that the proportion of craters with high EM values is less at lower latitudes and increases with increasing latitude, irrespective of region (Figs. 4a, 5a, 6a; Table 2). These results are true for both ejecta layers but are more apparent for outer layers. For example, Figure 4a shows the distribution of binned outer layer EM data (0.1 increments) within each region, where higher EM bins (reds) are observed dominantly at higher latitudes, and lower EM bins (blues) are concentrated at lower latitudes. The same is generally seen with the inner layers (Fig. 4b). An exception for these general distribution patterns is Southern Tharsis, which appears to have a range of high and low EM values for both outer and inner layers (Fig. 4). Excluding S Tharsis, the EM distributions suggests that there is a weak trend of increasing EM with latitude for at least the outer layers. Figures 4a and 5a show

normalized frequencies of binned EM data (0.5 increments) against latitudinal bins to help recognize any trends with latitude. Concentrating on the middle latitude ranges (10–30° and 30–50°) in Figure 5a, we see a higher frequency of DLEs with lower EM (bins 1.5–2 and 2–2.5; light and dark blue respectively) within the 10–30° latitude range and a lower frequency of the same bins within the 30–50° latitude range. This appears to continue into the 0–10° latitude range. Conversely, we find that the frequency of higher EM (bins 2.5–3, 3–3.5, and 3.5–4 or green, yellow, and red respectively) increases from the 10–30° to the 30–50° latitude ranges (Fig. 5a). Again, this appears to persist into the adjacent higher latitude range (50–70°) (Fig. 5a).

Figures 5b and 6b display box plot distributions of our data for each region. We note that regions in this plot (and successive box plots) are listed in increasing order by the average latitude of each respective region regardless of hemisphere to better visualize any trends in the overall data. From the bulk of the data (quartiles 1 and 3), one could argue there is a very weak trend of increasing EM with latitude for the outer layers; however, considering the error bars, the trend disappears. No such trend is recognized for inner layers (Fig. 6b). S Tharsis, Syrtis Major, and Hesperia all appear to have similar EM ranges and means while N Tharsis and Elysium are both similar. Considering the locations of each region (e.g., latitude wise), Hesperia should have values similar to that of N Tharsis and Elysium, yet it doesn't (Fig. 5b). This may suggest Hesperia is an outlier from the rest of the data. We have also plotted all data from each region against latitude (not presented here), but do not recognize any strong trends within any particular region. Using a linear least squares fit, the outer layer R^2 values range from ~ 0.03 (S Tharsis) to ~ 0.56 (Elysium), suggesting there are indeed no trends with latitude within each region. In addition, there are no trends with elevation.

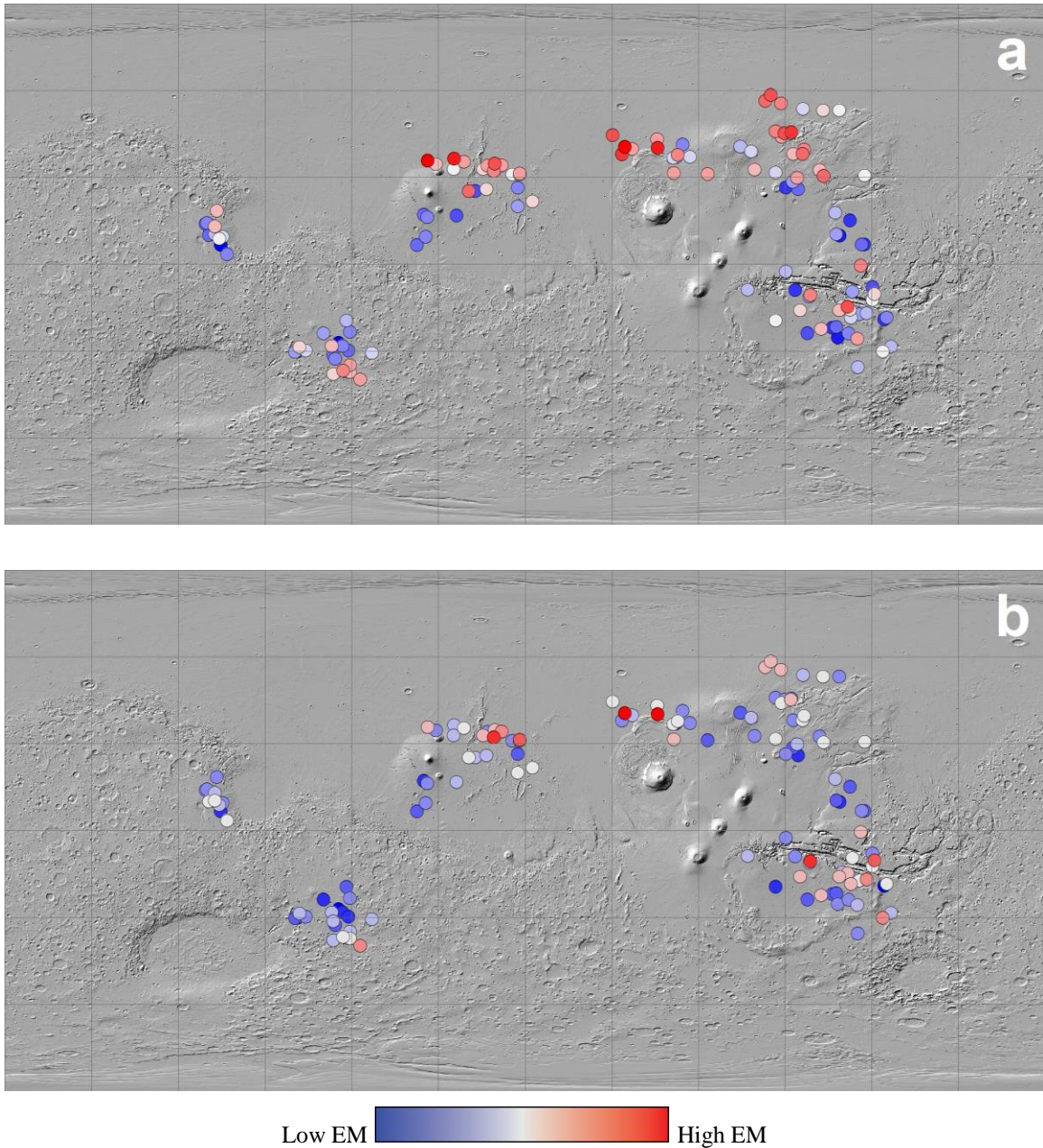


Figure 2.4: Distribution of binned EM data on MOLA shaded relief map of Mars. Data is binned by 0.1 increments. (a) Outer layer EM. (b) Inner layer EM.

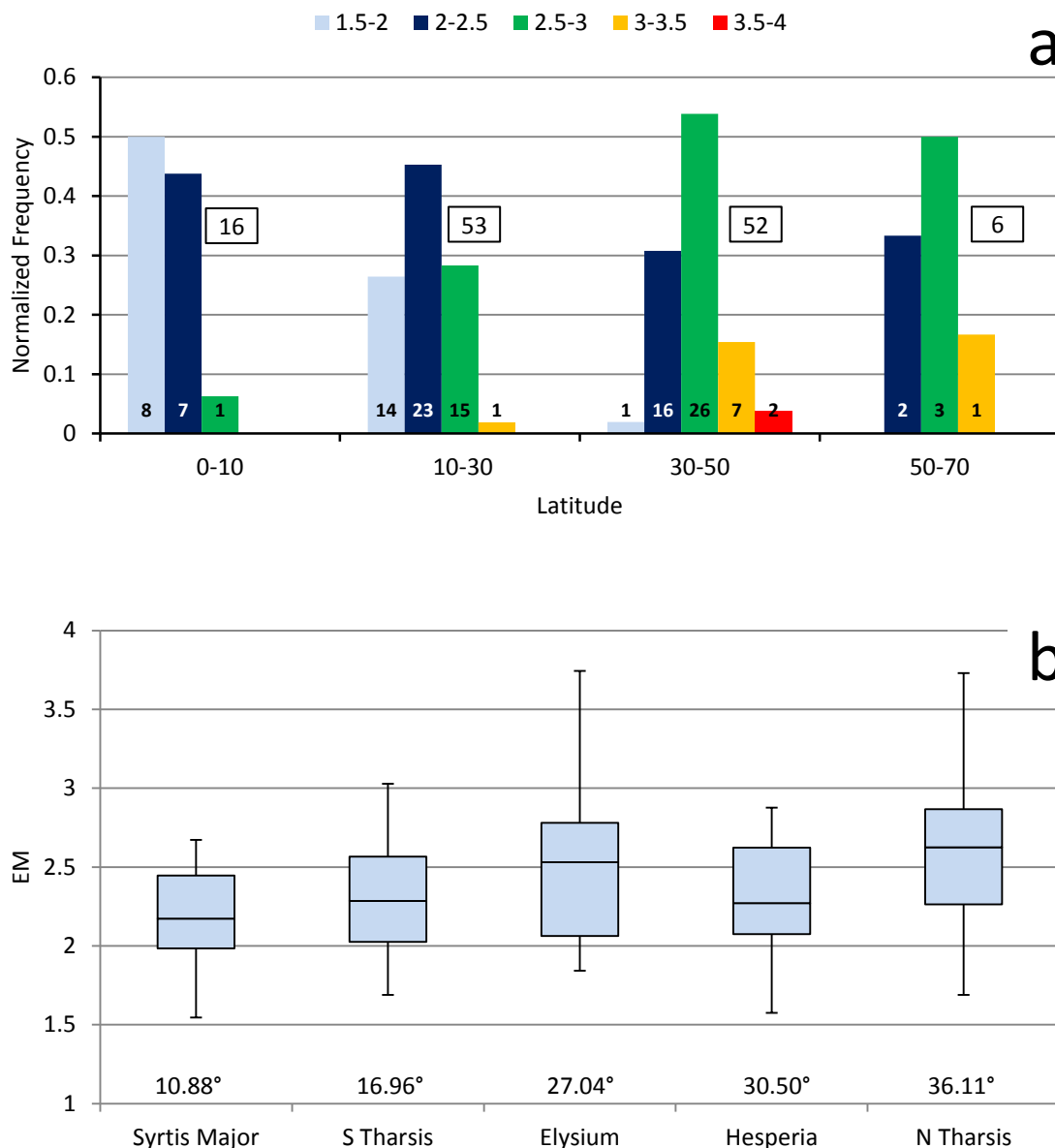


Figure 2.5: Ejecta mobility (EM) of outer layers. (a) Normalized frequency of EM values across latitude. EM values in legend are grouped in 0.5 intervals. Number of craters within a specific series is labeled within each respective bar while total number of craters in each latitude bin are labeled in white boxes. (b) Box plot showing the distribution of EM values within each region. Whiskers represent minimum and maximum values. Average (positive) latitudes are listed with each respective region.

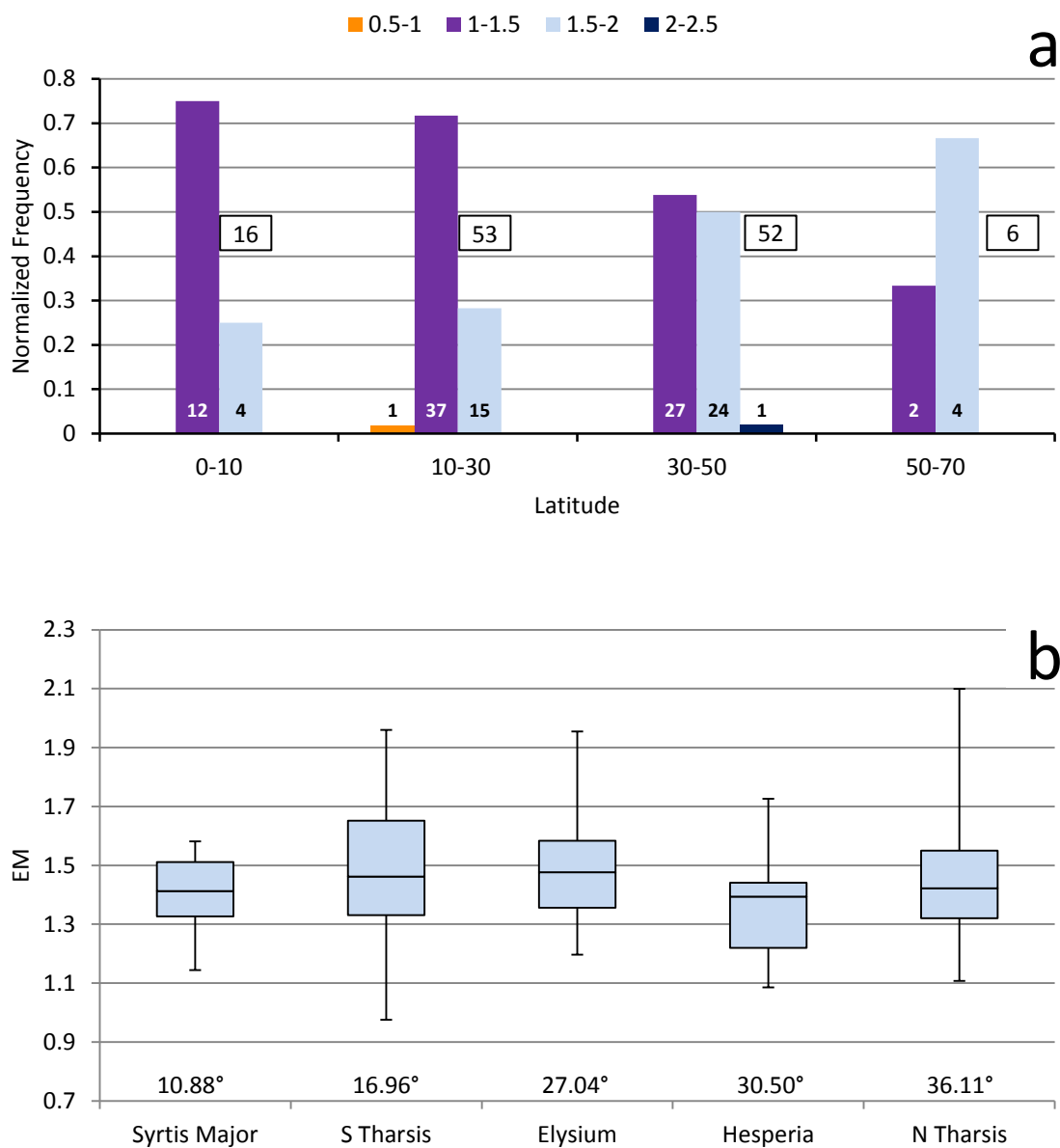


Figure 2.6: Ejecta mobility (EM) of inner layers. (a) Normalized frequency of EM values across latitude. EM values in legend are grouped in 0.5 intervals. Number of craters in a specific series is labeled within each respective bar while total number of craters in each latitude bin are labeled in white boxes. (b) Box plot showing the distribution of EM values within each region. Whiskers represent minimum and maximum values. Average (positive) latitudes are listed with each respective region.

Table 2.2: Average ejecta mobility (EM) and lobateness (Γ) for outer and inner layers of DLEs.

Region	(n) DLEs	Diameter range (km)	Layer	Avg. EM	SD	EM Range	Avg. Γ	SD	Γ Range
Northern Tharsis	44	3 – 24	Outer	2.56	0.45	1.69-3.73	1.42	0.13	1.21-1.63
			Inner	1.45	0.19	1.11-2.10	1.32	0.11	1.15-1.63
Elysium	24	3.2 – 20.3	Outer	2.52	0.50	1.84-3.74	1.47	0.20	1.23-2.11
			Inner	1.49	0.19	1.20-1.95	1.30	0.11	1.15-1.58
Syrtis Major	10	8.1 – 23.7	Outer	2.23	0.36	1.54-2.67	1.62	0.11	1.44-1.87
			Inner	1.39	0.13	1.14-1.58	1.50	0.09	1.36-1.65
Southern Tharsis	31	4 – 19.6	Outer	2.29	0.37	1.69-3.03	1.58	0.22	1.27-2.06
			Inner	1.48	0.22	0.98-1.96	1.45	0.18	1.19-1.85
Hesperia	18	4.7 – 19.7	Outer	2.32	0.35	1.57-2.88	1.53	0.17	1.21-1.82
			Inner	1.36	0.16	1.08-1.73	1.42	0.14	1.20-1.65

2.3.2 Lobateness (Γ)

Our results show that DLEs located at lower latitudes generally have a higher lobateness than those at higher latitudes, and is consistent with previous studies (c.f., Kargel, 1986) (Fig. 7, Table 2). This pattern also appears to be inversed from our EM results (e.g., higher EM at higher latitudes and lower EM at lower latitudes), where we find that at lower latitudes both ejecta layers are more lobate than those at higher latitudes. This may suggest a relationship between EM and lobateness. However, after simply plotting EM against lobateness, no trends arose; if there is indeed a relationship between EM and lobateness, it is likely more complex. Figure 7 shows the distribution of binned lobateness data (0.1 increments) within each region, where lower lobateness values (blues) are generally more frequent at higher latitudes, and higher lobateness values (reds) more frequent at lower latitudes. Figures 8a and 9a show the frequency of craters having a certain lobateness value within a given latitude range. Both graphs show a greater number of craters with higher lobateness values at lower latitudes and less craters at higher latitudes. Like EM, the bulk of the data (quartiles 1 and 3) in Figures 8b and 9b could potentially show a very weak trend with latitude; but considering the error bars, the trend may be nonexistent. This is excluding Hesperia, which could again be considered an outlier based on the ranges of lobateness values with region location (latitude wise).

Scatter plots of lobateness against latitude within each individual region show no strong trends (not presented here). In addition, elevation does not seem to affect the lobateness of either layer (not presented here).

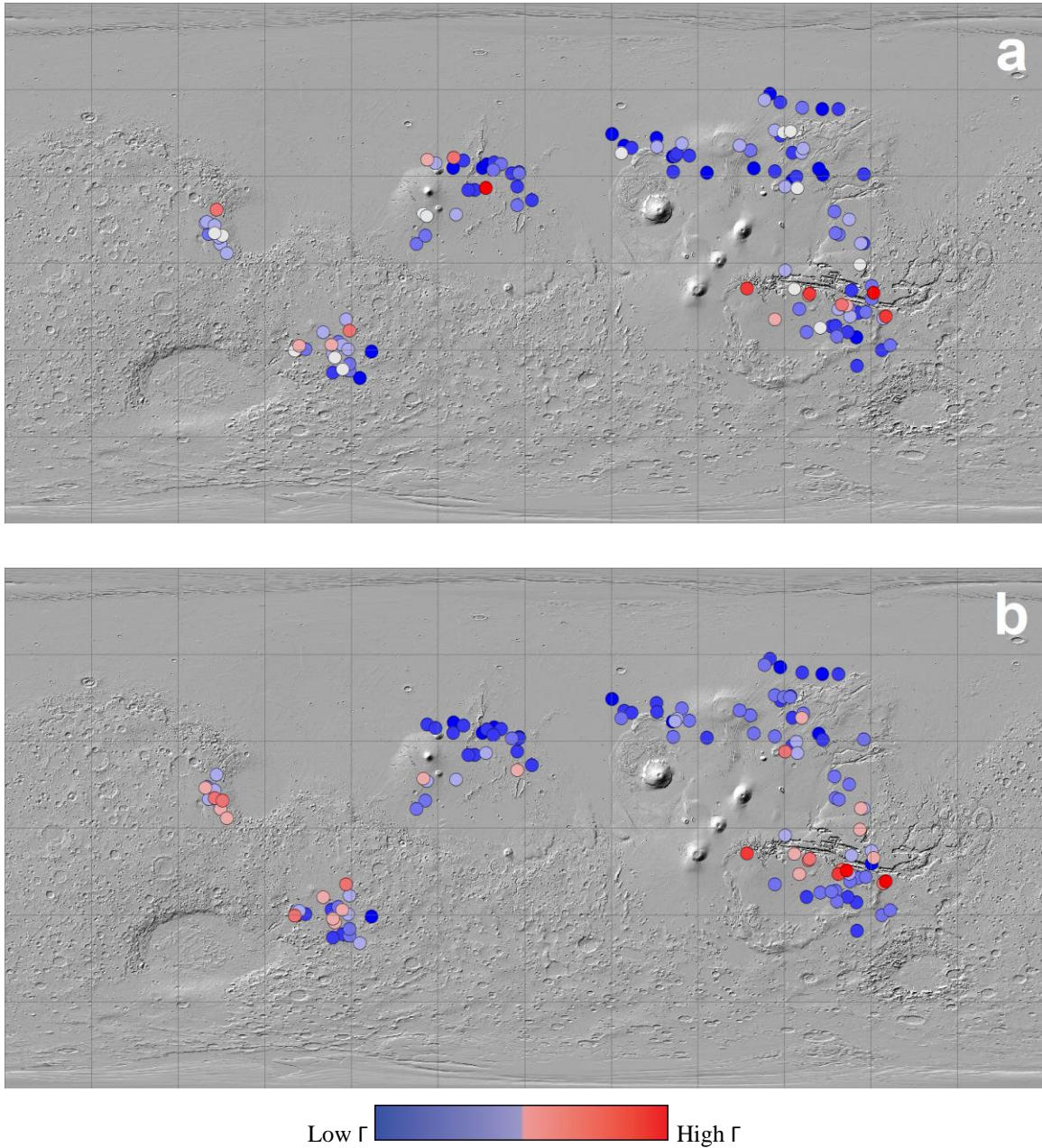


Figure 2.7: Distribution of binned lobateness data on MOLA shaded relief map of Mars. Data is binned by 0.1 increments. (a) Outer layer EM. (b) Inner layer EM.

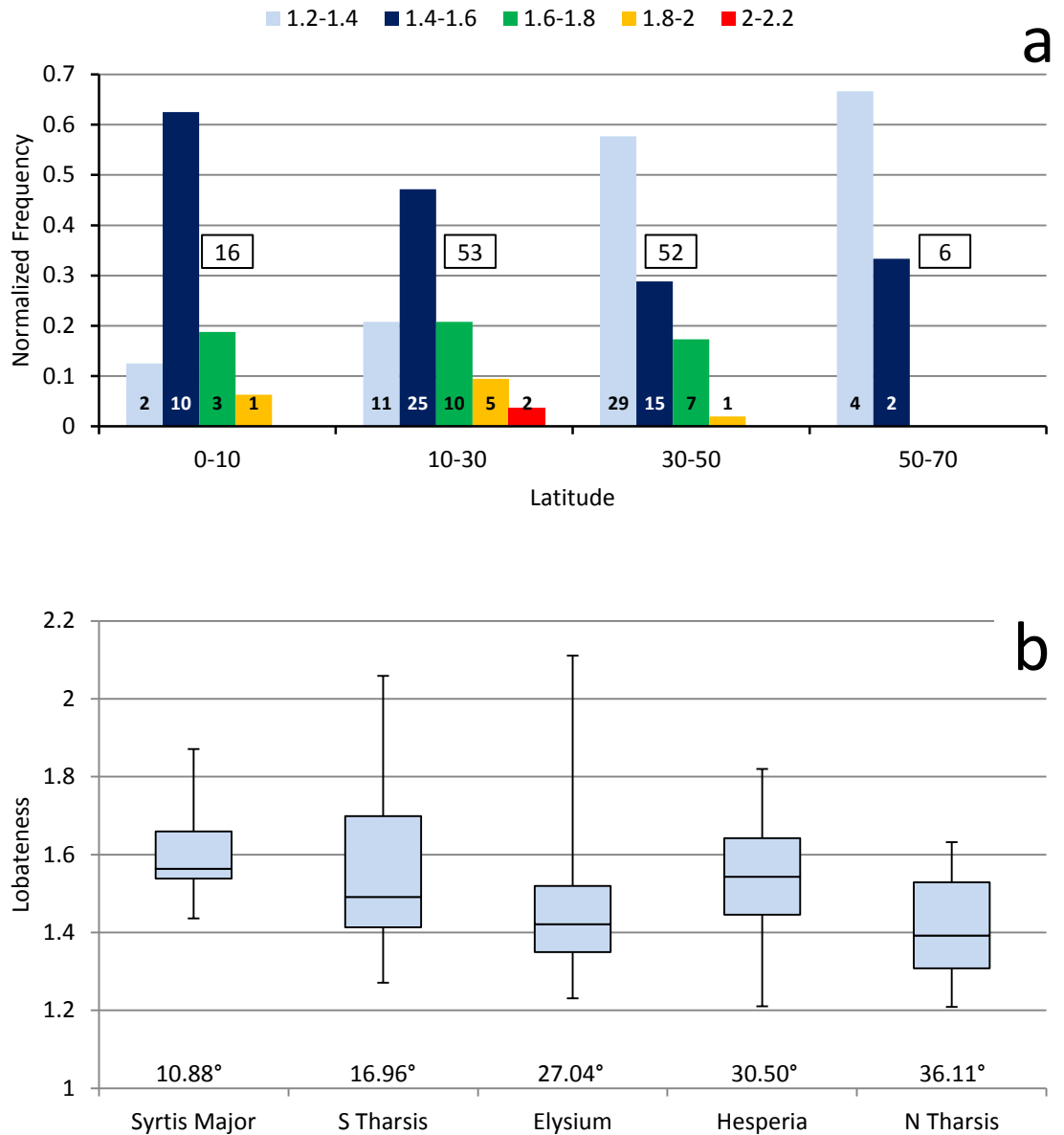


Figure 2.8: Lobateness of outer layers. (a) Normalized frequency of lobateness values across latitude. Lobateness values in legend are grouped in 0.5 intervals. Number of craters in a specific series is labeled within each respective bar while total number of craters in each latitude bin are labeled in white boxes. (b) Box plot showing the distribution of lobateness values within each region. Whiskers represent minimum and maximum values. Average (positive) latitudes are listed with each respective region.

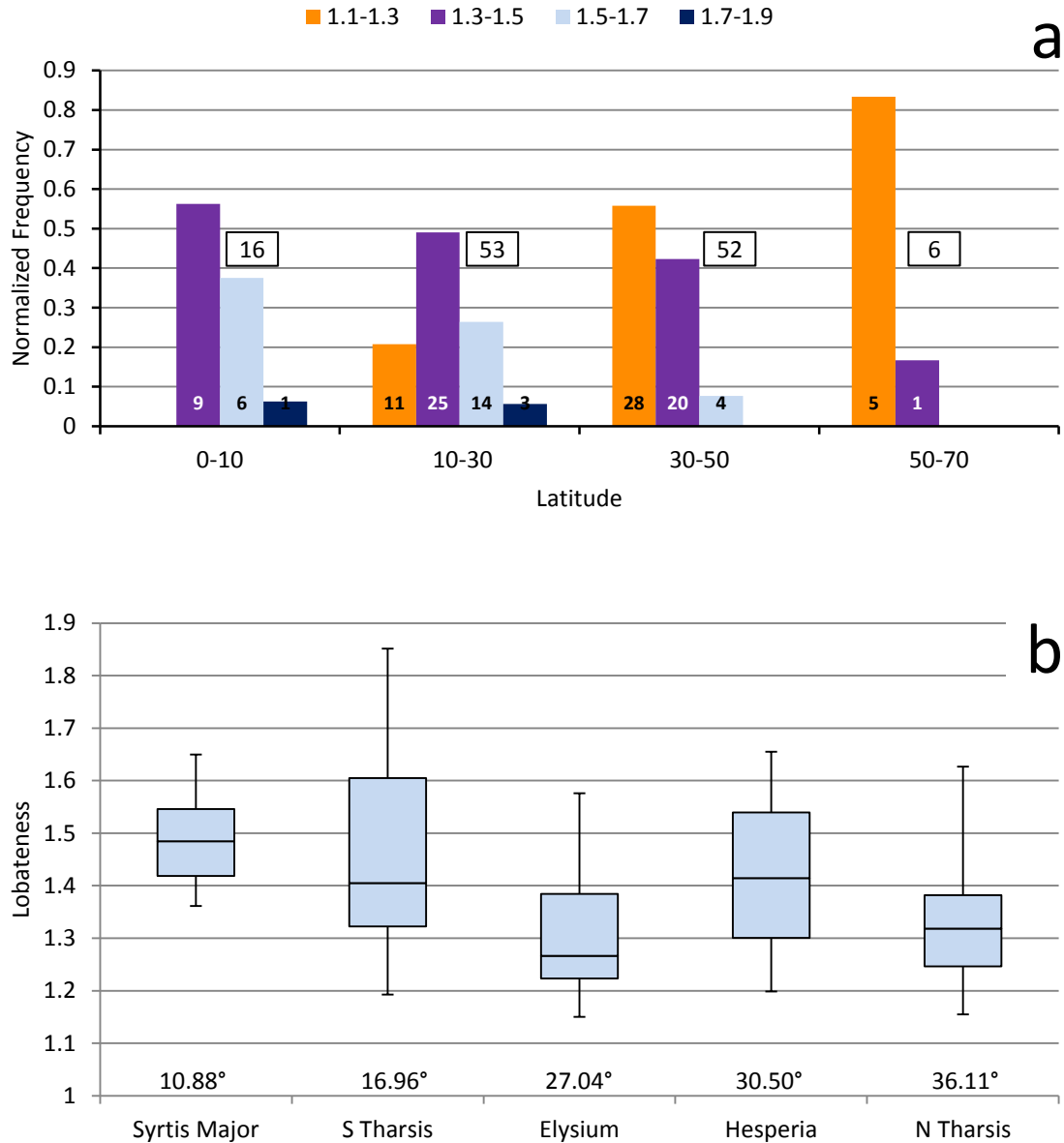


Figure 2.9: Lobateness of inner layers. (a) Normalized frequency of lobateness values across latitude. Lobateness values in legend are grouped in 0.5 intervals. Number of craters in a specific series is labeled within each respective bar while total number of craters in each latitude bin are labeled in white boxes. (b) Box plot showing the distribution of lobateness values within each region. Whiskers represent minimum and maximum values. Average (positive) latitudes are listed with each respective region.

2.3.3 Other Morphologic and Morphometric Attributes

Some morphologic features such as radial grooves and the lack of secondary craters and distal ramparts have originally been attributed to DLE craters (e.g., Mouginis-Mark and Boyce, 2004). However, recent studies have challenged these previous observations as (1) radial grooves have been recognized on some SLEs and MLEs (Boyce et al., 2015a); (2) distal ramparts do occur on DLEs, though the morphology differs from SLEs and MLEs (Boyce and Mouginis-Mark, 2006); and (3) secondary craters (not considered in this study) are recognized around “fresh” DLE craters (e.g., Barlow, 2015a; Wulf and Kenkmann, 2015). An important observation from this study is that seventy-three of the 127 DLE craters we surveyed have grooves present on either the inner, outer, or both ejecta layers, while grooves are absent on either layer of the other 54 DLEs (Fig. 10). Importantly, the occurrence of grooves correlates with latitude. DLEs observed with no grooves occur predominately at low latitudes equatorward of $\sim 30^\circ$ in both hemispheres, while those with grooves are predominately seen at higher latitudes poleward (Fig. 11). Furthermore, DLEs without grooves show on average a lower fraction of surface dust coverage than those with grooves.

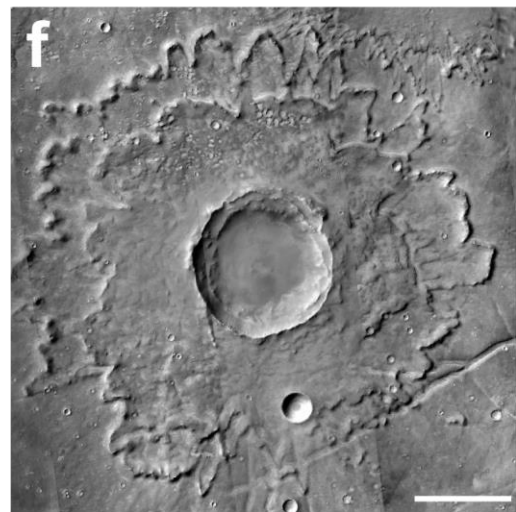
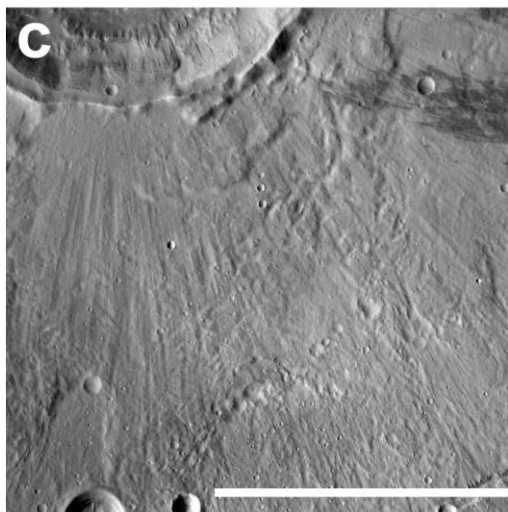
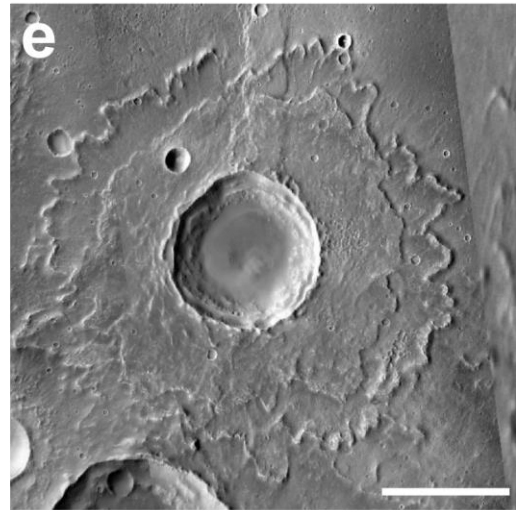
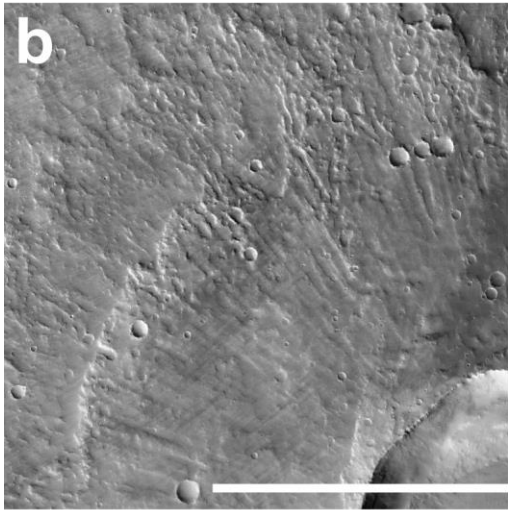
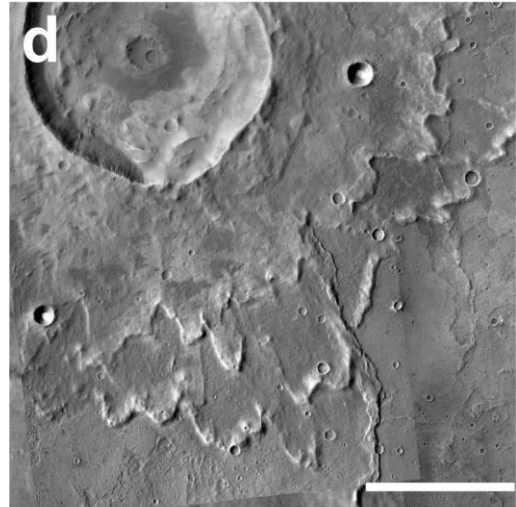
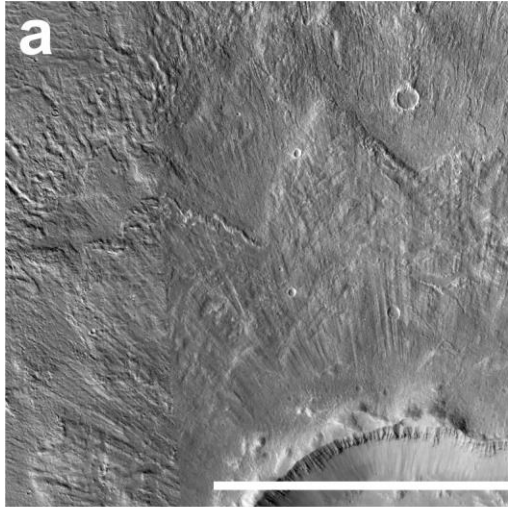
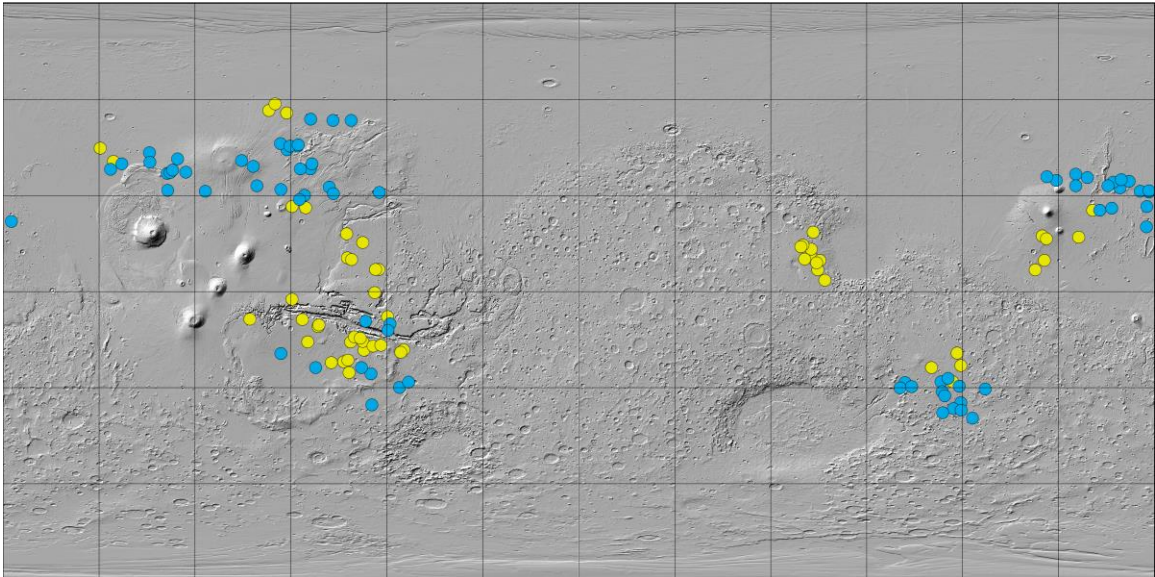


Figure 2.10: DLEs located in Tharsis with grooves (a, b, c) and without grooves (d, e, f). All scale bars 10 km except b (5 km). North is up in all images. (a) N Tharsis (276.54° E, 39.73°), CTX mosaic: P12_005663_2185_XI_38N083W, B19_016884_2181_XI_38N083W; (b) N Tharsis (266.85° E, 31.69°), CTX image ID: P13_006204_2139_XN_33N093W; (c) N Tharsis (283.36° E, 30.50°), CTX image ID: B17_016475_2099_XI_29N076W; (d) N Tharsis (296.50° E, 6.81°), CTX mosaic: B02_010554_1869_XN_06N063W, G22_026628_1876_XN_07N063W; (e) N Tharsis (288.96° E, 9.83°), CTX image ID: D03_028580_1898_XI_09N071W; (f) S Tharsis (278.54° E, -11.10°), CTX mosaic: P02_001760_1690_XI_11S081W, B17_016449_1673_XN_12S081W, D01_027631_1682_XN_11S081W, F04_037547_1684_XN_11S081W, D22_035991_1684_XN_11S081W.



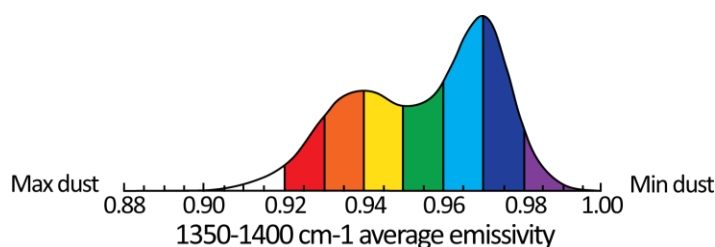
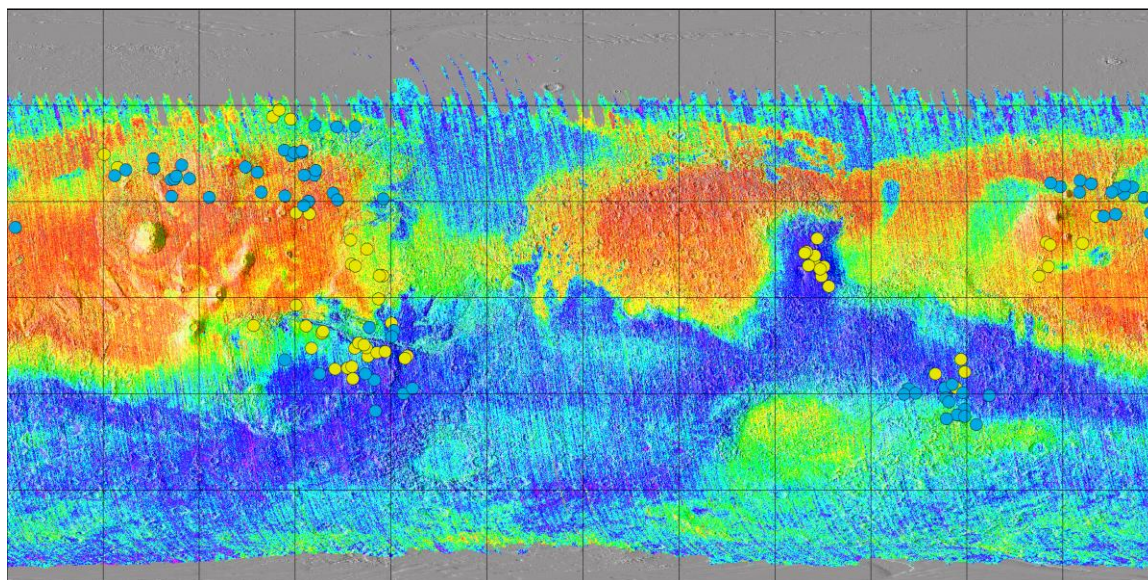
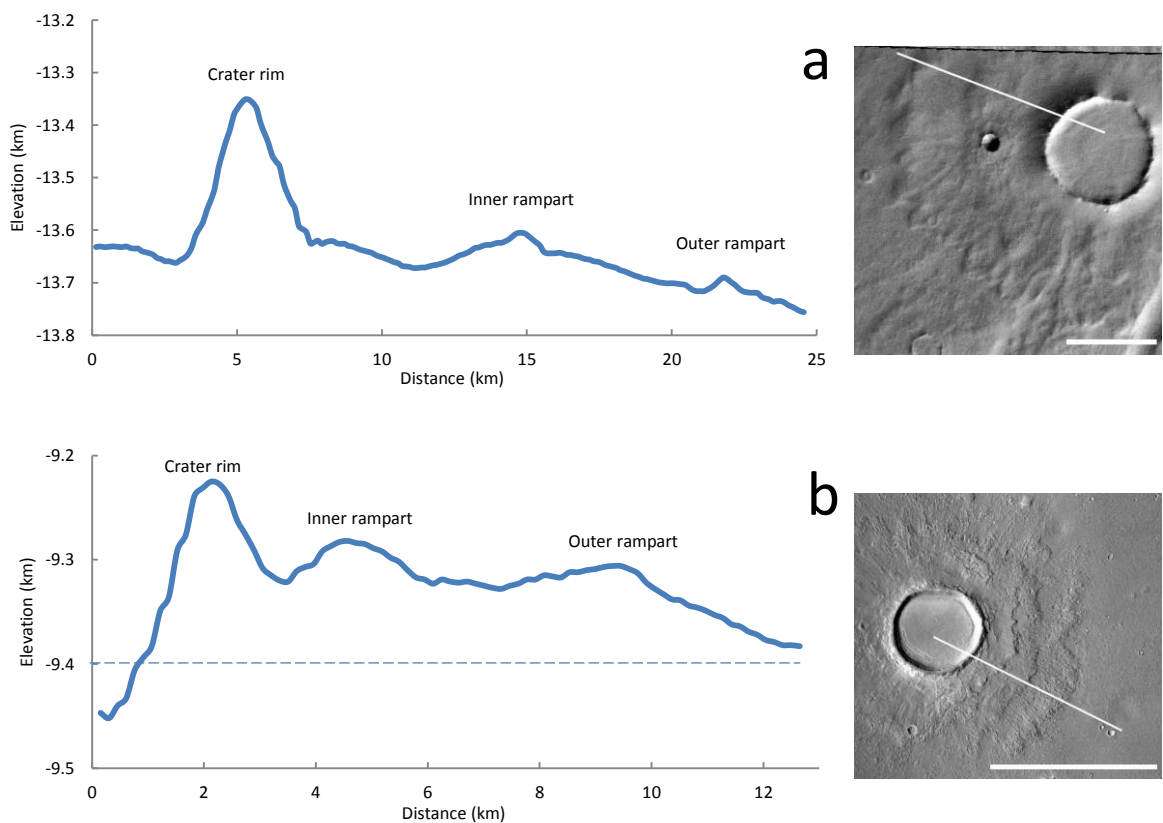


Figure 2.11: Distribution of DLEs displaying grooves (blue) and those lacking grooves (yellow) over MOLA shaded relief map of Mars (top) and TES colorized dust cover index (bottom). Warmer colors represent areas of higher dust cover; cooler colors represent areas of lower dust cover. Values in Tables 3 and 4 were derived from the map sampling feature in JMARS where the average DCI (after Ruff and Christensen, 2002) was calculated for the total area of a DLE (i.e., area of outer layer) and then averaged with the total DLEs within a specific region.

Profiles of a representative crater from each of our 5 study regions are shown in Figure 12. The profiles of the craters in Figures 12a and 12b (North Tharsis and Elysium respectively) have been exaggerated to a great extent ($\sim 17x$) in order to see the ramparts. Because these two craters are in heavily dusty areas, ejecta may be mantled by dust resulting in the subdued topographic profiles. In each region, the inner layer sits topographically higher than the outer layers and all appear to have an inner ejecta moat at $\sim 0.3\text{--}0.8$ crater radii. In addition, ramparts at the edge of the inner ejecta blanket are

apparent for all DLEs with the exception of the southern Tharsis representative (Fig. 12d). Average rampart heights above the surrounding terrain are ~ 100 m with the exception of the Syrtis Major representative (~ 200 m). In comparison, ramparts on the outer ejecta blankets are present on each of our 5 representative DLEs with an average height above the surrounding terrain between ~ 50 and ~ 100 m. The consistency of one rampart being more prominent than the other is not recognized here as it varies for each crater.



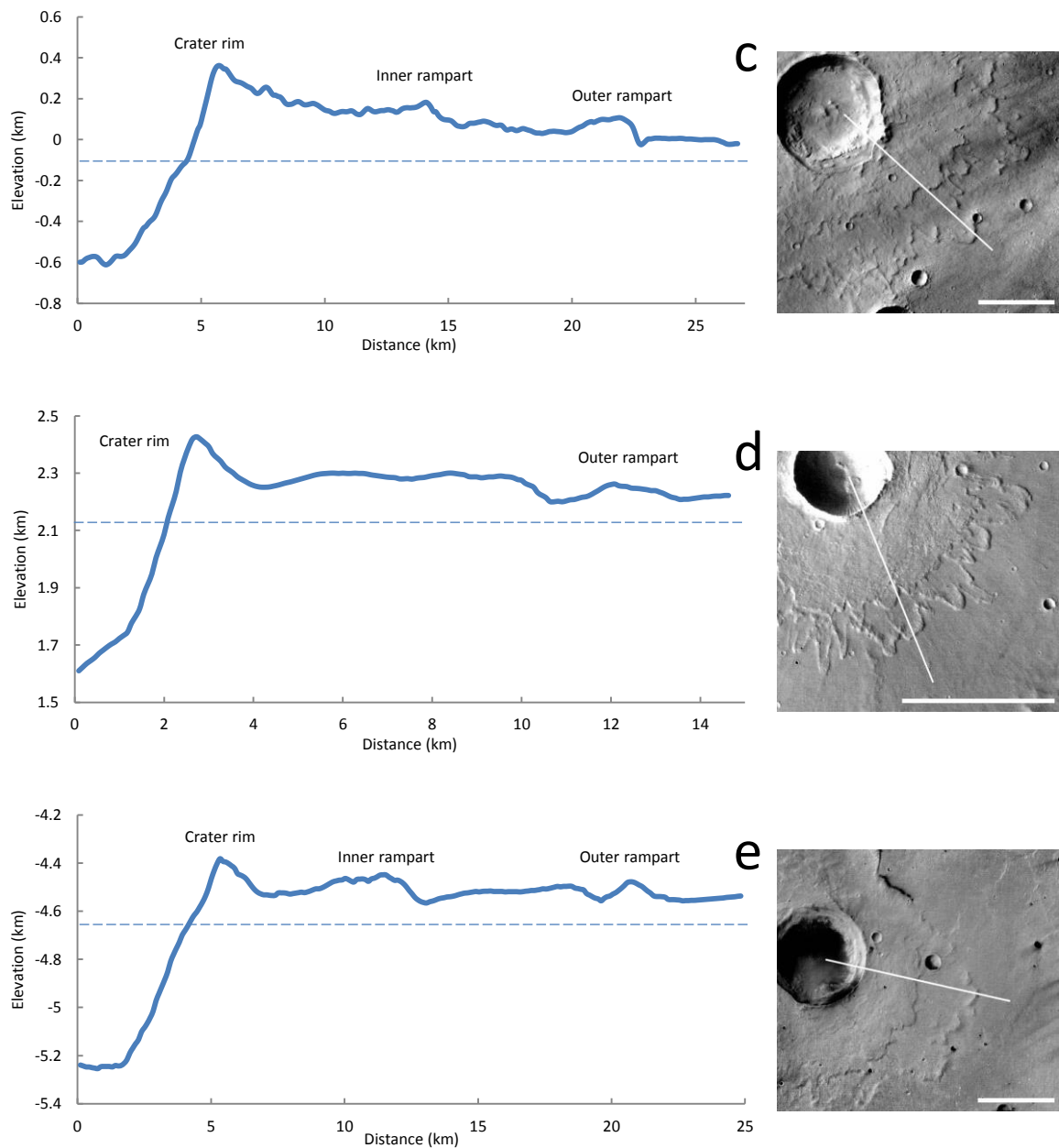


Figure 2.12: Topographic profiles of representative DLEs from each study region using HRSC DTMs. Dotted lines are planes of reference. All scale bars are 10 km. North is up in all images. (a) 11.7 km diameter crater located in N Tharsis (268.69° E, 55.58°). Vertically exaggerated $\sim 17\times$. Image ID: H1594_0000. (b) 4.9 km diameter crater located in Elysium (178.26° E, 31.40°). Vertically exaggerated $\sim 17\times$. Image ID: H1540_0009. (c) 14.7 km diameter crater located in Syrtis Major (75.47° E, 9.61°). Vertically exaggerated $\sim 8\times$. Image ID: H3025_0000. (d) 5.9 km diameter

crater located in S Tharsis (301.04° E, -10.21°). Vertically exaggerated ~6x. Image ID: H1918_0000. (e) 12.8 km diameter crater located in Hesperia Planum (100.44° E, -30.14°). Vertically exaggerated ~9x. Image ID: H0022_0000.

Figure 13 shows potential examples of the two recently proposed DLE types suggested by some authors (e.g., Barlow, 2015b; Barlow and Boyce, 2015; Boyce et al., 2015c), all located within the Hesperia region. Based on the criteria for distinguishing between the two proposed DLE types in Barlow and Boyce (2015), Figure 13a would likely be classified as a type 1 DLE, while Figures 13c and 13d are likely type 2 DLEs. Figure 13b could potentially be classified as transitional between the two types; if so, this may suggest that the varying morphologies are a continuum of the term “DLE” and not two distinct DLE types. Indeed, we find a range of DLE morphologies throughout this study, some which would fit the criteria for the “type 1”, “type 2”, and “transitional” DLE classification, but in no particular distribution that may suggest these are distinct based on location. Regardless, further work needs to be done to confirm if these recent observations of the two proposed DLE types are a result of varying emplacement processes/mechanisms or simply a continuum of the original term “DLE” (e.g., Barlow et al., 2000) where environmental factors (e.g., target lithology, surface properties, preservational/degradational phenomenon) could potentially affect the observed morphologies.

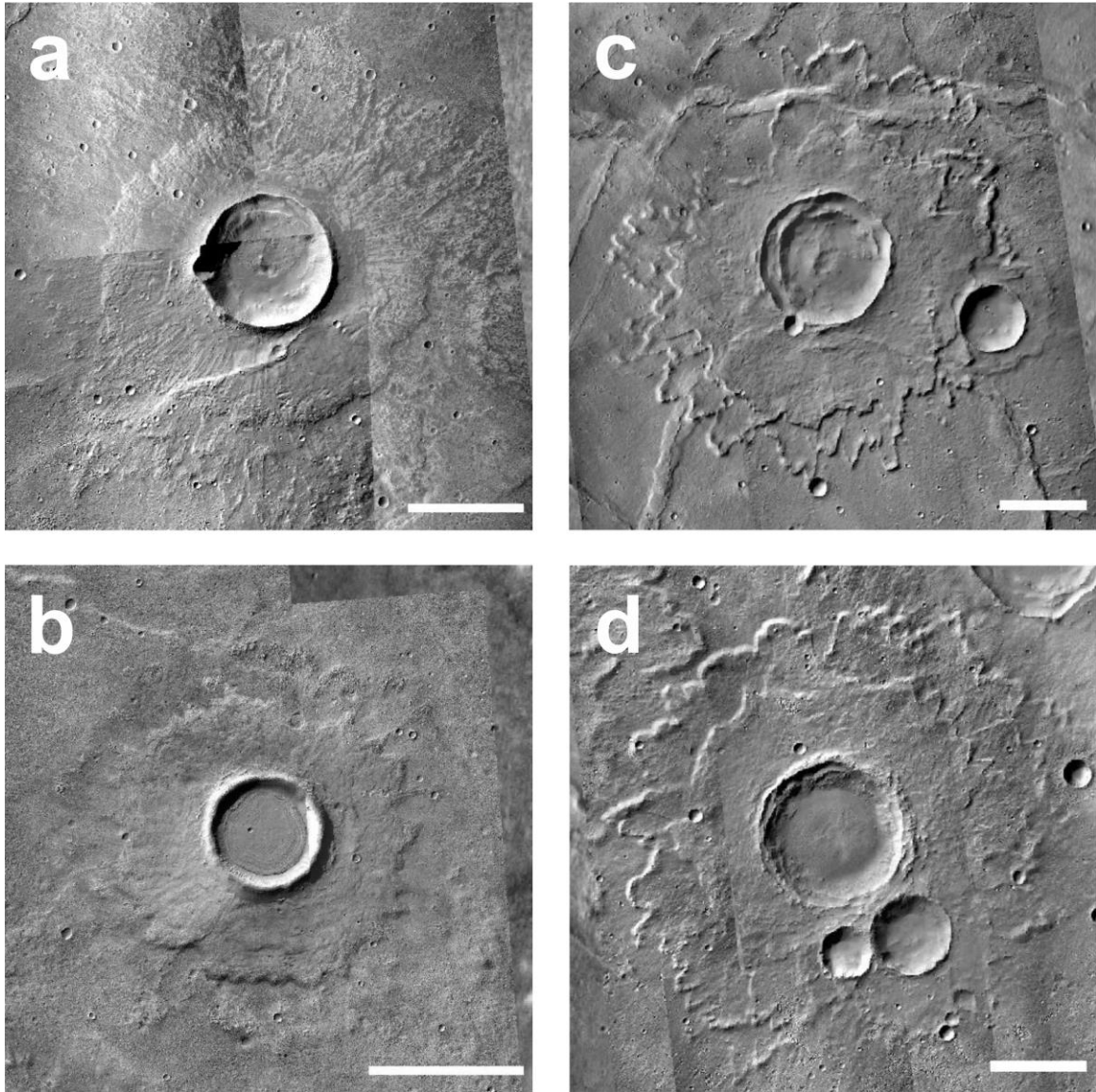


Figure 2.13: Examples of the two recently proposed DLE types in the Hesperia region. All scale bars are 10 km. North is up in all images. CTX mosaic: (a) G07_020807_1528_XN_27S258W, B20_017550_1486_XI_31S258W, D13_032345_1512_XN_28S258W; (b) G19_025461_1417_XN_38S237W, F02_036432_1391_XN_40S236W; (c) B20_017312_1564_XN_23S240W, B18_016745_1551_XN_24S240W, B09_013066_1565_XN_23S240W; (d) D21_035417_1540_XN_26S249W, G19_025646_1564_XN_23S249W, B18_016508_1568_XN_23S250W, G19_025646_1564_XN_23S249W, B17_016297_1565_XN_23S249W, B16_016086_1566_XN_23S249W, F02_036617_1531_XN_26S249W.

2.4 Discussion

2.4.1 Effect of the Target Properties on Ejecta Mobility

Despite all DLEs in this study being situated on volcanic terrains, their morphology and morphometric attributes (e.g., EM and lobateness) vary considerably. We have shown that EM is generally higher at higher latitudes and lower at lower latitudes, while lobateness appears inverted (e.g., higher at lower latitudes and lower at higher latitudes). We see no correlation between EM and lobateness with elevation. The bulk basaltic composition of the target alone cannot explain the differences seen from our results, as they should be very similar. Therefore, some other target variable(s) must be influencing emplacement.

Based on current models of the impact cratering process throughout the Solar System, initial emplacement of the first layer of ejecta is via a process of ballistic sedimentation where material is ejected out of the transient cavity at different angles, following parabolic flight paths that strike the ground at different distances away from the crater rim (Oberbeck, 1975; Melosh, 1989; Osinski et al., 2011). Materials ejected at higher velocities can form secondary craters, which excavate and incorporate local materials into the ejecta blanket (e.g., Oberbeck, 1975; Hörz et al., 1983; Melosh, 1989; Osinski et al., 2013). This incorporation of local material allows ejecta to become more mobile and essentially “flow” across the surface (e.g., Hörz et al., 1983; Osinski et al., 2013). Studies of impact craters on Earth support this hypothesis and provide evidence that local target material can become incorporated into an ejecta layer (Oberbeck, 1975; Hörz et al., 1983; Melosh, 1989; Osinski et al., 2013). For example, at the Ries impact structure, a significant portion (~69 vol. % average) of the local target is included in the ejecta layer, indicating incorporation during emplacement (Hörz et al., 1983). Importantly, the properties of the target material outside the transient cavity can also have an effect on ejecta mobility where more volatiles and/or less cohesive surficial materials can allow ejecta to runout further. This is seen at the Ries structure where the ballistic ejecta has a greater runout distance in regions where loose surface sediments were present at the surface, with correspondingly lesser runout distances in regions where the hard, competent Malm limestone was at the surface (Hörz et al., 1983). Thus, one explanation

for higher EM values is that these craters formed in targets covered with loose, surficial sediments. While we cannot rule this out for individual craters, it is difficult to imagine how this mechanism would result in the latitudinal variation we see here.

A related mechanism is that accumulation of dust on the surface of Mars could also potentially have the same effect on ejecta mobility, if accumulations are thick enough. Data from the Thermal Emission Spectrometer (TES) shows the highest concentrations of dust largely in the northern hemisphere, including northern Tharsis and Elysium (Fig. 11) (Ruff and Christensen, 2002), where dust accumulations are predicted to be 0.1–2 m thick (Christensen, 1986). High Resolution Imaging Science Experiment (HiRISE) observations confirm this and revise the estimate to ~4 m thick, at least in the Tharsis region (Keszthelyi et al., 2008; Bridges et al., 2010). Based on Viking Orbiter Infrared Thermal Mapper (IRTM) and TES observations, particle sizes in these regions are implied to be less than ~100 μm in diameter (Christensen, 1986; Ruff and Christensen, 2002). Particle sizes this small would have very little cohesion between particles and may potentially aid in the higher EM values observed within N Tharsis and Elysium (i.e., most dusty regions on Mars) (Fig. 4). Polar-layered terrains are evidence that the climate on Mars and the rate of dust generation and deposition has changed periodically throughout history and likely reflects changes in orbital parameters (e.g., Murray et al., 1973). Changes in climate will, in turn, affect dust cover (Christensen, 1986). Therefore, the current state of the Martian surface, based on TES data, likely represents the most recent, cyclic process of deposition and removal (Christensen, 1986). Topographic effects on regional wind patterns (e.g., Tharsis bulge) are suggested to be low since the current topography on Mars was constructed very early in geologic time (Noachian to early Hesperian) (e.g., Fenton and Richardson, 2001; Carr and Head, 2010). Together, this suggests that the cyclic process of deposition and removal of dust mentioned by Christensen (1986), likely occurs in the same general regions on Mars, and could quite possibly aid, and enhance, ejecta emplacement at higher northern latitudes.

In addition to dust, a volatile component may enhance fluidization further by reducing friction between particles. The distribution of ice throughout Mars' history has likely changed numerous times as a consequence of the planets obliquity; it has been estimated

to have undergone cyclic fluctuations between ~ 15 and 60° (Laskar et al., 2004) which may result in extreme climate change and global redistribution of ice. At the current obliquity ($\sim 25^\circ$), subsurface volatile (i.e., water-ice) concentrations are suggested to be more abundant near the poles and decrease equatorward (Rossbacher and Judson, 1981; Clifford, 1993; Clifford and Parker, 2001; Clifford et al., 2010). Thicknesses of the cryosphere are estimated to be ~ 0 – 9 km at the equator to ~ 10 – 22 km near the poles (Clifford, 1993; Clifford and Parker, 2001; Clifford et al., 2010) with an ice-rich layer proposed to begin at ~ 100 m depth equatorward of $\pm 40^\circ$ latitude (Clifford and Hillel, 1983; Barlow and Bradley, 1990). Model predictions indicate ground ice is stable with the current atmosphere poleward of $\pm 40^\circ$ latitude (e.g., Fanale, 1976; Clifford and Hillel, 1983; Madeleine et al., 2009) therefore, ice is expected to be present in the uppermost surficial layer at these latitudes (e.g., Byrne et al., 2009; Smith et al., 2009; Dundas and Byrne, 2010). In addition, mid-latitude glaciation is suggested to have occurred throughout the Amazonian (Head et al., 2003, 2005, 2006, 2010; Madeleine et al., 2009; Souness and Hubbard, 2012). There is, thus, ample evidence for a relative abundance of volatiles at higher latitudes, which may contribute to the increase in EM observed at these latitudes.

Large-scale flume experiments on debris flows indicate that Coulomb friction between particles dominates the shear strength of an overall flow (Iverson and LaHusen, 1993). Subsequently, yield strength decreases with increasing liquid concentrations (Rodine, 1974). Volatiles within the target material in the excavated zone of the transient cavity can be incorporated both in the solid (i.e., clasts of ice) or liquid form (i.e., impact melt derived from melting ground-ice and/or initially liquid water). Indeed, Stewart and Ahrens (2005) showed that H_2O ice will undergo complete melting at 2.5 ± 0.1 GPa at 263 K and 4.1 ± 0.3 GPa at 100 K. In other words, the melt content of primary ejecta will be higher in regions of Mars with substantial ground-ice. Jones and Osinski (2015) developed a simple regional stratigraphic model of the subsurface (e.g., low, medium, and high viscosity layers) based on SLE and DLE variations in EM, onset diameter and the correlation between EM and diameter. They suggest a low viscosity layer buried beneath a high viscosity layer at lower latitudes, whereas, at higher latitudes a low

viscosity layer overlies a high viscosity layer. The fraction of low to high viscosity layers incorporated into the ejecta should control how mobile the ejecta will be (e.g., higher fraction of a low viscosity layer equals greater EM) (Jones and Osinski, 2015). This is generally consistent with our results. In addition, ice present on the surface may also provide a ‘frictionless’ surface (e.g., Weiss and Head, 2013) for the ballistically emplaced outer layer to glide across, which may enhance runout distance further. Ice concentrations are generally thought to be much lower near the equator and our EM values reflect this. With no ice on the surface and less volatile content in the subsurface (Madeleine et al., 2009; Clifford et al., 2010), ejecta will experience a lot more friction, which can reduce the distance it travels (i.e., EM).

2.4.2 Effect of the Target Properties on Lobateness

Early studies of ejecta lobateness found some evidence to suggest that this property varies with latitude (e.g., Johansen, 1979; Kargel, 1986); however, distinction between ejecta morphologies in these studies were not recognized. In a later study, Barlow (1994) distinguished layered ejecta into single- (SL), double- (DL), and multiple-lobed (ML) morphologies based on the number of ejecta layers yet found no such correlation of lobateness with latitude for each morphology. This author suggested that the inconsistency between studies could be attributed to varying lobateness of distinct ejecta morphologies (Barlow, 1994). We find that lobateness of both layers of DLE craters varies with latitude and is generally consistent with the very early studies over ejecta lobateness (e.g., Johansen, 1979; Kargel, 1986). The inconsistency of Barlow’s results to ours may be attributed to the small latitudinal variance of their DLE distribution (concentrated $\sim 30^\circ$ to 50° N), where similar results may be observed (Barlow, 1994). In comparison, our study DLEs range from $\sim 60^\circ$ N to 40° S, which may explain the variability observed in our lobateness values.

Johansen (1979) proposed the variation in their data was the result of impact into different volatiles (i.e., water verses ice), which subsequently affects the viscosity of the ejecta. Kargel (1986) suggested that the highly lobate ejecta observed at lower latitudes resulted from impact into water-rich targets (lower viscosity); whereas, lower lobateness at higher latitudes result from impact into ice-rich targets (higher viscosity). However,

based on thermal model predictions, if surface ice should be unstable at lower latitudes under present climatic conditions (e.g., Farmer and Doms, 1979; Clifford and Hillel, 1983; Zent et al., 1986), so too should near-surface liquid water. Craters excavating to depths of a potential liquid water reservoir seems unlikely anywhere on Mars, given current temperatures and pressures. Clifford et al. (2010) suggests that if there is indeed liquid water reservoirs on Mars, they would exceed ~3–5 km depth; well beyond the excavation depth of an average DLE crater [10 km diameter crater excavates ~0.7 km to ~1.2 km (Croft, 1985; Melosh, 1989). Note: although these equations were developed using terrestrial craters, they still factor in gravity, which affects crater diameter].

Instead, we suggest that the variation in lobateness with latitude could be related to ejecta viscosity and/or surface drag (i.e., friction). For example, viscous ejecta sliding over hard rock (e.g., basalt) would experience more friction than less viscous ejecta over loose sediment, or ice (Senft and Stewart, 2008; Weiss and Head, 2014). More friction between an ejecta layer and the target may cause an ejecta layer to split into more pronounced lobes, therefore, becoming more lobate, or sinuous. We have already established that there is more dust cover and presumably more near-surface ice at higher latitudes (Christensen, 1986; Clifford, 1993; Clifford and Parker, 2001; Head et al., 2003, 2005, 2006, 2010; Madeleine et al., 2009; Clifford et al., 2010; Souness and Hubbard, 2012), where we observe DLEs with lower lobatenesses. Impact into a target with these conditions would have less friction on an ejecta layer, allowing it to glide more easily across the surface. In addition, the abundance of volatiles at higher latitudes may produce ejecta that is very low in viscosity. This would potentially allow ejecta to extend outwards from the crater rim at roughly equal distances, resulting in less lobate (more circular) ejecta morphologies as seen in our results. In comparison, equatorial regions involved with this study are less dusty and icy, leaving hard basaltic rock as the uppermost surficial layer. Less volatile concentrations at lower latitudes may also result in ejecta that is more viscous, and may produce more friction between ejecta and the surface.

We recognize that the low-aspect ratio layered ejecta (LARLE) craters are located in areas under these same conditions (e.g., fine-grained, volatile-rich targets at higher

latitudes), yet have high observed lobateness values (1.45–4.35; 2.05 avg.) (Barlow et al., 2014; Boyce et al., 2015b). The normal layered ejecta morphology (i.e., SLE, DLE, MLE) accompanying LARLE craters, however are less lobate (SLE, 1.00 – 3.57; DLE outer layer, 1.01 – 2.27; MLE outer layer, 1.02 – 1.74 (Barlow, 2005; Barlow et al., 2014)) and are similar to results from this study. Because the emplacement mechanism for LARLE craters is proposed to be different from that of layered ejecta (driven by gravity currents rather than momentum from initial ejection) (Barlow et al., 2014; Boyce et al., 2015b), we do not compare the lobateness of LARLE craters to that of normal layered ejecta morphologies. Surface conditions (e.g., fine-grained, volatile-rich material) should affect the layered ejecta morphologies differently than the additional LARLE ejecta layers.

2.4.3 Radial Grooves

It has previously been suggested that radial grooves are characteristic of DLE morphologies (e.g., Boyce and Mouginis-Mark, 2006); however, the results from this study clearly shows that not all DLEs display this feature. Figure 11 shows that DLEs located within $\pm 25^\circ$ of the equator typically do not display grooves and that grooves are present on DLEs poleward of $\pm \sim 30^\circ$. There are, however, 5 ‘outlier’ DLEs at $\sim 40\text{--}60^\circ\text{N}$ that do not display grooves, and 3 outlier DLEs at $\sim 10^\circ\text{S}$ that do display grooves. While dust, other aeolian deposits, and/or erosion could have obscured or removed radial grooves on these outliers within the “grooved” regions, the same cannot be said for outliers within the “non-grooved” regions. Three DLEs in this band appear to have grooves present. The possibility of all these DLEs near the equator being dust covered, excluding the three outliers, is highly unlikely as they appear relatively dust free. A dust cover index (DCI) for Mars is derived from Thermal Emission Spectrometer (TES) spectral data onboard Mars Global Surveyor (MGS) and is based off of the average surface emissivity spectra spanning 1350 to 1400 cm^{-1} range (~ 7.1 to $7.4\ \mu\text{m}$) of TES spectra from fine silicate particles on the surface (i.e., dust) (Ruff and Christensen, 2002). Figure 11 shows a color-coded average ~ 1350 to $1400\ \text{cm}^{-1}$ emissivity map (i.e. DCI), where lower average emissivity over this range indicates an increased abundance of dust on the surface. Based on this, TES DCI supports our initial observations of near-

equatorial DLEs appearing relatively dust free and shows that most DLEs in this study near the equator being situated in less dusty regions compared to more northern regions (Table 3, 4, Fig. 11) (Ruff and Christensen, 2002). Observations of largely aeolian erosional features from various Martian landers and rovers infer that aeolian erosion has been the dominant erosional agent for the past ~ 3 Ga (Golombek and Bridges, 2000; Hartmann and Neukum, 2001; Greeley et al., 2004; Golombek et al., 2006) and it is possible that the lack of dust in these regions are a result of erosion. If this is the case, any grooves on ejecta would certainly not be obscured by dust but may be subject to aeolian erosion.

Table 2.3: Dust cover index (DCI) for each region.

Region	(n) DLEs	Avg. DCI	SD	Min. DCI	Max. DCI	Color
N Tharsis	44	0.94	0.009	0.93	0.97	Red–yellow
Elysium	24	0.94	0.007	0.93	0.96	Red–yellow
Syrtis Major	10	0.98	0.001	0.97	0.98	Blue–purple
S Tharsis	31	0.97	0.009	0.94	0.98	Orange–blue
Hesperia	18	0.97	0.006	0.96	0.98	Green–purple

Table 2.4: Average DCI for DLEs with grooves and without.

	Avg. DCI
Grooved DLEs	0.95
Non-grooved DLEs	0.96

Figures 10c and 10d show two DLEs located in northern Tharsis both on the same geological unit (ridged plains material) and in relatively dusty areas. These two craters are spaced $\sim 1,500$ km apart, have the same prevailing wind directions (NE – E) (based on THEMIS Day and Night IR), and are roughly at the same elevation (~ 400 m difference). One crater displays grooves (Fig. 10c), while the other does not (Fig. 10d). The DLE in Figure 10c appears to be in a region with slightly greater dust coverage (i.e., lower TES DCI) (Fig. 11) and there are aeolian bedforms on the ejecta blanket – yet the ejecta grooves are still visible. No aeolian bedforms are observed on the ejecta blanket of the DLE in Figure 10d with CTX imagery and no higher-resolution images (i.e., HiRISE) are

available for this particular DLE; any grooves present on this DLE should still be visible. If there are indeed aeolian bedforms on this ejecta blanket, it is unlikely they mantle the total ejecta blanket (area $\sim 1,700 \text{ km}^2$). These observations suggest that DLE craters with no grooves cannot just represent formerly grooved ejecta that is now buried. It is also unlikely that aeolian erosion has degraded the grooves on these craters. For example, the DLE in Figure 10b appears extensively eroded, yet the grooves are still visible. The ramparts on this DLE are also quite eroded compared to the ones in Figure 10d, which still appear to be distinctly raised. If the DLE in Figure 10d has undergone substantial erosion similar to that of the one in Figure 10b, then the ramparts should be degraded, suggesting that the crater in Figure 10d is younger or better-preserved. These observations suggest that the grooves, if present, could not have been eroded away from the ejecta blanket in Figure 10d. Thus, we propose that the absence of grooves on most “equatorial” DLEs is a primary feature that must, therefore, be linked with the emplacement process.

Based on morphological similarities to terrestrial analogs (e.g., explosion craters, explosive volcanoes), we propose that grooves on DLEs form during the impact process by a base surge-like process in which grooves are etched into ejecta layers (cf., Boyce and Mouginis-Mark, 2006; Harrison et al., 2013). Boyce and Mouginis-Mark (2006) suggest the outer layer is deposited over the inner layer during this process. In their model, material suspended in an ejecta plume falls and extends radially outwards creating a base surge, in which grooves are etched into the already emplaced inner layer. Grooves on the outer layer form simultaneously with the deposition of this layer. We favor an alternative base surge model that we first suggested in Harrison et al. (2013), where both the inner and outer layers are emplaced *before* the base surge. Experimental studies of high explosive shots into alluvium and basaltic rock have shown that target material can affect the size and density of the base surge (Knox and Rohrer, 1963; Rohrer, 1965). Results from these experiments show that an explosion into an alluvial target will produce a base surge nearly twice as large as an explosion into basaltic rock (Knox and Rohrer, 1963; Rohrer, 1965). This is dominantly due to expanding gases from vaporized water within the pore spaces of the alluvium (Knox and Rohrer, 1963; Rohrer, 1965). Based on these results, the size of a base surge could possibly explain the presence or

absence of grooves on DLEs, where larger, stronger base surges carve grooves, and smaller, weaker base surges simply don't generate enough energy to carve grooves. A simple explanation, then, would be that DLEs with grooves occur within higher volatile-content or dust-cover regions (producing a stronger surge), while DLEs without grooves occur in lower volatile-content or less dusty regions. Looking at Figure 11, not all of the grooved/non-grooved craters align this way as there are DLEs with no grooves present in dusty areas (~18%) (as discussed above). Thus, there must be an additional factor involved, or that at the time of an individual impact, the area simply was, or was not, volatile-rich or dust covered depending on the presence or absence of grooves.

As mentioned earlier, volatile concentrations on Mars presently are highest near the poles and decrease equatorward (Rossbacher and Judson, 1981; Clifford, 1993; Clifford and Parker, 2001; Clifford et al., 2010) in addition to Amazonian mid-latitude glaciation (Head et al., 2003, 2005, 2006, 2010; Madeleine et al., 2009; Souness and Hubbard, 2012). It is not known whether present conditions have persisted throughout Mars' history but it is suggested that at the time of the late Hesperian there was an inventory of water equivalent to a global ocean ~0.5 – 1 km deep of which the majority is believed to be stored as ground ice and/or water (e.g., Clifford et al., 2010). If the majority of this reservoir of ice has stayed underground throughout time, and has resided at mid- to high-latitudes (e.g., Head et al., 2005, 2006, 2010; Madeleine et al., 2009; Souness and Hubbard, 2012), it could help explain the possible role it has on the grooves observed on some DLEs. We know that solid or liquid water will sublime or evaporate, respectively, under heat and/or pressure, and that impact events generate more than enough energy to vaporize ice or liquid water (e.g., Stewart and Ahrens, 2005; Osinski et al., 2013). Impact into a volatile rich target may produce a larger base surge as compared to impact into a 'drier' target and may explain why we see grooves on DLEs at mid- to high-latitudes and not on DLEs near the equator. A larger base surge would have more energy to etch grooves into ejecta layers. This corresponds to the high concentrations of volatiles thought to reside at mid- to high-latitudes (Rossbacher and Judson, 1981; Clifford, 1993; Clifford and Parker, 2001; Head et al., 2005, 2006, 2010; Madeleine et al., 2009; Clifford et al., 2010; Souness and Hubbard, 2012) and supports our hypothesis of volatiles being an important factor controlling DLE groove formation.

2.4.4 Hesperia Planum – An Outlier?

The morphometric measurements of DLEs located in Hesperia Planum may suggest that this region is an outlier compared to other regions located at similar latitude ranges in this study. Referring back to Figures 5b, 6b, 8b, 9b, the EM distribution of Hesperia DLEs seem to be lower than what is expected based on the locality of the region (e.g., higher latitude); values should reflect those of DLEs at higher latitude regions (e.g., Elysium and northern Tharsis), yet DLEs in Hesperia are more comparable to those located in Syrtis Major and southern Tharsis (e.g., lower latitude regions). An explanation may result from Hesperia being located in the southern highlands where it is shown to be less dusty and is comparable to the amount of dust in Syrtis Major and southern Tharsis (Table 3; Fig. 11). In addition, Hesperia would be a candidate for mid-latitude glaciation given its location at a middle latitude. This is also evident from lobate debris aprons (e.g., Holt et al., 2008) found on the eastern part of the Hellas region and would suggest that there has indeed been ice in the area throughout the Amazonian (Head et al., 2003, 2005). Assuming there is a volatile variable within the Hesperia region could explain why morphometric values differ only slightly from those of Syrtis Major and southern Tharsis. The volatile variable in Syrtis Major and southern Tharsis may be less given their locations near the equator. Comparing Hesperia DLE morphometric values to northern Tharsis and Elysium values, the difference is more noticeable and may be due to the abundance of a dust and volatile variable in these two regions (Fig. 11) (Christensen, 1986; Ruff and Christensen, 2002; Head et al., 2005, 2006, 2010; Madeleine et al., 2009; Souness and Hubbard, 2012). Because Hesperia is less dusty, a volatile variable would only be applicable, while northern Tharsis and Elysium would have dust and volatiles present in abundance (e.g., Clifford et al., 2010; Head et al., 2010; Madeleine et al., 2009; Ruff and Christensen, 2002; Souness and Hubbard, 2012). Together, these observations suggest that surface and near-subsurface properties are an essential variable for morphometric properties of DLEs.

2.5 Concluding Remarks

We have shown that EM is generally higher at higher latitudes and is consistent with previous global studies (Mouginis-Mark, 1979; Costard, 1989; Barlow, 2006; Barlow et al., 2014; Jones and Osinski, 2015), while lobateness is generally higher at lower

latitudes, also consistent with previous studies (cf., Kargel, 1986). Because previous studies are global, a range of terrain types are involved, yet our results of DLEs situated solely on volcanic terrains still show that EM and lobateness varies with latitude. The general distribution of higher EM values at higher latitudes and lower values at lower latitudes correlates well with the concentrations of volatiles throughout the whole planet. However, this distribution is not conclusive enough to say that volatiles are the sole variable contributing to ejecta morphometry, as we would expect a simple trend of increasing EM correlated *well* with increasing latitude. Because of this, factors affecting DLE morphometric parameters are likely much more complex than solely volatile content. Furthermore, the very fact that DLEs are found at the equator where there are less volatile concentrations suggests that little volatile content is needed to form a DLE morphology. We suggest that the interaction of ejecta with the surface is a major factor causing the EM and lobateness variations that we see with latitude. High-concentrations of surface dust may aid in the enhanced mobility of ejecta and act as a low friction layer between ejecta and volcanic rock. In addition, impact into a target with a greater abundance of volatiles will create less viscous ejecta, resulting in less friction between ejecta and the surface. Surface drag plus a higher ejecta viscosity in lower volatile targets (e.g., volcanic rock) may also affect morphometric parameters, producing more friction between the ejecta-target interface.

A result and critical observation of this study is that not all DLEs display radial grooves. Even though the “radial groove” attribute of a “double-layered-ejecta” crater has been considered a diagnostic property, we recognize that some DLEs (predominantly $\pm 25^\circ$ equatorward) do not have grooves present, yet still display two distinct layers of ejecta. Current data suggest that the lack of grooves on some DLEs are not due to any erosional or other secondary process, and that the presence or absence of grooves is a primary feature. These craters all conform to the definition of a DLE crater so we propose that the presence of grooves should not be used as a diagnostic criterion for the identification and classification of DLE craters.

Returning to the recent suggestion that there are two distinct types of DLEs each with different emplacement mechanisms (Barlow, 2015b), we have not found any evidence to

support this proposition in our study. We see no systematic variation in morphology that warrants a sub-classification of the DLE morphology into two distinct groups. Instead, we suggest that there is a continuum of DLE morphologies with differences being due to a number of target factors as described herein (e.g., surficial sediments, dust, volatiles) and not because there are two different types with different emplacement mechanisms.

2.6 References

- Baloga, S.M., Fagents, S.A., Mouginis-Mark, P.J., 2005. Emplacement of Martian rampart crater deposits. *J. Geophys. Res.* 110. doi:10.1029/2004JE002338.
- Barlow, N.G., 1988. Crater size-frequency distributions and a revised Martian relative chronology. *Icarus* 75, 285–305. doi:10.1016/0019-1035(88)90006-1.
- Barlow, N.G., 1994. Sinuosity of Martian rampart ejecta deposits. *J. Geophys. Res.* 99, 10927 – 10935. doi:10.1029/94JE00636.
- Barlow, N.G., 2004. Martian subsurface volatile concentrations as a function of time: Clues from layered ejecta craters. *Geophys. Res. Lett.* 31, L05703. doi:10.1029/2003GL019075.
- Barlow, N.G., 2005. A review of Martian impact crater ejecta structures and their implications for target properties, in: Kenkmann, T., Hörz, F., Deutsch, A. (Eds.), *Large Meteorite Impacts III*, *Geol. Soc. Am. Spec. Pap.* 384. pp. 433 – 442.
- Barlow, N.G., 2006. Impact craters in the northern hemisphere of Mars: Layered ejecta and central pit characteristics. *Meteorit. Planet. Sci.* 41, 1425–1436. doi:10.1111/j.1945-5100.2006.tb00427.x.
- Barlow, N.G., 2015a. Characteristics of impact craters in the northern hemisphere of Mars. *Large Meteor. Impacts Planet. Evol.* V, *Geol. Soc. Am. Spec. Pap.* 518.
- Barlow, N.G., 2015b. Sizes and distributions of the two morphologic types of double layer ejecta craters in the northern hemisphere of Mars. *Lunar Planet. Sci. Conf. XLIV Abstract #2216*.

- Barlow, N.G., Bradley, T.L., 1990. Martian impact craters: Correlations of ejecta and interior morphologies with diameter, latitude, and terrain. *Icarus* 87, 156–179.
- Barlow, N.G., Perez, C.B., 2003. Martian impact crater ejecta morphologies as indicators of the distribution of subsurface volatiles. *J. Geophys. Res.* 108, 5085. doi:10.1029/2002JE002036.
- Barlow, N.G., Boyce, J.M., 2015. Criteria for distinguishing between the two types of double layer ejecta (DLE) craters on Mars. 6th Planet. Crater Consort. Meet. Abstract #1512.
- Barlow, N.G., Boyce, J.M., Costard, F.M., Craddock, R.A., Garvin, J.B., Sakimoto, S.E.H., Kuzmin, R.O., Roddy, D.J., Soderblom, L.A., 2000. Standardizing the nomenclature of Martian impact crater ejecta morphologies. *J. Geophys. Res.* 105, 26733 – 26738.
- Barlow, N.G., Boyce, J.M., Cornwall, C., 2014. Martian Low-Aspect-Ratio Layered Ejecta (LARLE) craters: Distribution, characteristics, and relationship to pedestal craters. *Icarus* 239, 186–200. doi:10.1016/j.icarus.2014.05.037.
- Barnouin-Jha, O.S., Schultz, P.H., 1998. Lobateness of impact ejecta deposits from atmospheric interactions. *J. Geophys. Res.* 103, 25739 – 25756.
- Barnouin-Jha, O.S., Schultz, P.H., Lever, J.H., 1999a. Investigating the interactions between an atmosphere and an ejecta curtain 1. Wind tunnel tests. *J. Geophys. Res.* 104, 27105–27115.
- Barnouin-Jha, O.S., Schultz, P.H., Lever, J.H., 1999b. Investigating the interactions between an atmosphere and an ejecta curtain 2. Numerical experiments. *J. Geophys. Res.* 104, 27117–27131.
- Barnouin-Jha, O.S., Baloga, S., Glaze, L., 2005. Comparing landslides to fluidized crater ejecta on Mars. *J. Geophys. Res.* 110. doi:10.1029/2003JE002214.

- Boyce, J.M., Mouginis-Mark, P.J., 2006. Martian craters viewed by the Thermal Emission Imaging System instrument: Double-layered ejecta craters. *J. Geophys. Res.* 111. doi:10.1029/2005JE002638.
- Boyce, J.M., Barlow, N.G., Mouginis-Mark, P.J., Stewart, S., 2010. Rampart craters on Ganymede: Their implications for fluidized ejecta emplacement. *Meteorit. Planet. Sci.* 45, 638–661. doi:10.1111/j.1945-5100.2010.01044.x.
- Boyce, J.M., Mouginis-Mark, P.J., Wilson, L., 2015a. Flow features on Martian layered ejecta. *Lunar Planet. Sci. Conf. XLVI Abstract #1043*. doi:10.102/2004JE00233.
- Boyce, J.M., Wilson, L., Barlow, N.G., 2015b. Origin of the outer layer of martian low-aspect ratio layered ejecta craters. *Icarus* 245, 263–272. doi:10.1016/j.icarus.2014.07.032.
- Boyce, J.M., Barlow, N.G., Mouginis-Mark, P.J., 2015c. Morphometric evidence for two types of double layer ejecta (DLE) craters. 6th Planet. Crater Consort. Meet. Abstract #1507.
- Bridges, N.T., Banks, M.E., Beyer, R.A., Chuang, F.C., Noe Dobrea, E.Z., Herkenhoff, K.E., Keszthelyi, L.P., Fishbaugh, K.E., McEwen, A.S., Michaels, T.I., Thomson, B.J., Wray, J.J., 2010. Aeolian bedforms, yardangs, and indurated surfaces in the Tharsis Montes as seen by the HiRISE Camera: Evidence for dust aggregates. *Icarus* 205, 165–182. doi:10.1016/j.icarus.2009.05.017.
- Byrne, S., Dundas, C.M., Kennedy, M.R., Mellon, M.T., Mcewen, A.S., Cull, S.C., Daubar, I.J., Shean, D.E., Seelos, K.D., Murchie, S.L., Cantor, B.A., Arvidson, R.E., Edgett, K.S., Reufer, A., Thomas, N., Harrison, T.N., Posiolova, L. V., Seelos, F.P., 2009. Distribution of mid-latitude ground ice on Mars from new impact craters. *Science* (80-.). 325, 1674–1676.
- Carr, M.H., 1986. Mars: A water-rich planet? *Icarus* 68, 187–216. doi:10.1016/0019-1035(86)90019-9.

- Carr, M.H., Head, J.W., 2010. Geologic history of Mars. *Earth Planet. Sci. Lett.* 294, 185–203. doi:10.1016/j.epsl.2009.06.042.
- Carr, M.H., Crumpler, L.S., Cutts, J.A., Greeley, R., Guest, J.E., Masursky, H., 1977. Martian impact craters and emplacement of ejecta by surface flow. *J. Geophys. Res.* 82, 4055–4065. doi:10.1029/JS082i028p04055.
- Cattermole, P., 1990. Volcanic flow development at Alba Patera, Mars. *Icarus* 83, 453–493. doi:10.1016/0019-1035(90)90079-O.
- Christensen, P.R., 1986. Regional dust deposits on Mars: Physical properties, age, and history. *J. Geophys. Res.* 91, 3533 – 3545. doi:10.1029/JB091iB03p03533.
- Christensen, P.R., Jakosky, B.M., Kieffer, H.H., Malin, M.C., Mcswen, H.Y., Neelson, K., Mehall, G.L., Silverman, S.H., Ferry, S., Caplinger, M., Ravine, M., 2004. The thermal emission imaging system (THEMIS) for the Mars 2001 Odyssey mission. *Space Sci. Rev.* 110, 85–130.
- Christensen, P.R., Engle, E., Anwar, S., Dickenshied, S., Noss, D., Gorelick, N., Weiss-Malik, M., 2009. JMARS - A planetary GIS. AGU Fall Meet. Abstract #IN22A-06.
- Clifford, S.M., 1993. A model for the hydrologic and climatic behavior of water on Mars. *J. Geophys. Res.* 98, 10973–11016. doi:10.1029/93JE00225.
- Clifford, S.M., Hillel, D., 1983. The stability of ground ice in the equatorial region of Mars. *J. Geophys. Res.* 88, 2456–2474. doi:10.1029/JB088iB03p02456.
- Clifford, S.M., Parker, T.J., 2001. The evolution of the Martian hydrosphere: Implications for the fate of a primordial ocean and the current state of the northern plains. *Icarus* 154, 40–79. doi:10.1006/icar.2001.6671.
- Clifford, S.M., Lasue, J., Heggy, E., Boisson, J., McGovern, P., Max, M.D., 2010. Depth of the Martian cryosphere: Revised estimates and implications for the existence and detection of subpermafrost groundwater. *J. Geophys. Res.* 115. doi:10.1029/2009JE003462.

- Costard, F.M., 1989. The spatial distribution of volatiles in the Martian hydrolithosphere. *Earth. Moon. Planets* 45, 265–290.
- Croft, S.K., 1985. The scaling of complex craters. *J. Geophys. Res.* 90, C828 – C842.
- Crown, D.A., Price, K.H., Greeley, R., 1992. Geologic evolution of the east rim of the Hellas basin, Mars. *Icarus* 100, 1–25. doi:10.1016/0019-1035(92)90014-X.
- Davis, P.A., Golombek, M.P., 1990. Discontinuities in the shallow Martian crust at Lunae, Syria, and Sinai Plana. *J. Geophys. Res.* 95, 14231–14248. doi:10.1029/JB095iB09p14231.
- Dundas, C.M., Byrne, S., 2010. Modeling sublimation of ice exposed by new impacts in the martian mid-latitudes. *Icarus* 206, 716–728. doi:10.1016/j.icarus.2009.09.007.
- Edwards, C.S., Nowicki, K.J., Christensen, P.R., Hill, J., Gorelick, N., Murray, K., 2011. Mosaicking of global planetary image datasets: 1. Techniques and data processing for Thermal Emission Imaging System (THEMIS) multi-spectral data. *J. Geophys. Res.* 116, E10008. doi:10.1029/2010JE003755.
- Fanale, F.P., 1976. Martian volatiles: Their degassing history and geochemical fate. *Icarus* 28, 179–202.
- Farmer, C.B., Doms, P.E., 1979. Global seasonal variation of water vapor on Mars and the implications for permafrost. *J. Geophys. Res.* 84, 2881–2888.
- Fenton, L.K., Richardson, M.I., 2001. Martian surface winds: Insensitivity to orbital changes and implications for aeolian processes. *J. Geophys. Res.* 106, 32885–32902. doi:10.1029/2000JE001407.
- Gault, D.E., Greeley, R., 1978. Exploratory experiments of impact craters formed in viscous-liquid targets: Analogs for Martian rampart craters? *Icarus* 34, 486–495. doi:10.1016/0019-1035(78)90040-4.

- Golombek, M.P., Bridges, N.T., 2000. Erosion rates on Mars and implications for climate change: Constraints from the Pathfinder landing site. *J. Geophys. Res.* 105, 1841–1853.
- Golombek, M.P., Grant, J.A., Crumpler, L.S., Greeley, R., Arvidson, R.E., Bell, J.F., Weitz, C.M., Sullivan, R., Christensen, P.R., Soderblom, L.A., Squyres, S.W., 2006. Erosion rates at the Mars Exploration Rover landing sites and long-term climate change on Mars. *J. Geophys. Res.* 111. doi:10.1029/2006JE002754.
- Greeley, R., Guest, J.E., 1987. Geologic map of the eastern equatorial region of Mars (1:15,000,000). USGS Misc. Inv. Ser. Map I-1802-B.
- Greeley, R., Crown, D.A., 1990. Volcanic geology of Tyrrhena Patera, Mars. *J. Geophys. Res.* 95, 7133–7149.
- Greeley, R., Squyres, S.W., Arvidson, R.E., Bartlett, P., Bell, J.F., Blaney, D., Cabrol, N.A., Farmer, J., Farrand, B., Golombek, M.P., Gorevan, S.P., Grant, J.A., Haldemann, A.F.C., Herkenhoff, K.E., Johnson, J., Landis, G., Madsen, M.B., McLennan, S.M., Moersch, J., Rice, J.W., Richter, L., Ruff, S., Sullivan, R.J., Thompson, S.D., Wang, A., Weitz, C.M., Whelley, P., 2004. Wind-related processes detected by the Spirit Rover at Gusev Crater, Mars. *Science* (80-.). 305, 810–821. doi:10.1126/science.1100108.
- Gregg, T.K.P., Farley, M.A., 2006. Mafic pyroclastic flows at Tyrrhena Patera, Mars: Constraints from observations and models. *J. Volcanol. Geotherm. Res.* 155, 81–89. doi:10.1016/j.jvolgeores.2006.02.008.
- Gwinner, K., Scholten, F., Spiegel, M., Schmidt, R., Giese, B., Oberst, J., Heipke, C., Jaumann, R., Neukum, G., 2009. Derivation and validation of high-resolution digital terrain models from Mars Express HRSC data. *Photogramm. Eng. Remote Sens.* 75, 1127–1142. doi:10.14358/PERS.75.9.1127.
- Harrison, T.N., Tornabene, L.L., Osinski, G.R., 2013. Emplacement chronology of double layer crater ejecta on Mars. *Lunar Planet. Sci. Conf. XLIV Abstract #1702.*

- Hartmann, W.K., Berman, D.C., 2000. Elysium Planitia lava flows: Crater count chronology and geological implications. *J. Geophys. Res.* 105, 15011 – 15025.
- Hartmann, W.K., Neukum, G., 2001. Cratering chronology and the evolution of Mars. *Space Sci. Rev.* 96, 165–194.
- Head, J.W., Mustard, J.F., Kreslavsky, M.A., Milliken, R.E., Marchant, D.R., 2003. Recent ice ages on Mars. *Nature* 426, 797–802. doi:10.1038/nature02114.
- Head, J.W., Neukum, G., Jaumann, R., Hiesinger, H., Hauber, E., Carr, M.H., Masson, P., Foing, B., Hoffmann, H., Kreslavsky, M., Werner, S., Milkovich, S., van Gasselt, S., 2005. Tropical to mid-latitude snow and ice accumulation, flow and glaciation on Mars. *Nature* 434, 346–351.
- Head, J.W., Marchant, D.R., Agnew, M.C., Fassett, C.I., Kreslavsky, M.A., 2006. Extensive valley glacier deposits in the northern mid-latitudes of Mars: Evidence for Late Amazonian obliquity-driven climate change. *Earth Planet. Sci. Lett.* 241, 663–671. doi:10.1016/j.epsl.2005.11.016.
- Head, J.W., Marchant, D.R., Dickson, J.L., Kress, A.M., Baker, D.M., 2010. Northern mid-latitude glaciation in the Late Amazonian period of Mars: Criteria for the recognition of debris-covered glacier and valley glacier landsystem deposits. *Earth Planet. Sci. Lett.* 294, 306–320. doi:10.1016/j.epsl.2009.06.041.
- Hiesinger, H., Head, J.W., 2004. The Syrtis Major volcanic province, Mars: Synthesis from Mars Global Surveyor data. *J. Geophys. Res.* 109, E01004. doi:10.1029/2003JE002143.
- Hill, J., Edwards, C.S., Christensen, P.R., 2014. Mapping the Martian surface with THEMIS global infrared mosaics. Eighth Int. Conf. Mars, Abstract #1141.
- Holt, J.W., Safaeinili, A., Plaut, J.J., Head, J.W., Phillips, R.J., Seu, R., Kempf, S.D., Choudhary, P., Young, D.A., Putzig, N.E., Biccari, D., Gim, Y., 2008. Radar sounding evidence for buried glaciers in the southern mid-latitudes of Mars. *Science* (80-.). 322, 1235–1238.

- Horner, V.M., Greeley, R., 1982. Pedestal craters on Ganymede. *Icarus* 51, 549–562. doi:10.1016/0019-1035(82)90145-2.
- Hörz, F., Ostertag, R., Rainey, D.A., 1983. Bunte Breccia of the Ries: Continuous deposits of large impact craters. *Rev. Geophys. Sp. Phys.* 21, 1667–1725.
- Iverson, R.M., LaHusen, R.G., 1993. Friction in Debris Flows: Inferences from Large-scale Flume Experiments. in: *Hydraulic Engineering (1993)*. Hsieh Wen Shen, S.T. Su, Feng Wen (eds). Proc. 1993 Conf., San Fr. CA, July 25-30, 1993. *Am. Soc. Civ. Eng.* 1604–1609.
- Johansen, L.A., 1979. The latitude dependence of Martian splosted cratering and its relationship to water. *Rep. Planet. Geol. Prog. 1978-1979*, NASA Tech. Memo., 80339 123–125.
- Jones, E., Osinski, G.R., 2015. Using martian single and double layered ejecta craters to probe subsurface stratigraphy. *Icarus* 247, 260–278. doi:10.1016/j.icarus.2014.10.016.
- Kargel, J.S., 1986. Morphologic variations of Martian rampart crater ejecta and their dependencies and implications. *Lunar Planet. Sci.* XVII 410–411.
- Kargel, J.S., 1989. First and second-order equatorial symmetry of Martian rampart crater ejecta morphologies. *Fourth Int. Conf. Mars* 132–133.
- Keszthelyi, L., Jaeger, W., McEwen, A., Tornabene, L., Beyer, R.A., Dundas, C., Milazzo, M., 2008. High resolution imaging science experiment (HiRISE) images of volcanic terrains from the first 6 months of the Mars reconnaissance orbiter primary science phase. *J. Geophys. Res.* 113, E04005. doi:10.1029/2007JE002968.
- Knox, J.B., Rohrer, R., 1963. Base surge analysis: Project Pre-Buggy. Lawrence Radiat. Lab. Livermore PNE–304.

- Komatsu, G., Ori, G.G., Di Lorenzo, S., Rossi, A.P., Neukum, G., 2007. Combinations of processes responsible for Martian impact crater “layered ejecta structures” emplacement. *J. Geophys. Res.* 112. doi:10.1029/2006JE002787.
- Laskar, J., Correia, A.C.M., Gastineau, M., Joutel, F., Levrard, B., Robutel, P., 2004. Long term evolution and chaotic diffusion of the insolation quantities of Mars. *Icarus* 170, 343–364. doi:10.1016/j.icarus.2004.04.005.
- Li, L., Yue, Z., Di, K., Peng, M., 2015. Observations of Martian layered ejecta craters and constraints on their formation mechanisms. *Meteorit. Planet. Sci.* 50, 508–522. doi:10.1111/maps.12438.
- MacKinnon, D.J., Tanaka, K.L., 1988. A two-layer hydrologic model for the impacted Martian crust. *Lunar Planet. Sci. Conf. XIX* 707–708.
- Madeleine, J.-B., Forget, F., Head, J.W., Levrard, B., Montmessin, F., Millour, E., 2009. Amazonian northern mid-latitude glaciation on Mars: A proposed climate scenario. *Icarus* 203, 390–405. doi:10.1016/j.icarus.2009.04.037.
- Malin, M.C., Bell, J.F., Cantor, B.A., Caplinger, M.A., Calvin, W.M., Clancy, R.T., Edgett, K.S., Edwards, L., Haberle, R.M., James, P.B., Lee, S.W., Ravine, M.A., Thomas, P.C., Wolff, M.J., 2007. Context Camera Investigation on board the Mars Reconnaissance Orbiter. *J. Geophys. Res.* 112, E05S04. doi:10.1029/2006JE002808.
- McCauley, J.F., 1973. Mariner 9 evidence for wind erosion in the equatorial and mid-latitude regions of Mars. *J. Geophys. Res.* 78, 4123–4137. doi:10.1029/JB078i020p04123.
- Melosh, H.J., 1989. *Impact Cratering: A Geologic Process*. Oxford University Press, 245 p.
- Mouginis-Mark, P.J., 1979. Martian fluidized crater morphology: Variations with crater size, latitude, altitude, and target material. *J. Geophys. Res.* 84, 8011 – 8022. doi:10.1029/JB084iB14p08011.

- Mouginis-Mark, P.J., 1981. Ejecta emplacement and modes of formation of Martian fluidized ejecta craters. *Icarus* 45, 60–76. doi:10.1016/0019-1035(81)90006-3.
- Mouginis-Mark, P.J., 1987. Water or ice in the Martian regolith?: Clues from rampart craters seen at very high resolution. *Icarus* 71, 268–286. doi:10.1016/0019-1035(87)90152-7.
- Mouginis-Mark, P.J., Boyce, J.M., 2004. The unique characteristics of double layered ejecta craters on Mars. *Eos Trans. AGU*, 85, Fall Meet. Suppl., Abstract #P33B–04.
- Murray, B.C., Ward, W.R., Yeung, S.C., 1973. Periodic Insolation Variations on Mars. *Science* (80-.). 180, 638–640.
- Mustard, J.F., Erard, S., Bibring, J.-P., Head, J.W., Hurtrez, S., Langevin, Y., Pieters, C.M., Sotin, C.J., 1993. The surface of Syrtis Major: Composition of the volcanic substrate and mixing with altered dust and soil. *J. Geophys. Res.* 98, 3387 – 3400. doi:10.1029/92JE02682.
- Neukum, G., Jaumann, R., Team, the H.C.-I., Team, the H.E., 2004. The High Resolution Stereo Camera of Mars Express. *ESA Spec. Publ. SP-1240*, 1–19.
- Oberbeck, V.R., 1975. The role of ballistic erosion and sedimentation in Lunar stratigraphy. *Rev. Geophys. Sp. Phys.* 13, 337–362.
- Oberbeck, V.R., 2009. Layered ejecta craters and the early water/ice aquifer on Mars. *Meteorit. Planet. Sci.* 44, 43–54. doi:10.1111/j.1945-5100.2009.tb00716.x.
- Osinski, G.R., 2006. Effect of volatiles and target lithology on the generation and emplacement of impact crater fill and ejecta deposits on Mars. *Meteorit. Planet. Sci.* 41, 1571–1586. doi:10.1111/j.1945-5100.2006.tb00436.x.
- Osinski, G.R., Tornabene, L.L., Grieve, R.A.F., 2011. Impact ejecta emplacement on terrestrial planets. *Earth Planet. Sci. Lett.* 310, 167–181. doi:10.1016/j.epsl.2011.08.012.

- Osinski, G.R., Grieve, R.A.F., Tornabene, L.L., 2013. Excavation and impact ejecta emplacement, in: Osinski, G.R., Pierazzo, E. (Eds.), *Impact Cratering: Processes and Products*. pp. 43–59.
- Platz, T., Michael, G., 2011. Eruption history of the Elysium Volcanic Province, Mars. *Earth Planet. Sci. Lett.* 312, 140–151. doi:10.1016/j.epsl.2011.10.001.
- Robbins, S.J., Hynek, B.M., 2012. A new global database of Mars impact craters ≥ 1 km: 1. Database creation, properties, and parameters. *J. Geophys. Res.* 117. doi:10.1029/2011JE003966.
- Rodine, J.D., 1974. Analysis of mobilization of debris flows (PhD Thesis). Stanford University.
- Rohrer, R., 1965. Base surge and cloud formation: Project pre-Schooner. Lawrence Radiat. Lab. Livermore.
- Rossbacher, L.A., Judson, S., 1981. Ground ice on Mars: Inventory, distribution, and resulting landforms. *Icarus* 45, 39–59. doi:10.1016/0019-1035(81)90005-1.
- Ruff, S.W., Christensen, P.R., 2002. Bright and dark regions on Mars: Particle size and mineralogical characteristics based on Thermal Emission Spectrometer data. *J. Geophys. Res.* 107, 5127. doi:10.1029/2001JE001580.
- Schaber, G.G., 1982. Syrtis Major: A Low-Relief Volcanic Shield. *J. Geophys. Res.* 87, 9852–9866.
- Schneeberger, D.M., Pieri, D.C., 1991. Geomorphology and stratigraphy of Alba Patera, Mars. *J. Geophys. Res.* 96, 1907–1930.
- Schultz, P.H., 1992. Atmospheric effects on ejecta emplacement. *J. Geophys. Res.* 97, 11623–11662. doi:10.1029/92JE00613.
- Schultz, P.H., Gault, D.E., 1979. Atmospheric effects on martian ejecta emplacement. *J. Geophys. Res.* 84, 7669–7687.

- Scott, D.H., Tanaka, K.L., 1986. Geologic map of the western equatorial region of Mars (1:15,000,000). USGS Misc. Inv. Ser. Map I-1802-A.
- Senft, L.E., Stewart, S.T., 2008. Impact crater formation in icy layered terrains on Mars. *Meteorit. Planet. Sci.* 43, 1993–2013. doi:10.1111/j.1945-5100.2008.tb00657.x.
- Skinner, J.A., Hare, T.M., Tanaka, K.L., 2006. Digital renovation of the atlas of Mars 1:15,000,000-scale global geologic series maps. *Lunar Planet. Sci.* XXXVII, Abstract #2331.
- Smith, P.H., Tamppari, L.K., Arvidson, R.E., Bass, D., Blaney, D., Boynton, W. V., Carswell, A., Catling, D.C., Clark, B.C., Duck, T., DeJong, E., Fisher, D., Goetz, W., Gunnlaugsson, H.P., Hecht, M.H., Hipkin, V., Hoffman, J., Hviid, S.F., Keller, H.U., Kounaves, S.P., Lange, C.F., Lemmon, M.T., Madsen, M.B., Markiewicz, W.J., Marshall, J., McKay, C.P., Mellon, M.T., Ming, D.W., Morris, R. V., Pike, W.T., Renno, N., Stauffer, U., Stoker, C., Taylor, P., Whiteway, J.A., Zent, A.P., 2009. Water at the Phoenix Landing Site. *Science* (80-.). 58, 58–61. doi:10.1126/science.1172339.
- Souness, C., Hubbard, B., 2012. Mid-latitude glaciation on Mars. *Prog. Phys. Geogr.* 36, 238–261. doi:10.1177/0309133312436570.
- Stewart, S.T., Ahrens, T.J., 2005. Shock properties of H₂O ice. *J. Geophys. Res.* 110, E03005. doi:10.1029/2004JE002305.
- Tanaka, K.L., Skinner, J.A., Dohm, J.M., Irwin, R.P., Kolb, E.J., Fortezzo, C.M., Platz, T., Michael, G.G., Hare, T.M., 2014. Geologic map of Mars (1:20,000,000). USGS Sci. Investig. Map 3292.
- Wada, K., Barnouin-Jha, O.S., 2006. The formation of fluidized ejecta on Mars by granular flows. *Meteorit. Planet. Sci.* 41, 1551–1569. doi:10.1111/j.1945-5100.2006.tb00435.x.
- Weiss, D.K., Head, J.W., 2013. Formation of double-layered ejecta craters on Mars: A glacial substrate model. *Geophys. Res. Lett.* 40, 3819–3824. doi:10.1002/grl.50778.

- Weiss, D.K., Head, J.W., 2014. Ejecta mobility of layered ejecta craters on Mars: Assessing the influence of snow and ice deposits. *Icarus* 233, 131–146. doi:10.1016/j.icarus.2014.01.038.
- Wohletz, K.H., Sheridan, M.F., 1983. Martian Rampart Crater Ejecta: Experiments and Analysis of Melt-Water Interaction. *Icarus* 37, 15–37.
- Wulf, G., Kenkmann, T., 2015. High-resolution studies of double-layered ejecta craters: Morphology, inherent structure, and a phenomenological formation model. *Meteorit. Planet. Sci.* 1–31. doi:10.1111/maps.12416.
- Zent, A.P., Fanale, F.P., Salvail, J.R., Postawko, S.E., 1986. Distribution and state of H₂O in the high-latitude shallow subsurface of Mars. *Icarus* 67, 19–36.

Chapter 3

3 A Morphometric Comparison of Martian Double Layered Ejecta Craters and Implications for the Effect of Target Lithology

3.1 Introduction

Layered ejecta is the dominant type of ejecta morphology surrounding craters ≥ 5 km in diameter on Mars (Barlow, 1988, 2007). These include single- (SLE), double- (DLE), and multiple- (MLE) layered ejecta morphologies (Barlow et al., 2000) and are considered to have been emplaced via ground hugging flow (Carr et al., 1977; Mouginis-Mark, 1979, 1981; Baloga et al., 2005; Komatsu et al., 2007). Volatile content within (or on) the target (Carr et al., 1977; Gault and Greeley, 1978; Mouginis-Mark, 1981, 1987; Wohletz and Sheridan, 1983; Costard, 1989; Barlow and Bradley, 1990; Barlow and Perez, 2003; Barlow, 2005; Osinski, 2006; Boyce and Mouginis-Mark, 2006; Komatsu et al., 2007; Oberbeck, 2009) and/or atmosphere (Schultz and Gault, 1979; Schultz, 1992; Barnouin-Jha and Schultz, 1998; Barnouin-Jha et al., 1999a, 1999b) is generally recognized as the dominant variable enhancing mobility during emplacement, though it has also been suggested that the presence of unconsolidated surface materials may aid in mobility as well (Osinski, 2006; Osinski et al., 2011). Previous studies have shown that ejecta mobility (the distance ejecta travels from the crater rim divided by radius) increases with increasing latitude (Mouginis-Mark, 1979; Costard, 1989; Li et al., 2015; Jones and Osinski, 2015; Chapter 2) and appears to largely reflect volatile concentrations on Mars (e.g., Rossbacher and Judson, 1981; Clifford, 1993; Clifford and Parker, 2001; Clifford et al., 2010). Other studies have shown that lobateness (sinuosity of ejecta) is greater at lower latitudes and less at higher latitudes (Kargel, 1986). One question that has yet to be addressed is: Does the bulk target lithology also play a role? Here, we aim to determine whether the bulk target lithology has any effect on morphometric properties by comparing and contrasting the morphologic and morphometric properties of DLEs situated into volcanic targets and sedimentary targets.

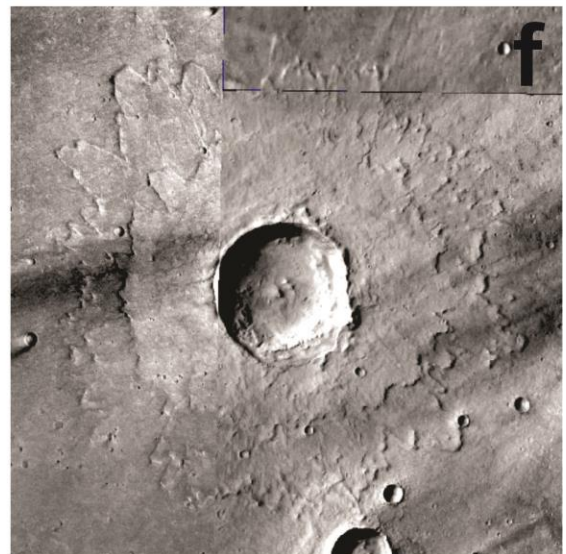
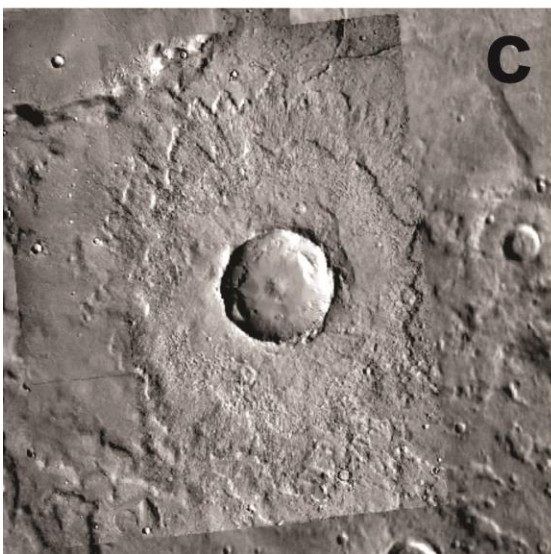
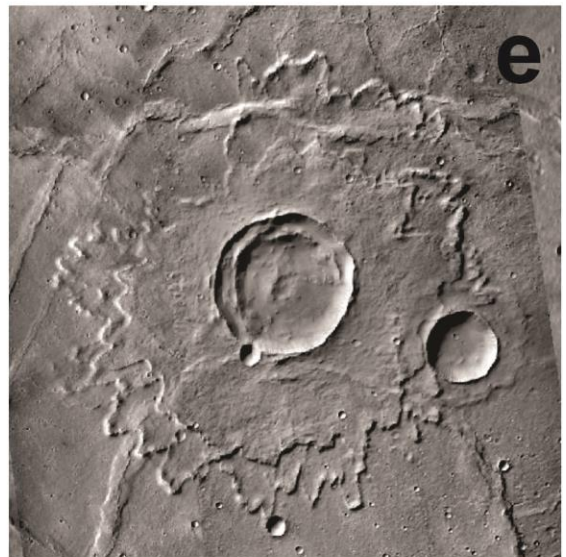
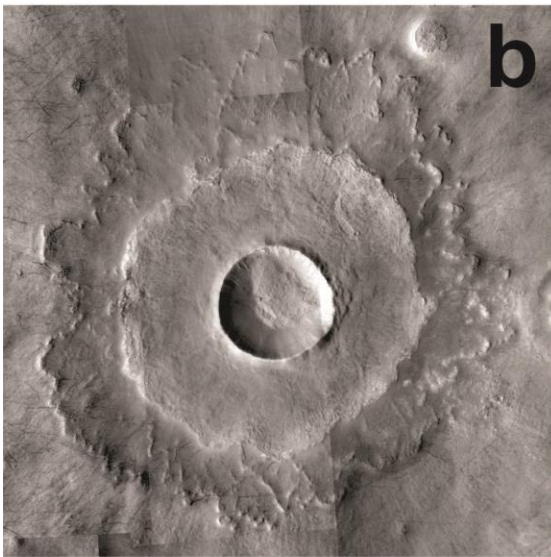
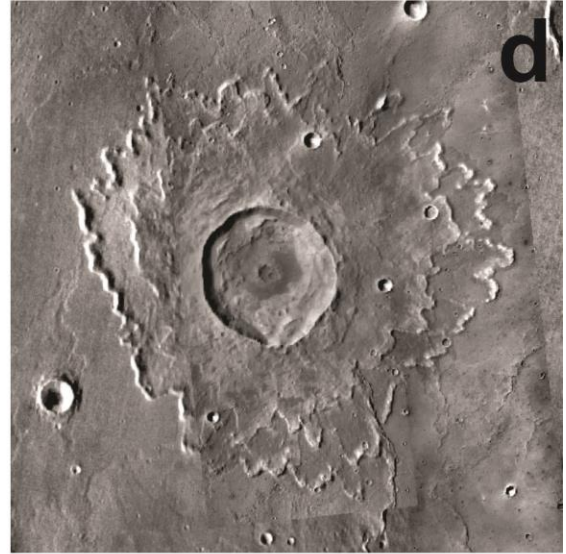
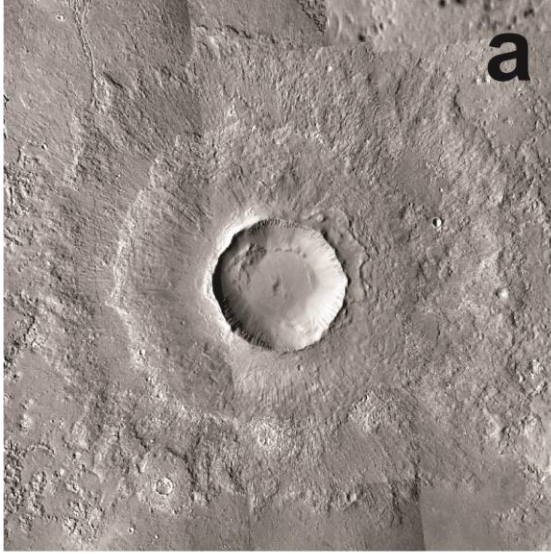


Figure 3.1: Examples of non-volcanic (a, b, c) and volcanic (d, e, f) DLEs. (a) 12.2 km diameter crater located at 120.53° E, 34.71°N; CTX mosaic: D04_028863_2145_XN_34N239W, D15_033122_2158_XN_35N239W, P20_008833_2149_XN_34N239W, G22_026964_2131_XN_33N239W, G20_025975_2135_XN_33N288W. (b) 10.7 km diameter crater located at 95.71° E, 57.00° N; CTX mosaic: D21_035549_2381_XN_58N265W, D22_035694_2379_XN_57N263W, G01_018420_2372_XN_57N264W, P16_007344_2382_XN_58N264W. (c) 10.8 km diameter crater located at 308.86° E, 42.54° N; CTX mosaic: B02_010527_2228_XN_42N051W, B17_016118_2250_XN_45N051W. (d) 16.7 km diameter crater located at 296.50° E, 6.81° N; CTX mosaic: B02_010554_1869_XN_06N063W, G22_026628_1876_XN_07N063W. (e) 14.8 km diameter crater located at 119.51° E, 23.24° S; CTX mosaic: B20_017312_1564_XN_23S240W, B18_016745_1551_XN_24S240W, B09_013066_1565_XN_23S240W. (f) 14.7 km diameter crater located at 75.47° E, 9.61° N; HRSC image ID: H0232_0000; H3025_0000.

3.2 Methodology

We have reevaluated the DLEs in Robbins Crater Database (3413 craters ≥ 1 km in diameter) to compile our own database of 1345 DLEs ~ 2 –25 km in diameter (see Chapter 2). Classification of DLEs in our database are based on the original definition of a “DLE” (Barlow et al., 2000), which includes any crater that clearly displays two distinct layers of ejecta. Data was then superposed onto the geologic map of Mars (USGS I-1802-A and -B) (Scott and Tanaka, 1986; Greeley and Guest, 1987; Skinner et al., 2006), where we select 79 DLEs situated on what is largely interpreted as sedimentary material and grouped into 3 regions (Acidalia/Chryse, Utopia, and Arcadia Planitiae) based on location (Fig. 2; Tables 1 and 2). DLEs in the Highlands were not considered because these targets are highly degraded, complex admixtures of impact, sedimentary, and volcanic rock (Tanaka et al., 2014). We also utilize the data from our previous work on DLEs on volcanic terrains (127 total) (Chapter 2). These were also grouped into regions based on location: Northern and southern Tharsis, Elysium, Syrtis Major, and Hesperia

Planum (Tables 1 and 2) (Chapter 2). We also note that the older geologic map of Mars (USGS I-1802-A and -B) (Scott and Tanaka, 1986; Greeley and Guest, 1987; Skinner et al., 2006) was chosen over the newer map (USGS SIM 3292) (Tanaka et al., 2014), because units were previously mapped in more detail (1:15M compared to 1:20M).

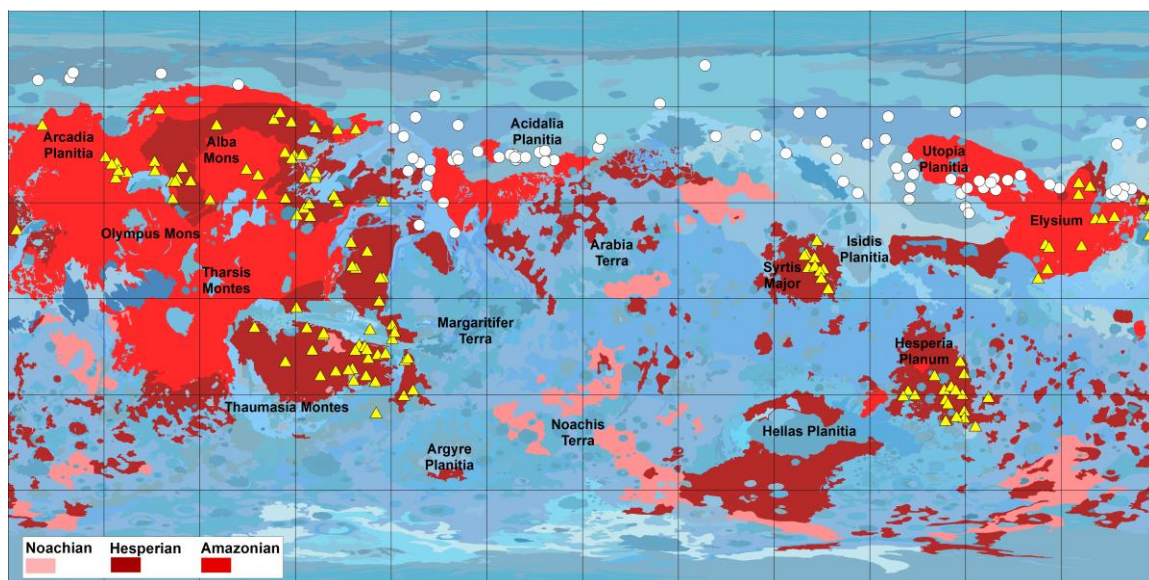


Figure 3.2: Geologic map of Mars modified after Scott and Tanaka (1986), Greeley and Guest (1987), and digitized into ArcGIS by Skinner et al. (2006). Shades of red are interpreted as largely volcanic terrains while blues represent non-volcanic terrains. DLEs are plotted as white circles (non-volcanic) and yellow triangles (volcanic). Though there are some lava flows within Utopia Planitia, we consider it largely a non-volcanic terrain based on the regional interpretation (Table 2).

Table 3.1: Number of volcanic and non-volcanic DLEs within each region.

	Region	# DLEs	Diameter (km)	Latitude
Volcanic DLEs	N Tharsis	51	3.0–24.0	06.81–59.61 °N
	Elysium	17	3.2–17.9	06.64–36.56 °N
	Syrtis Major	10	8.1–23.7	03.43–18.46 °N
	S Tharsis	31	4.0–19.6	00.47–35.49 °S
	Hesperia	18	4.7–19.7	19.33–39.64 °S
Non-volcanic DLEs	Acidalia/Chryse	33	3.0–17.4	20.66–72.99 °N
	Utopia	31	3.3–21.4	26.76–58.53 °N
	Amazonis/Arcadia	15	4.3–20.3	32.27–70.81 °N

Table 3.2: Study regions showing the number of DLEs corresponding to each geologic with regional interpretation (see Scott and Tanaka, 1986 and Greeley and Guest, 1987 for full unit descriptions).

Region	(n) DLEs	Unit	Regional Interpretation
Northern Tharsis	9	Aa1	Generally around the Alba Patera region. Emplacement began in the early Hesperian and continues throughout the Amazonian Period (Cattermole, 1990; Schneeberger and Pieri, 1991). Four main eruptive phases: (1) fissure erupted extensive flood-like flows; (2) emplacement of pyroclastic materials; (3) voluminous lava flows erupted from a central vent; (4) effusive flows followed by collapse of summit caldera (Schneeberger and Pieri, 1991). Estimated to be hundreds of meters thick (Tanaka et al., 2014).
	3	Aa3	
	3	Aam	
	2	AHcf	
	14	Hal	
	1	Hf	
	10	Hr	
	3	Ht2	
Elysium	3	Htl	Bulk of edifice constructed during Noachian with episodic activity through to the Amazonian (Platz and Michael, 2011). Primarily effusive lava flows overlying heavily cratered terrain (Hartmann and Berman, 2000; Platz and Michael, 2011). Sedimentary layers possible between flows (Hartmann and Berman, 2000). Thickness estimated to be on the order of hundreds of meters (Tanaka et al., 2014).
	3	Htm	
	10	Ael1	
	1	AHpe	
Syrtris Major	5	Hr	First episode of eruption in late Noachian or early Hesperian as extensive ridge-plains unit followed by flows from calderas (Schaber, 1982). Surface heterogeneous, but basaltic in composition (Mustard et al., 1993; Hiesinger and Head, 2004). Overall thickness ~0.5 – 1 km (Hiesinger and Head, 2004).
	1	Npld	
Southern Tharsis	10	Hs	Heavily fractured basement from heavy bombardment overlain by a 2–3 km thick friable impact generated megaregolith layer (Carr, 1986; MacKinnon and Tanaka, 1988; Davis and Golombek, 1990). Multiple lava flows superposed at surface and are estimated to be a few hundred meters thick (Davis and Golombek, 1990; Tanaka et al., 2014). Emplacement continuous since Noachian (Carr and Head, 2010).
	1	Hf	
	1	Hpl3	
	21	Hr	
Hesperia Planum	6	Hsu	Pyroclastic deposits from Tyrrhena Patera overlain by lava flows originating from same vent (Greeley and Crown, 1990; Crown et al., 1992; Gregg and Farley, 2006). Region estimated to be few hundred meters thick (Tanaka et al., 2014). Emplacement began in the late Noachian or early Hesperian and ceased in late Hesperian to early Amazonian (Gregg and Farley, 2006).
	2	Npl2	
	18	Hr	
	2	Aa1	
Acidalia/Chryse Planitia	5	Hchp	Volcanism and fluvial sedimentation begin in the Noachian (Rotto and Tanaka, 1995). Outflow channel activity and sedimentation continue throughout the Hesperian ceasing in the early Amazonian (Lucchitta et al., 1986; Rotto and Tanaka, 1995; Tanaka, 1997; Kreslavsky and Head, 2002). Water sublimates from sediment during the Amazonian and produces polygonal fractures throughout the region (Tanaka, 1997; Kreslavsky and Head, 2002).
	11	Hvg	
	5	Hvk	
	6	Hvm	
	1	Npl1	
	3	Nple	
Utopia Planitia	9	Ael3	Site of ancient Noachian impact basin (~3300 km in diameter) (McGill, 1989). Early Hesperian lavas flood basin followed by later Hesperian sediment deposits derived from outflow channels (Vastitas Borealis Formation)(~100 m thick) (Thomson and Head, 2001; Kreslavsky and Head, 2002). Some early Amazonian lavas emplaced
	2	Apk	
	5	Aps	
	8	Hvg	

	7	Hvm	with subsequent sediment/ice deposition in the more recent past (Head et al., 2003; Platz and Michael, 2011).
Amazonis/ Arcadia Planitiae	3	Am	Amazonis Planitia suggested to be site of large, circa-Noachian impact event (Fuller and Head, 2002). Widespread Hesperian aged lavas infill basin and surrounding area (Plescia, 1993; Fuller and Head, 2002) followed by deposition of the Vastitas Borealis Formation (Fuller and Head, 2002; Head et al., 2002). Amazonian aged lavas, subsequent mass-wasting material, and unconsolidated sediments cover all or parts of the Vastitas Borealis Formation with the latter being dominant (Fuller and Head, 2002; Head et al., 2002; Tanaka et al., 2003, 2014).
	1	Apk	
	6	Aps	
	2	HNu	
	2	Hvk	
	1	Hvm	

Analysis of each DLE was performed using Java Mission-planning and Analysis for Remote Sensing (JMARS) software and included use of CTX (res. 6 m/pixel) and THEMIS visible (VIS) (res. 18 m/pixel) images superposed onto THEMIS daytime thermal infrared band 9 global mosaic base layer (Christensen et al., 2004, 2009; Malin et al., 2007; Edwards et al., 2011; Hill et al., 2014). The area and perimeter of each ejecta layer were calculated in JMARS by creating individual shape layers outlining both ejecta layers (e.g., inner and outer). Because JMARS calculates the total enclosed area of a shape, a shape layer of the crater itself was also created and subtracted from both ejecta shape layers to give just the area of each ejecta layer (e.g., inner and outer ejecta layers begin at the crater rim). Morphometric analysis included ejecta mobility (EM), which measures the extent of an ejecta blanket from the crater rim (Mouginis-Mark, 1979; Costard, 1989; Barlow, 2004; Boyce et al., 2010), and lobateness (Γ), the sinuosity of the outermost edge of an ejecta blanket (Johansen, 1979; Kargel, 1986, 1989; Barlow, 2004); these parameters were calculated for both DLE layers (i.e., inner and outer):

$$EM = \frac{\text{average extent of ejecta layer from crater rim}}{\text{crater radius}}$$

$$\Gamma = \frac{\text{perimeter of ejecta layer}}{[4\pi(\text{area of ejecta layer})]^{1/2}}$$

As in Chapter 2, we have modified the EM equation to determine an “effective” radius of an ejecta layer using the area of a circle:

$$EM = \frac{\sqrt{\frac{A}{\pi}} - r}{r}$$

where A is the total enclosed area inside an ejecta layer (including the crater itself), and r is the radius of the crater. This gives a more precise average radius of an individual ejecta layer by essentially averaging every radii along the circumference of a layer.

3.3 Results

3.3.1 Ejecta Mobility (EM)

DLEs on non-volcanic terrains are binned separately from those on volcanic terrains (referred to as “non-volcanic” and “volcanic” DLEs respectively from here on) by 10° degree latitude increments; a plot of the distribution of EM for each bin is provided in Figure 3. This same process was repeated for crater diameters using 3 km bins (Fig. 4). Tables 3 and 4 list the number of craters within each respective bin. Collectively, ejecta mobility appears to generally increase with increasing latitude and is consistent with previous observations (e.g., Mouginis-Mark, 1979; Costard, 1989; Barlow, 2006; Barlow et al., 2014; Li et al., 2015; Jones and Osinski, 2015; Chapter 2). This is most apparent for the outer layers (Fig. 3a) and is less apparent for inner layers, which seem to be concentrated more or less around ~1.5 (Fig. 3b). The EM of the outer layers peaks around ~45° latitude for both groups (i.e., non-volcanic and volcanic DLEs) and then generally decreases (Fig. 3a).

Non-volcanic DLEs have slightly higher EM values than volcanic DLEs and this difference is most apparent for outer layers. This can be seen particularly well when EM for these targets are plotted against diameter (Fig. 4). Inner layers for these targets show less separation, but are generally consistent with results of outer layers. Additionally, we have binned the EM values of non-volcanic and volcanic DLEs, separately, by 0.2 increments and then plotted the data on the MOLA map of Mars to better show the distributions between both groups (Fig. 5). At latitudes greater than ~25°, there are higher

proportions of non-volcanic DLEs (61%) with higher (outer layer) EM values than volcanic DLEs with high EM values (20%) (Fig. 5a) – here an $EM \geq 3$ is considered as being a high value. This is also seen for inner layers, but is less apparent (Fig. 5b).

Table 3.3: Number of DLEs within each latitude bin.

Latitude bin (°N)	(n) Non-volcanic	(n) Volcanic
00–10	0	16
10–20	0	27
20–30	5	26
30–40	26	35
40–50	29	14
50–60	11	9
>60	8	0

Table 3.4: Number of DLEs within each crater diameter bin.

Crater diameter bin (km)	(n) Non-volcanic	(n) Volcanic
3–6	23	15
6–9	14	36
9–12	16	24
12–15	15	24
15–18	6	17
18–24	5	11

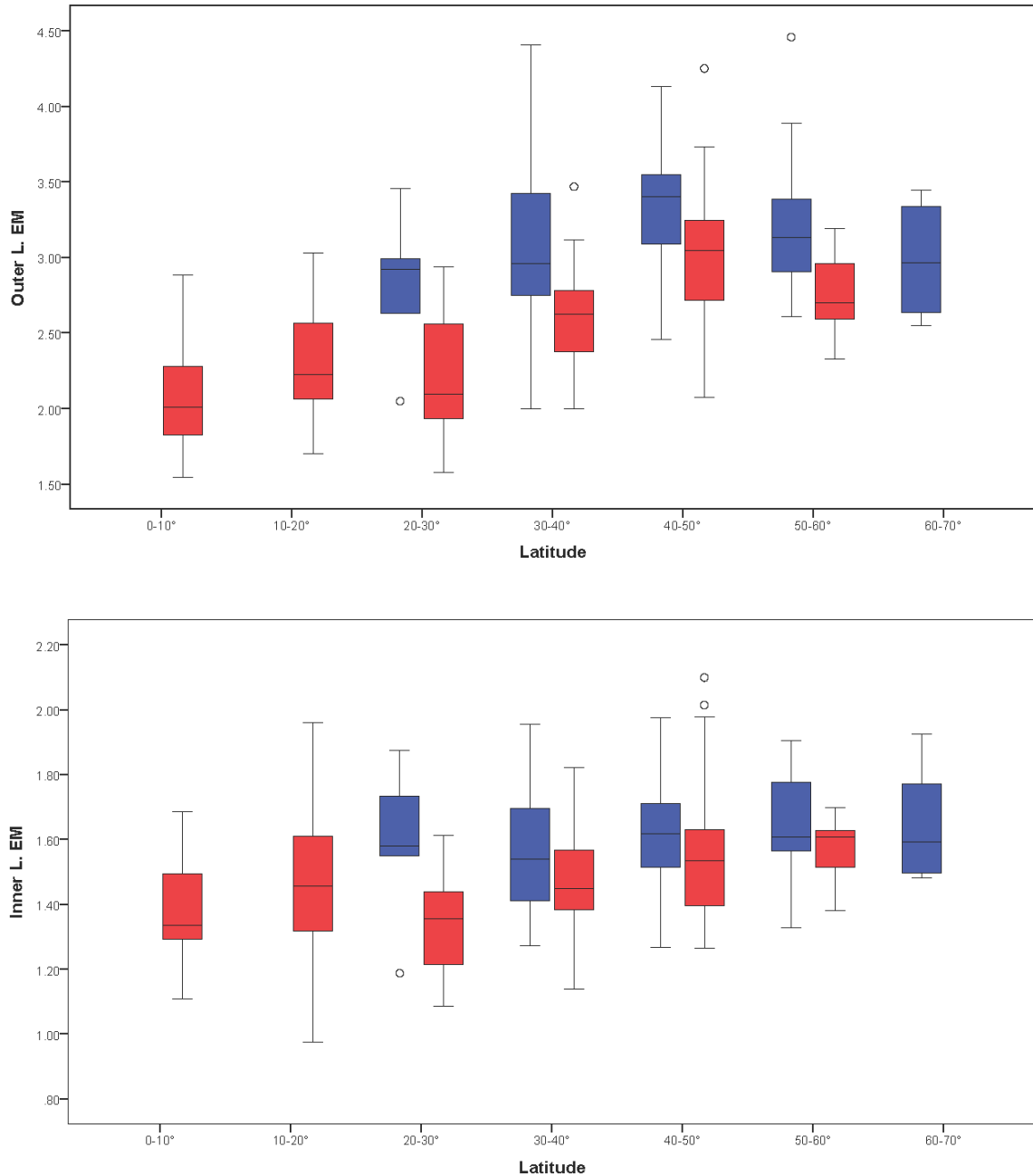


Figure 3.3: Box plots showing the distribution of EM values for the outer (a) and inner (b) layers. Data is binned by 10° latitude. Non-volcanic DLEs are plotted in blue, volcanic DLEs in red. Whiskers represent minimum and maximum values with outliers plotted as circles. The horizontal lines within each box represent the median EM value.

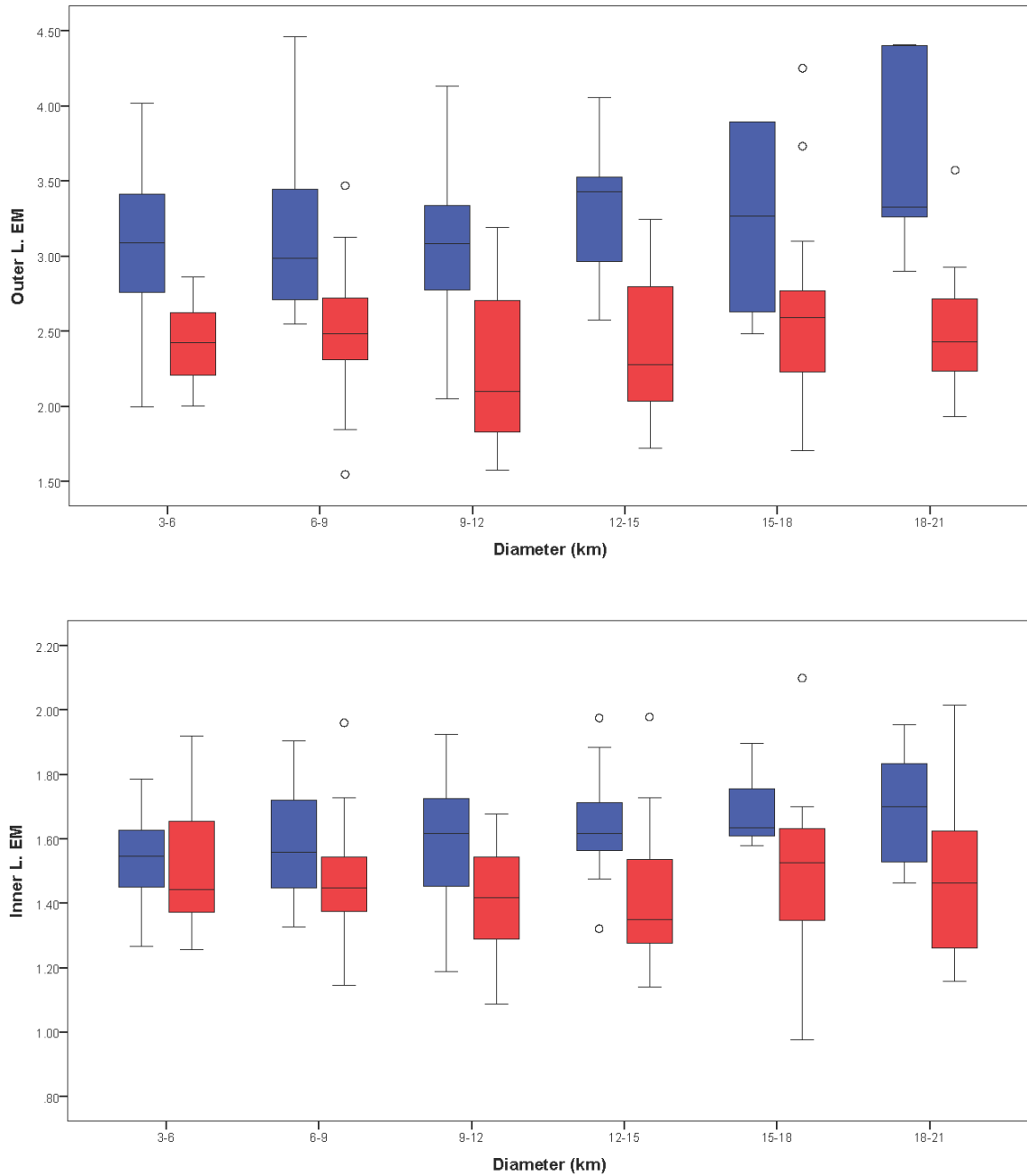


Figure 3.4: Box plots showing the distribution of EM values for the outer (a) and inner (b) layers. Data is binned by crater diameter (every 3 km). Non-volcanic DLEs are plotted in blue, volcanic DLEs in red. Whiskers represent minimum and maximum values with outliers plotted as circles. The horizontal lines within each box represent the median EM value.

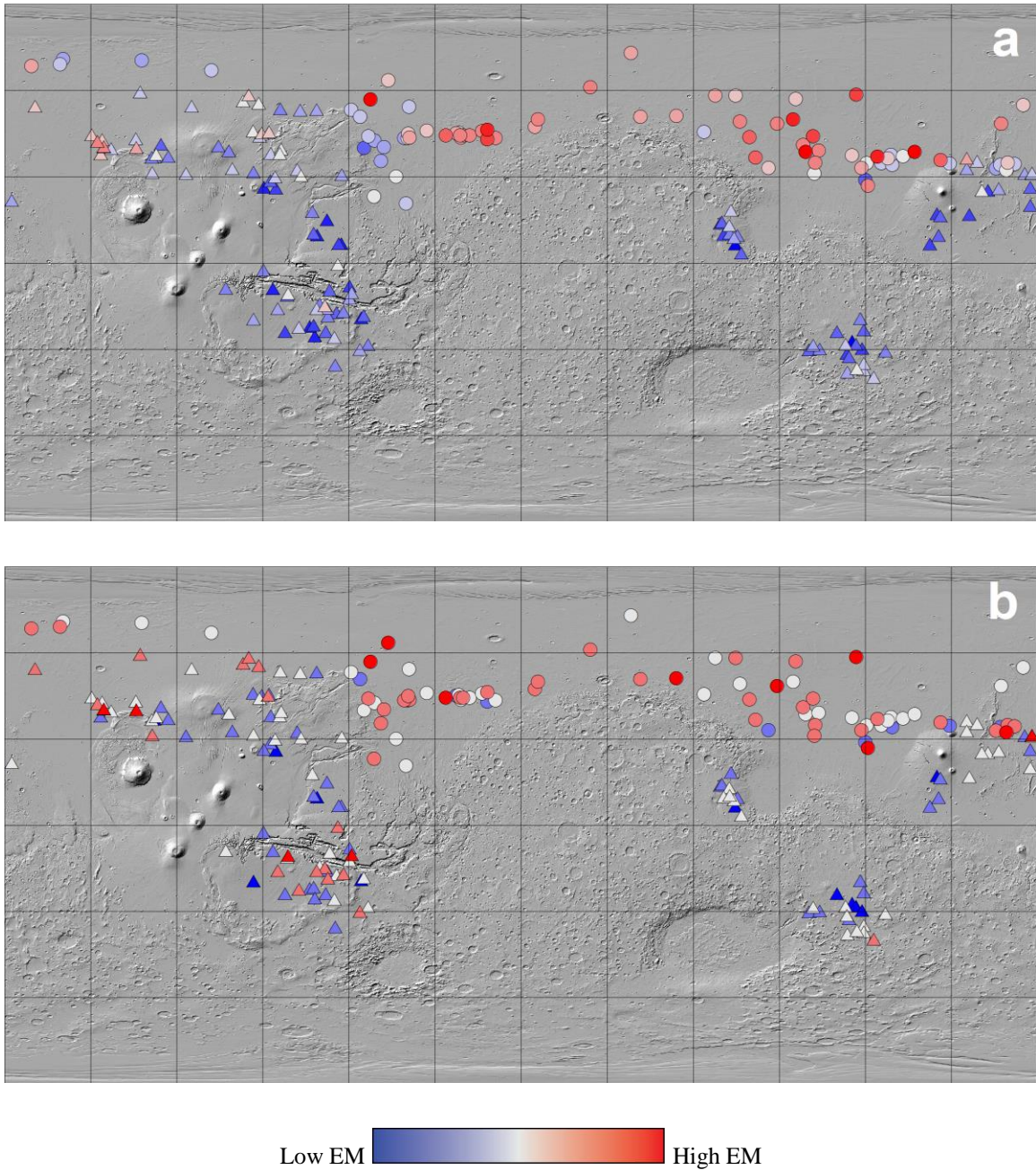
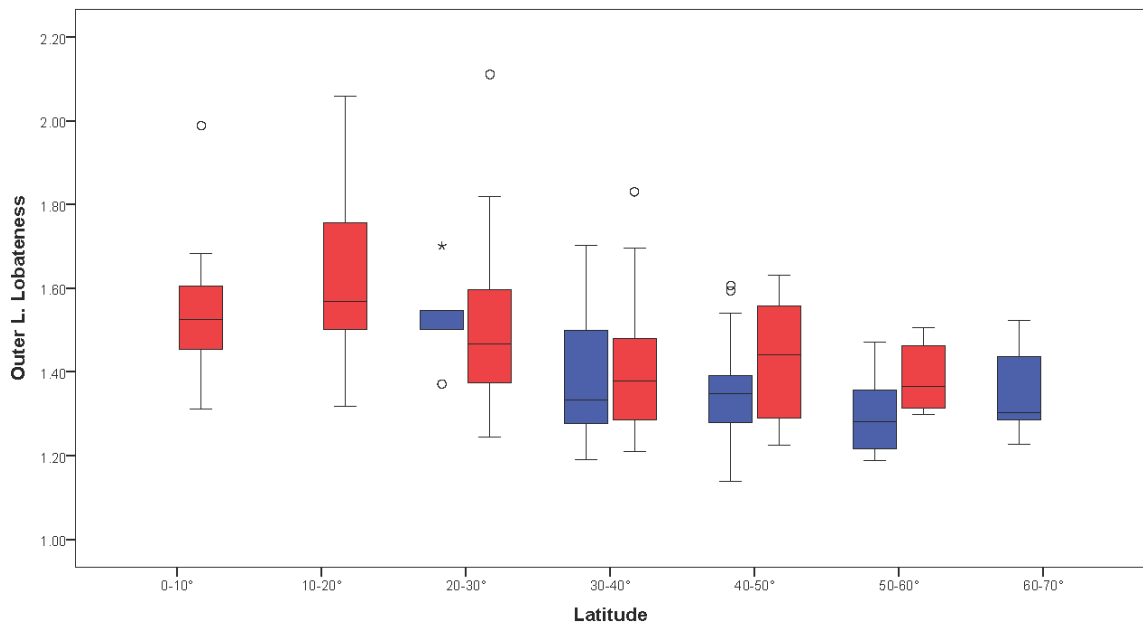


Figure 3.5: Distribution of binned EM data over MOLA shaded relief map of Mars. Top plot (a) shows the outer layer EM, bottom plot (b) shows the inner layer EM. Data is binned by 0.2 values. Non-volcanic DLEs are plotted as circles, volcanic DLEs are triangles.

3.3.2 Lobateness (Γ)

Results of lobateness are binned and displayed (Figs. 6 and 7) in a similar fashion as the EM plots. Overall, lobateness shows a subtle latitudinal trend only inverted from EM behaviors; lobateness appears to generally decrease with increasing latitude (Fig. 6). This trend is observed for both inner and outer layers but is more defined for inner layers. Figure 8 is plotted equivalent to Figure 5 but shows lobateness binned by 0.2 degree increments. This plot supports Figures 6 and 7 in that we see a higher proportion of DLEs with higher lobateness values near the equator and less poleward. From Figure 7, one can see that volcanic DLEs tend to be slightly more lobate when compared to non-volcanic DLEs, particularly for inner layers. This behavior is not observed between lobateness and latitude (e.g., Fig. 6). It also appears that lobateness for both layers and both groups gradually increases with increasing diameter. Overall, lobateness between the two groups are very similar when compared to EM results.



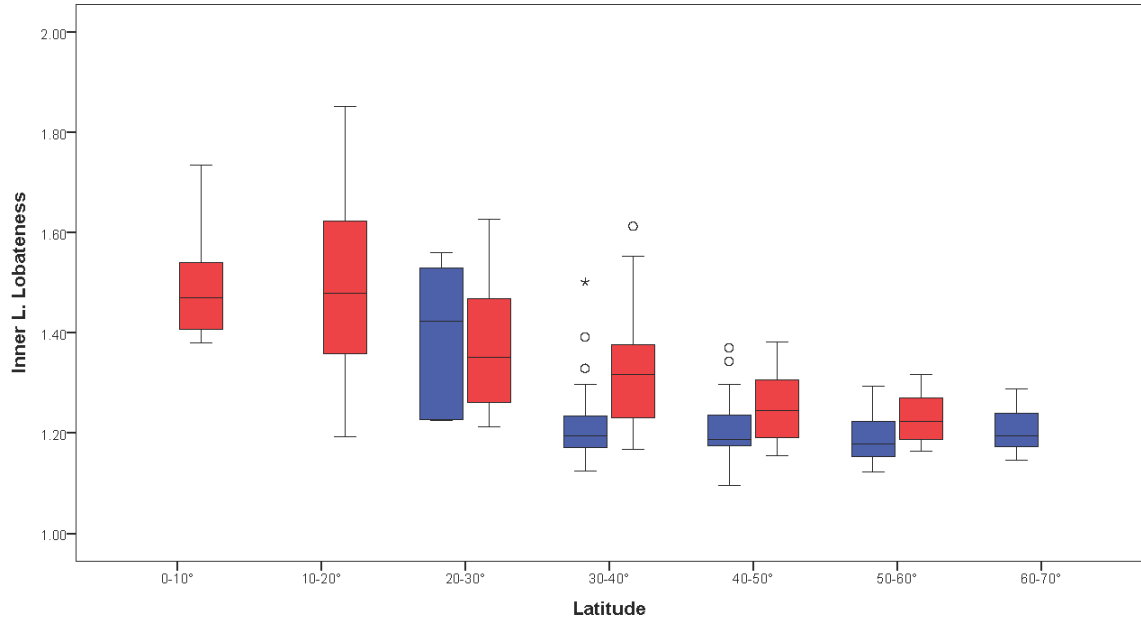
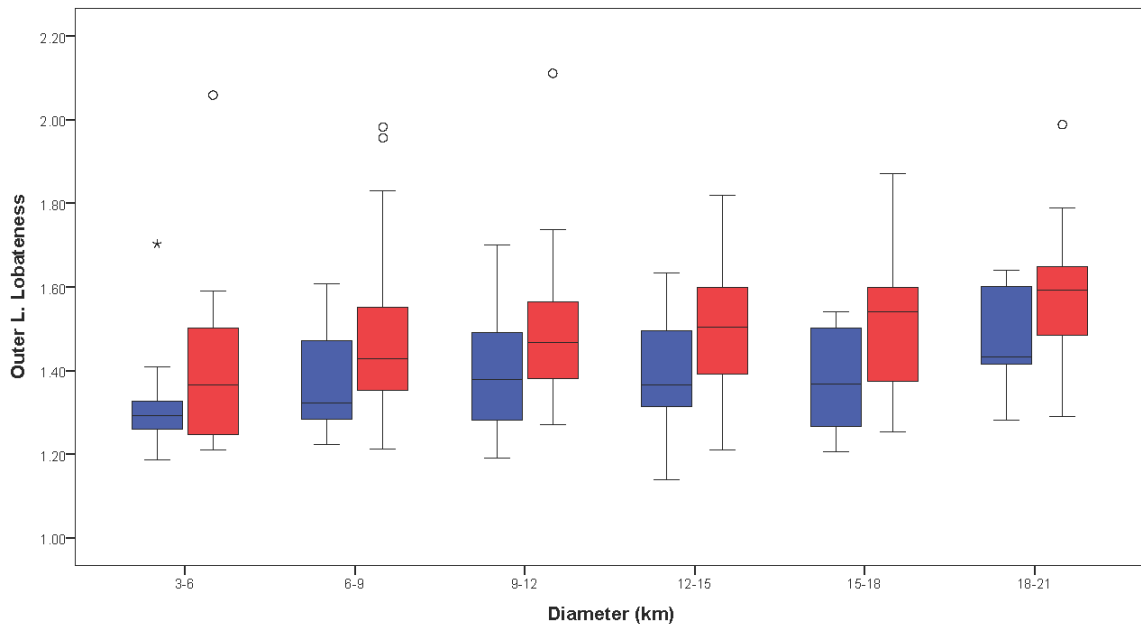


Figure 3.6: Box plots showing the distribution of lobateness values for the outer (a) and inner (b) layers. Data is binned by 10° latitude. Non-volcanic DLEs are plotted in blue, volcanic DLEs in red. Whiskers represent minimum and maximum values with outliers plotted as circles. The horizontal lines within each box represent the median lobateness value.



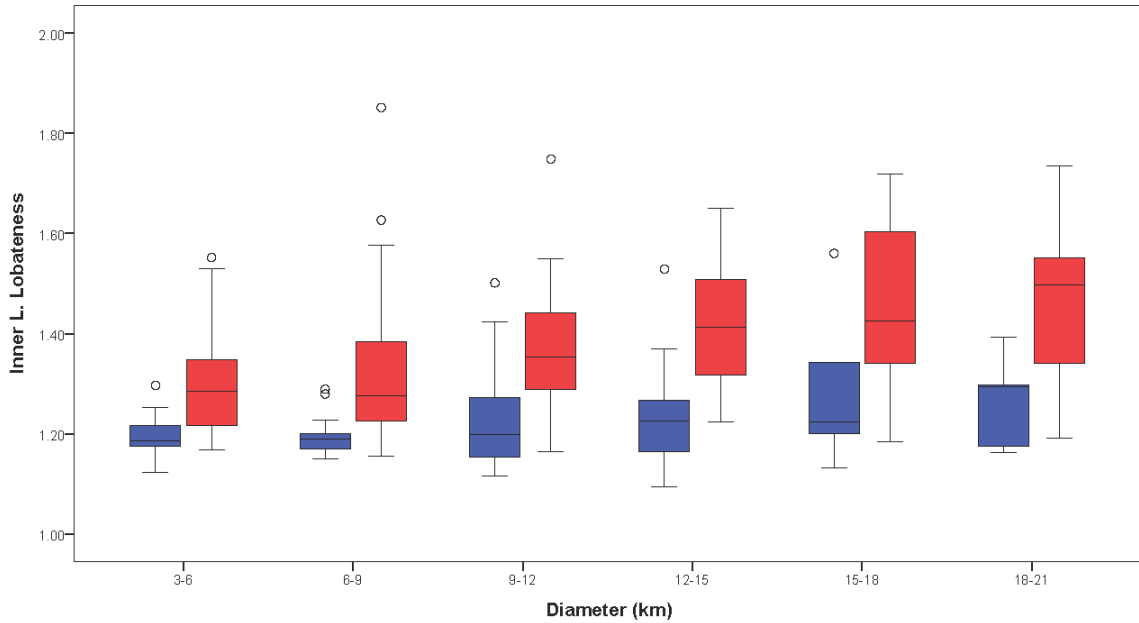
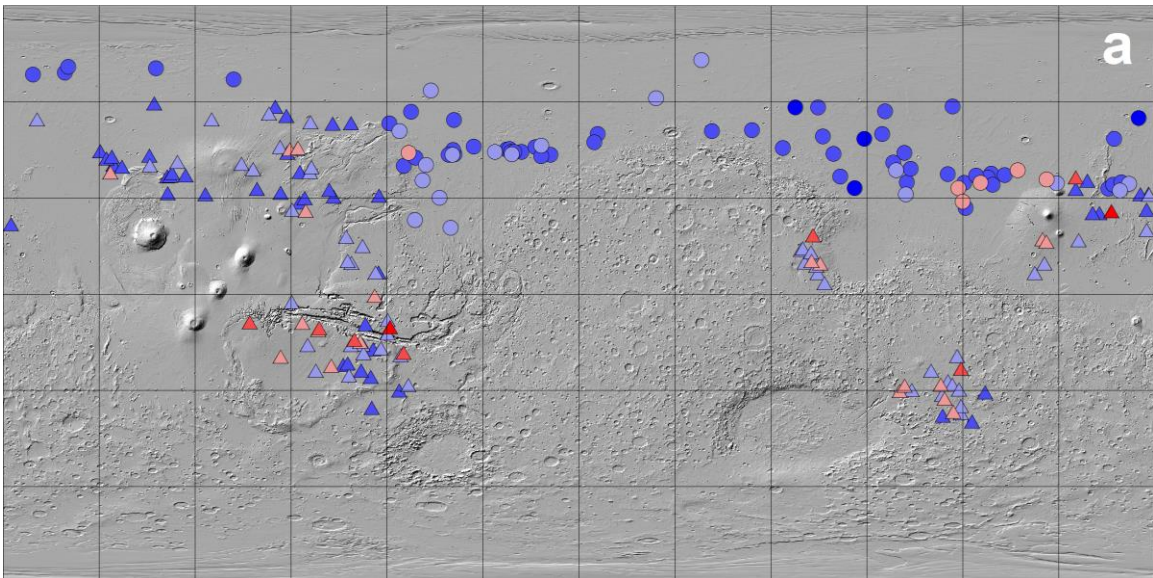


Figure 3.7: Box plots showing the distribution of lobateness values for the outer (a) and inner (b) layers. Data is binned by crater diameter (every 3 km). Non-volcanic DLEs are plotted in blue, volcanic DLEs in red. Whiskers represent minimum and maximum values with outliers plotted as circles. The horizontal lines within each box represent the median lobateness value.



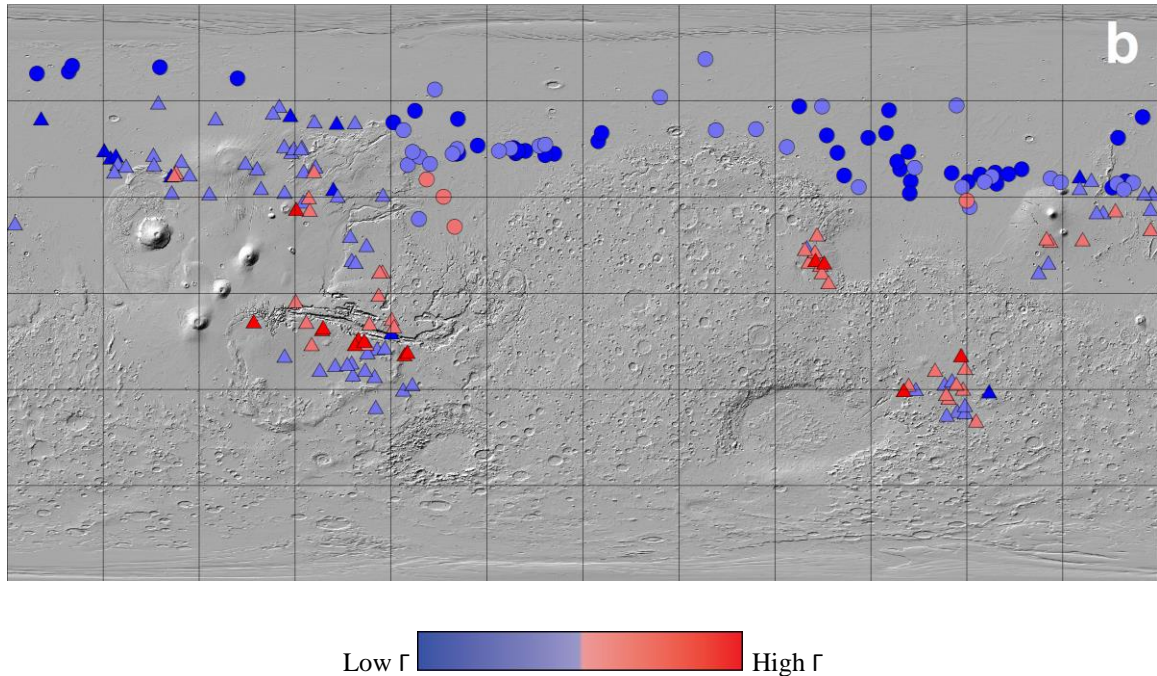


Figure 3.8: Distribution of binned lobateness data over MOLA shaded relief map of Mars. Top plot (a) shows the outer layer lobateness, bottom plot (b) shows the inner layer lobateness. Data is binned by 0.2 values. Non-volcanic DLEs are plotted as circles, volcanic DLEs are triangles.

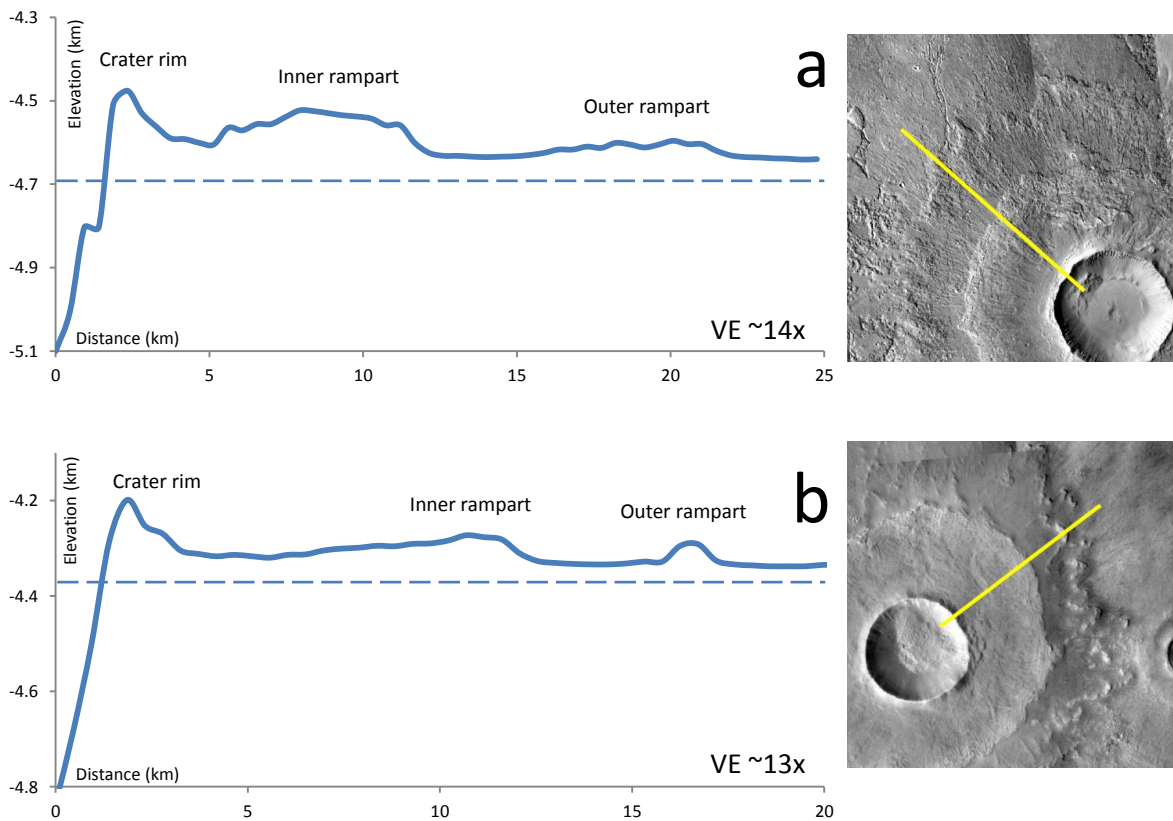
3.3.3 Morphology

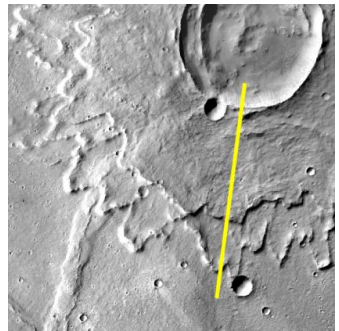
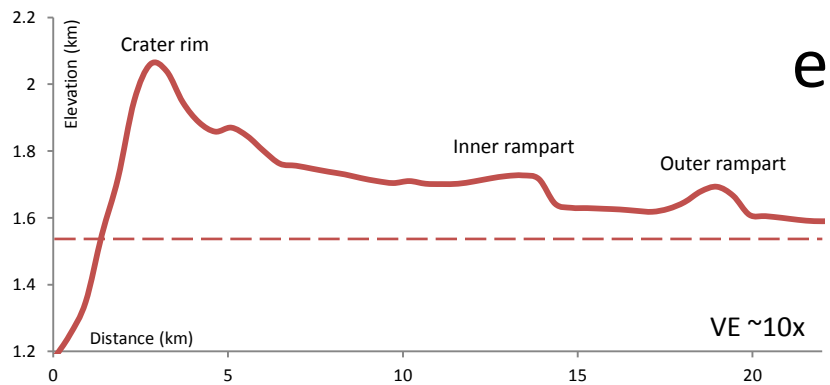
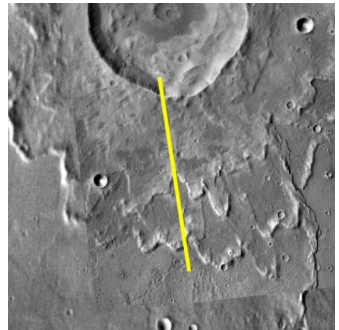
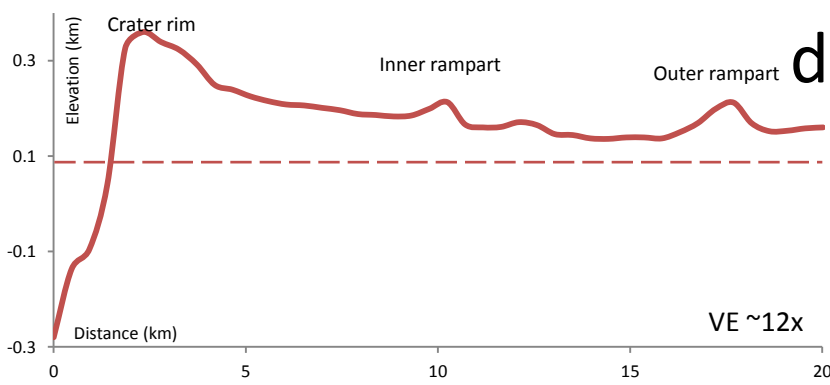
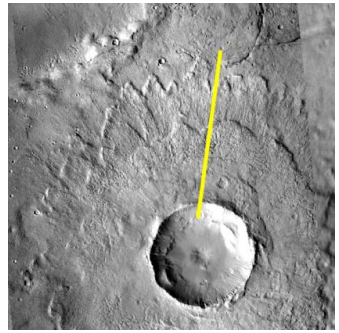
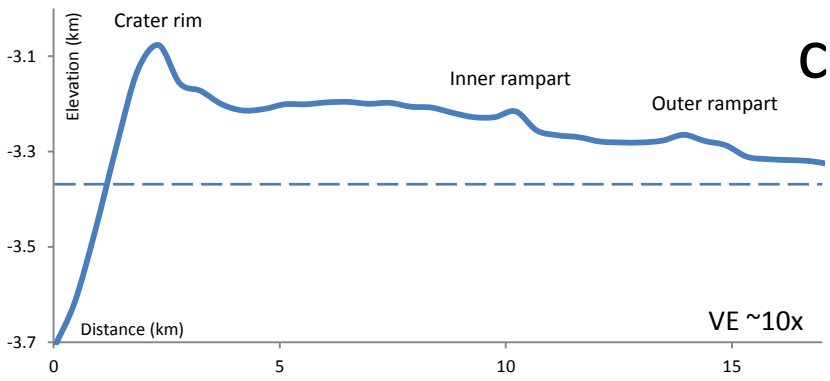
Radial grooves are a common feature observed on many DLEs and in the past have been used as a diagnostic criterion for DLEs (Mouginis-Mark and Boyce, 2004; Boyce and Mouginis-Mark, 2006). In our study set, 131 out of a total of 206 DLEs (~64%) display radial grooves on either the outer, inner, or both ejecta layers. It is notable that the majority of non-volcanic DLEs display grooves (77%) while only roughly half (55%) of volcanic DLEs do (Table 5).

Table 3.5: Number of DLEs with or without radial grooves.

	(n) DLEs w/ grooves	(n) DLEs w/o grooves
Volcanic DLEs	70	57
Non-volcanic DLEs	61	18
Total	131	75

Profiles of the DLE craters shown in Figure 1, derived from MOLA elevation data, are shown in Figure 9. These were taken along MOLA shot tracks (shots spaced 300 m apart (Smith et al., 2001)) to ensure the best possible representation of the true profile (e.g., no data gaps). Vertical accuracy for MOLA elevation is 1 m (Smith et al., 2001). For all these DLE craters, the elevation of the inner layers is higher than the surrounding outer layers. Ramparts are observed at the distal end of each ejecta layer and are relatively more distinctive for outer layers. It is interesting to note that the volcanic DLE examples appear to show more pronounced ramparts when compared to the non-volcanic examples, particularly the inner layers (Figures 9d–9f compared to Figures 9a–9c). Topographic lows, or “moats”, between the crater rim and the inner layer rampart are a commonly observed feature on DLEs (e.g., Boyce and Mouginis-Mark, 2006) and appear to be present in all our examples. They do, however, appear to differ between non-volcanic and volcanic DLEs. The non-volcanic DLE moats seem to be immediately adjacent to the crater rim while volcanic DLE moats appear to be much more subtle and extend out closer to the rampart.





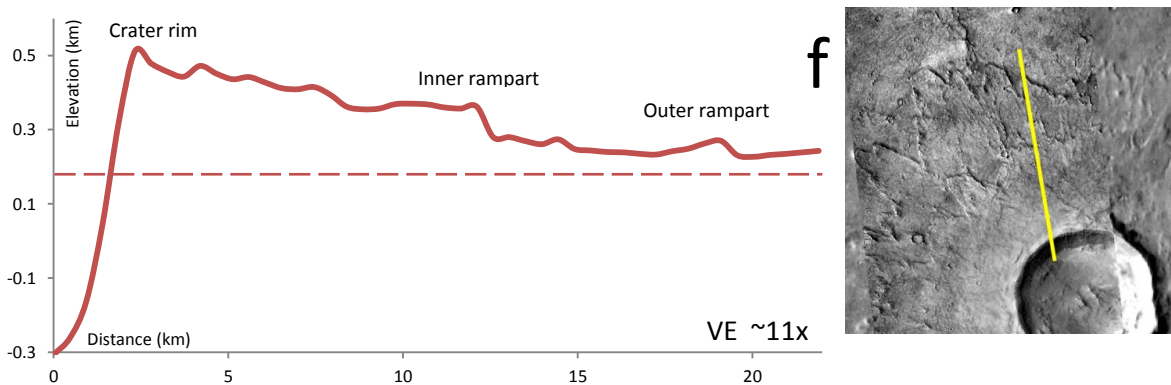


Figure 3.9: Topographic profiles of the craters in Fig. 1 derived from MOLA DTMs. Blue profiles are non-volcanic DLEs (a, b, c), red profiles are volcanic DLEs (d, e, f). Dashed lines are planes of reference to emphasize the topography of ejecta. Vertical exaggeration (VE) is included within each profile. IDs for context images are the same as those in Fig. 1 unless otherwise noted. (a) 12.2 km diameter crater located in Utopia Planitia (120.53° E, 34.71° N). (b) 10.7 km diameter crater located in Utopia Planitia (95.71° E, 57.00° N). (c) 10.8 km diameter crater located in Acidalia Planitia (308.86° E, 42.54° N). (d) 16.7 km diameter crater located in Tharsis (296.50° E, 6.81° N). (e) 14.8 km diameter crater located in Hesperia Planum (119.51° E, 23.24° S). (f) 14.7 km diameter crater located in Syrtis Major (75.47° E, 9.61° N). CTX image ID: G01_018698_1896_XN_09N284W.

3.4 Discussion

3.4.1 Effect of Target/Surface Properties on Ejecta Mobility and Lobateness

Our measured EM values seem to reflect general subsurface volatile concentrations on Mars (e.g., Rossbacher and Judson, 1981; Clifford, 1993; Clifford et al., 2010) in that both increase with increasing latitude, consistent with previous observations (e.g., Mouginis-Mark, 1979; Costard, 1989; Barlow, 2006; Barlow et al., 2014; Li et al., 2015; Jones and Osinski, 2015; Chapter 2). Because EM of both groups increases with latitude, the simplest explanation is that volatile content is the main variable controlling layered ejecta morphologic and morphometric properties. In comparison, results for lobateness

contrast with EM in that it decreases with increasing latitude. In addition, our results show a difference in morphometric properties (i.e., EM and lobateness) between non-volcanic and volcanic DLEs with non-volcanic DLEs having slightly higher EM values than volcanic DLEs but slightly lower lobateness values than their counterpart (Figs. 3–5, 7 and 8). This observation suggests that properties of the target and/or surface may indeed play a role during the emplacement process and final ejecta morphology and morphometry. We suggest a major factor responsible for this observation is the strength contrast between largely volcanic and sedimentary targets, plus their ability to host volatile-rich materials.

As explained in Chapter 2, the first layer of ejecta emplaced has been suggested to be via a process of ballistic sedimentation with subsequent radial flow (see Chapter 2). Greater amounts of surface materials are incorporated into the developing ejecta blanket if the uppermost target is loose, unconsolidated sediment (e.g., Hörz et al., 1983) when compared to competent volcanic rock (compressive strength of basalt ~100–300 MPa (Attewell and Farmer, 1976)). Thus the incorporation of a greater amount of weak or unconsolidated surface materials (including surficial dust) into the ejecta blanket should allow ejecta to become more mobile and result in increased runout distances (e.g., Hörz et al., 1983; Osinski, 2006; Osinski et al., 2011). Furthermore, a higher concentration of volatiles in the near-surface environment would effectively reduce friction between particles and enhance mobility further. On Mars, subsurface volatile concentrations generally increase with increasing latitude (Rossbacher and Judson, 1981; Clifford, 1993; Clifford and Parker, 2001; Clifford et al., 2010). In addition, climate models and geomorphologic evidence suggest that glacial ice was abundant at mid- to high-latitudes throughout the Amazonian (Head et al., 2003, 2005, 2006, 2010; Mellon et al., 2008; Plaut et al., 2009; Madeleine et al., 2009; Fastook et al., 2011; Kadish and Head, 2011; Souness and Hubbard, 2012). Together, this suggests that volatiles are abundant at higher latitudes. Based on permeability, sedimentary targets generally host a greater concentration of volatiles than volcanic rock (e.g., Brace, 1980); as a result, a greater volatile to ejecta ratio is expected to exist for impacts into a sedimentary target versus a volcanic one. Jones and Osinski (2015) observed variations in EM, onset diameter, and correlation between EM and diameter to develop a regional stratigraphic model of the

subsurface of Mars. They ascribe targets with high volatile contents, small grain sizes, and poor cohesion as a “low viscosity layer” and targets with low volatile contents, coarser grain sizes, and higher cohesion as “higher viscosity” layers (Jones and Osinski, 2015). They suggest equatorward of $\sim 30^\circ$ latitude a higher viscosity layer overlays a lower viscosity layer while the converse is true (low viscosity layer over a higher viscosity layer) for targets poleward of $\sim 45^\circ$ latitude (Jones and Osinski, 2015). Correlating our distribution of DLE craters with their model, we find that the majority of our non-volcanic DLEs are located where a low viscosity layer is near the surface while volcanic DLEs are mostly in regions where a low viscosity layer is buried beneath a higher viscosity layer - An exception for the latter are DLEs located in northern Tharsis where a low viscosity layer is near the surface. In general, Jones and Osinski’s (2015) model support results of this study that non-volcanic DLEs have slightly higher EM values than volcanic DLEs, which may be attributed to differences in the target.

Results for lobateness suggest that this property decreases with increasing latitude and that DLEs on volcanic terrains are somewhat more lobate than those on non-volcanic ones (e.g., unconsolidated sediment) (Figs. 6–8). Lobateness measures the sinuosity of an ejecta layer and is dependent on the perimeter and area of the ejecta being measured (Kargel, 1986; Barlow, 1994). Individual lobes that radially make up the distal edge of ejecta determine the lobateness of the ejecta but does not necessarily mean that the quantity equates to a higher or lower lobateness value; how pronounced the lobes are in form determines the lobateness. Theoretically, two separate DLEs could have the same number of lobes around the perimeter of ejecta but have different lobateness values simply because one DLE has more pronounced lobes and the other DLE with more subdued, less pronounced lobes. Regardless of the size of the crater, the DLE with more pronounced lobes would equate to a higher lobateness value. The rheology and morphology of saturated masses of soil and fragmental rock (e.g., debris flows, pyroclastic flows, lahars) have been suggested to be analogous to that of layered ejecta (e.g., Carr et al., 1977; Melosh, 1989). Because debris flows and layered ejecta move as a ground hugging flow, surficial materials and properties likely have a strong influence on ejecta lobateness. Field observations and large-scale flume experiments show that poorly sorted debris flows move as one or more nonuniform surges that generally consist of an

abrupt flow front followed by a body that gradually transitions into a thin, watery tail (e.g., Iverson, 1997, 2003; Major, 1997). Larger sized particles migrate towards the flow front and margins while smaller particles stay near the center. Importantly, pore-fluid pressure drives the entire debris flow which is highest (e.g., liquefied) in the center and absent within the coarse-grained flow front and margins (high friction) (Iverson, 1997, 2003; Major, 1997; Major and Iverson, 1999; Iverson et al., 2010). Lobes may develop in places where grain-to-grain contacts (i.e., flow front and margins) have sufficient frictional resistance to cease the trailing liquefied portion of the flow (Iverson and LaHusen, 1993; Iverson, 1997, 2003; Major and Iverson, 1999).

Relating the rheology and depositional process of debris flows to layered ejecta, lobes should form where there is high frictional resistance (e.g., Iverson, 1997, 2003; Major and Iverson, 1999). If ejecta is viewed as an initial coalesced mass of debris moving radially outward at equal distances (e.g., a lobateness value of 1; perfect circle), lobes will start to form depending on how much friction, or drag, there is between the debris (i.e., ejecta) and the target surface. We suggest that this can explain the lower average lobateness values for non-volcanic DLEs. In other words, at higher latitudes where there is an abundance of surficial sediment and/or near-surface volatiles, friction between the ejecta blanket and the target can be expected to be low and may result in ejecta to run out at roughly equal distances from the crater rim. We suggest that this would produce more subdued (less pronounced) lobes and result in a lower lobateness values (Figs. 6–8). In comparison, ejecta emplaced on volcanic terrains should experience more friction between ejecta and the target – where there are less volatiles and/or more coherent bedrock – which could cause ejecta to split into more pronounced lobes equating to the observed higher lobateness values for volcanic DLEs (Figs. 6–8).

Experiments have also shown that that water content of the source material strongly influences the depositional process for debris flows, where more saturated flows ran out further than less saturated flows (Major, 1997). Successive surges in saturated flows commonly override already emplaced debris while less saturated flows shove forward debris and only partially overrides earlier deposited debris (Major, 1997). Our non-volcanic DLEs are situated on what is largely interpreted as sediment within the northern

plains. Because sediment is generally more permeable than volcanic rock (e.g., Brace, 1980), and our non-volcanic DLEs are located at favorable locations for abundant volatile concentrations (mid- to high-latitudes) (e.g., Clifford, 1993; Head et al., 2006; Madeleine et al., 2009; Clifford et al., 2010; Souness and Hubbard, 2012), we infer that non-volcanic targets contain higher volatile concentrations than volcanic ones. The amount of volatiles in the target may determine how saturated the ejecta becomes with non-volcanic DLEs likely being more saturated than volcanic DLEs. If this is true, non-volcanic DLEs may behave like the more saturated flows observed from large-scale experiments (e.g., Major, 1997), where successive surges may potentially be emplaced on top of earlier emplaced ejecta and/or in gaps between two lobes, which results in lobes with more subdued and ejecta that is less lobate. Figures 10a and 10b show two DLEs that appear to have the aforementioned qualities, where numerous lobes can be seen making up the outer layer of ejecta and overlap one another. In comparison, Figures 10c and 10d appear to have little to no overlap in lobes. Volcanic DLEs may behave like and resemble the less saturated experimental flows, where surges push earlier emplaced ejecta forward instead of dominantly overriding emplaced ejecta like the saturated flows (e.g., Major, 1997). This may make lobes more pronounced and contribute to a higher lobateness. However, these two different debris flow morphologies do not favor one DLE group over the other (e.g., volcanic or non-volcanic) but are instead assorted among our collective study DLEs. For example, the DLE in Figure 9a is a volcanic DLE and the one in Figure 9b is a non-volcanic DLE, both having the “saturated” morphology. Regardless, the DLEs having the more “saturated morphology” may indeed be more saturated causing lobes to overlap and contribute to a lower lobateness value. Our results would suggest that these types of morphologies are found at higher latitudes, where there are more volatile concentrations and generally lower lobateness values.

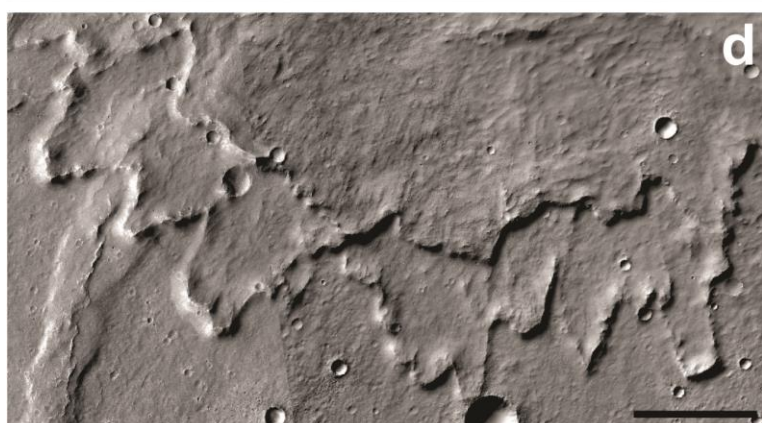
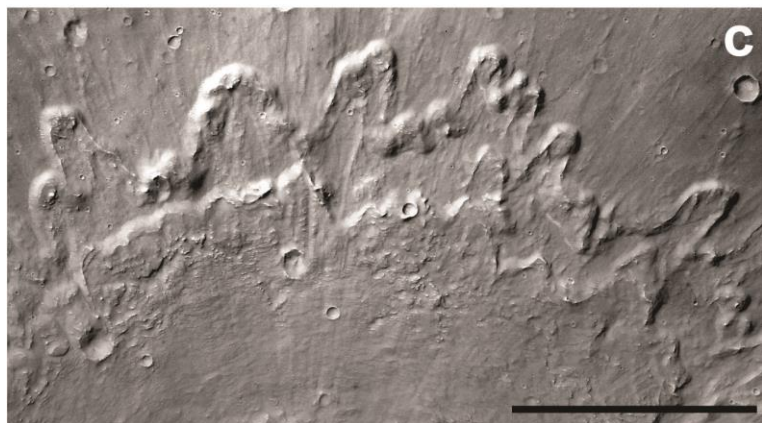
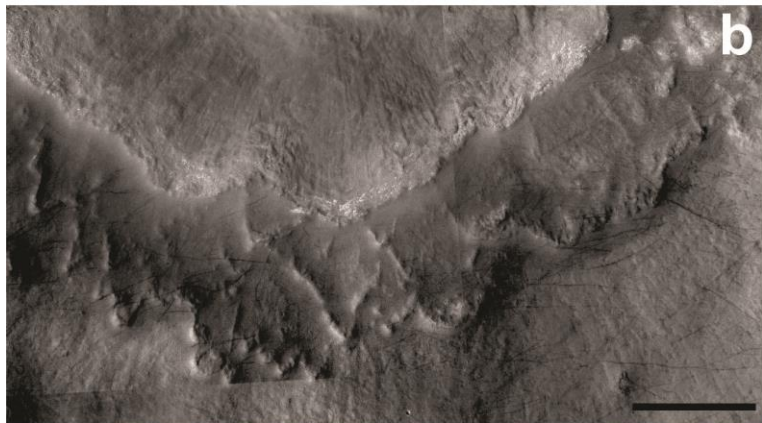


Figure 3.10: Examples of DLE outer layers that resemble the saturated and non-saturated large-scale debris flow experiment morphologies described in Major (1997). The DLEs depicted in a and b resemble the saturated debris flows where multiple surges commonly overrun earlier emplaced material and form numerous lobes. The DLEs in c and d resemble the non-saturated debris flows where subsequent surges push forward earlier emplaced material and overlapping of lobes is uncommon. All scale bars are 5 km.

3.4.2 Ejecta Emplacement Chronology

The chronological order of emplacement between the DLE inner and outer layers remains debated. Some workers propose that the inner layer is emplaced before the outer layer (e.g., Mougini-Mark, 1981; Boyce and Mougini-Mark, 2006), while others suggest the opposite (e.g., Osinski, 2006; Osinski et al., 2011; Weiss and Head, 2013, 2014; Wulf and Kenkmann, 2015). It has also been proposed that the outer layer is emplaced both before and after the inner layer (e.g., Komatsu et al., 2007). Regardless of chronological order, most models agree that at least one layer is emplaced ballistically with subsequent radial flow, generally the first layer emplaced. Because we have shown that surface and target properties affect the morphometry of DLEs, we should be able to establish which layer of ejecta was likely emplaced first (e.g., inner or outer), using results from our two DLE groups (non-volcanic and volcanic). The first layer of ejecta emplaced should be directly affected by surface properties (i.e., cohesiveness and volatile content) proximal to the transient crater, while the second layer of ejecta emplaced should principally be affected by the upper surface properties of the first layer of ejecta. For example, impact into an unconsolidated, volatile-rich target should result in an ejecta layer with a higher EM value than an ejecta layer derived from impact into a solid, volatile-poorer target. Subsequent layer(s) of ejecta (i.e., the second layer) would travel atop of a fragmental, unconsolidated first layer of ejecta, thereby, limiting the effect of pre-impact target surface on the emplacement of the subsequent layer. Because the effect of the initial target surface is essentially eliminated for subsequent ejecta layers, volatile content should be the dominant property controlling runout of the second ejecta layer and would be dependent on concentrations within the target (i.e., more volatiles = greater runout). In

theory, we should be able to determine which layer of ejecta (i.e., inner or outer) was emplaced first by observing EM values between DLEs situated on volcanic targets to those on sedimentary targets. Because there are distinct contrasts between target properties (e.g., cohesiveness of the surface, concentration of volatiles), the overall difference in EM between one layer of ejecta (i.e., inner or outer) of both groups (i.e., volcanic and non-volcanic DLEs) should be greater than the difference between the other layer. The layer (i.e., inner or outer) that has the greatest difference between both groups (i.e., volcanic and non-volcanic DLEs) likely represents the first layer emplaced. Figures 3 and 4 show some separation between the outer layers of both groups, while the inner layers show much less. Outer layers of the non-volcanic DLEs have larger EM values compared to the EM of the outer layer of volcanic DLEs. This suggests that the EM of the outer layers were affected more by the pre-impact target surface than the inner layers and suggests the outer layer is emplaced before the inner layer. Inner layers also, collectively, show a subtle increase of EM with latitude and support our suggestion of emplacement of subsequent ejecta layers (in this case, the inner layer) being largely affected by volatile content. This is based on subsurface volatile concentrations on Mars increasing with latitude (Rossbacher and Judson, 1981; Clifford, 1993; Clifford and Parker, 2001; Clifford et al., 2010).

3.5 Summary

We have shown that an impact into a sedimentary target will yield ejecta that is morphometrically different from that of an impact into a volcanic target. This is likely due to the strength contrast between the two lithologies plus their ability to host volatile-rich materials. The differences between the outer layer EM of the two groups is greater than the differences for the inner layer EM. This holds implications that the outer layer is affected by surface properties more than the inner layer and is also emplaced before the inner layer. Results from this study suggest that volatile content in the subsurface is the main variable controlling EM variations with latitude. In addition, target lithology seems to be the main variable controlling lobateness while the addition of volatiles will be an aiding variable. In summary, we suggest that impact into a sedimentary, volatile-rich target can enhance mobility and allow ejecta to runout further (higher EM) at

approximately equal distances (lower lobateness) while ejecta derived from impact into volcanic rock will experience more drag on the surface resulting in lower EM and higher lobateness.

3.6 References

- Attewell, P.B., Farmer, I.W., 1976. *Principles of Engineering Geology*. Chapman and Hall, London.
- Baloga, S.M., Fagents, S.A., Mouginis-Mark, P.J., 2005. Emplacement of Martian rampart crater deposits. *J. Geophys. Res.* 110. doi:10.1029/2004JE002338.
- Barlow, N.G., 1988. Crater size-frequency distributions and a revised Martian relative chronology. *Icarus* 75, 285–305. doi:10.1016/0019-1035(88)90006-1.
- Barlow, N.G., 1994. Sinuosity of Martian rampart ejecta deposits. *J. Geophys. Res.* 99, 10927 – 10935. doi:10.1029/94JE00636.
- Barlow, N.G., 2004. Martian subsurface volatile concentrations as a function of time: Clues from layered ejecta craters. *Geophys. Res. Lett.* 31, L05703. doi:10.1029/2003GL019075.
- Barlow, N.G., 2005. A review of Martian impact crater ejecta structures and their implications for target properties, in: Kenkmann, T., Hörz, F., Deutsch, A. (Eds.), *Large Meteorite Impacts III*, Geol. Soc. Am. Spec. Pap. 384. pp. 433 – 442.
- Barlow, N.G., 2006. Impact craters in the northern hemisphere of Mars: Layered ejecta and central pit characteristics. *Meteorit. Planet. Sci.* 41, 1425–1436. doi:10.1111/j.1945-5100.2006.tb00427.x.
- Barlow, N.G., 2007. New insights into impact crater morphologies from the revised Catalog of Large Martian Impact Craters. Seventh Int. Conf. Mars Abstract #3347.
- Barlow, N.G., Bradley, T.L., 1990. Martian impact craters: Correlations of ejecta and interior morphologies with diameter, latitude, and terrain. *Icarus* 87, 156–179.

- Barlow, N.G., Perez, C.B., 2003. Martian impact crater ejecta morphologies as indicators of the distribution of subsurface volatiles. *J. Geophys. Res.* 108, 5085. doi:10.1029/2002JE002036.
- Barlow, N.G., Boyce, J.M., Costard, F.M., Craddock, R.A., Garvin, J.B., Sakimoto, S.E.H., Kuzmin, R.O., Roddy, D.J., Soderblom, L.A., 2000. Standardizing the nomenclature of Martian impact crater ejecta morphologies. *J. Geophys. Res.* 105, 26733 – 26738.
- Barlow, N.G., Boyce, J.M., Cornwall, C., 2014. Martian Low-Aspect-Ratio Layered Ejecta (LARLE) craters: Distribution, characteristics, and relationship to pedestal craters. *Icarus* 239, 186–200. doi:10.1016/j.icarus.2014.05.037.
- Barnouin-Jha, O.S., Schultz, P.H., 1998. Lobateness of impact ejecta deposits from atmospheric interactions. *J. Geophys. Res.* 103, 25739 – 25756.
- Barnouin-Jha, O.S., Schultz, P.H., Lever, J.H., 1999a. Investigating the interactions between an atmosphere and an ejecta curtain 1. Wind tunnel tests. *J. Geophys. Res.* 104, 27105–27115.
- Barnouin-Jha, O.S., Schultz, P.H., Lever, J.H., 1999b. Investigating the interactions between an atmosphere and an ejecta curtain 2. Numerical experiments. *J. Geophys. Res.* 104, 27117–27131.
- Boyce, J.M., Mougini-Mark, P.J., 2006. Martian craters viewed by the Thermal Emission Imaging System instrument: Double-layered ejecta craters. *J. Geophys. Res.* 111. doi:10.1029/2005JE002638.
- Boyce, J.M., Barlow, N.G., Mougini-Mark, P.J., Stewart, S., 2010. Rampart craters on Ganymede: Their implications for fluidized ejecta emplacement. *Meteorit. Planet. Sci.* 45, 638–661. doi:10.1111/j.1945-5100.2010.01044.x.
- Brace, W.F., 1980. Permeability of crystalline and argillaceous rocks. *Int. J. Rock Mech. Min. Sci. Geomech. Abstr.* 17, 241–251. doi:10.1016/0148-9062(80)90807-4.

- Carr, M.H., 1986. Mars: A water-rich planet? *Icarus* 68, 187–216. doi:10.1016/0019-1035(86)90019-9.
- Carr, M.H., Head, J.W., 2010. Geologic history of Mars. *Earth Planet. Sci. Lett.* 294, 185–203. doi:10.1016/j.epsl.2009.06.042.
- Carr, M.H., Crumpler, L.S., Cutts, J.A., Greeley, R., Guest, J.E., Masursky, H., 1977. Martian impact craters and emplacement of ejecta by surface flow. *J. Geophys. Res.* 82, 4055–4065. doi:10.1029/JS082i028p04055.
- Cattermole, P., 1990. Volcanic flow development at Alba Patera, Mars. *Icarus* 83, 453–493. doi:10.1016/0019-1035(90)90079-O.
- Christensen, P.R., Jakosky, B.M., Kieffer, H.H., Malin, M.C., McSween, H.Y., Neelson, K., Mehall, G.L., Silverman, S.H., Ferry, S., Caplinger, M., Ravine, M., 2004. The thermal emission imaging system (THEMIS) for the Mars 2001 Odyssey mission. *Space Sci. Rev.* 110, 85–130.
- Christensen, P.R., Engle, E., Anwar, S., Dickenshied, S., Noss, D., Gorelick, N., Weiss-Malik, M., 2009. JMARS - A planetary GIS. AGU Fall Meet. Abstract #IN22A-06.
- Clifford, S.M., 1993. A model for the hydrologic and climatic behavior of water on Mars. *J. Geophys. Res.* 98, 10973–11016. doi:10.1029/93JE00225.
- Clifford, S.M., Parker, T.J., 2001. The evolution of the Martian hydrosphere: Implications for the fate of a primordial ocean and the current state of the northern plains. *Icarus* 154, 40–79. doi:10.1006/icar.2001.6671.
- Clifford, S.M., Lasue, J., Heggy, E., Boisson, J., McGovern, P., Max, M.D., 2010. Depth of the Martian cryosphere: Revised estimates and implications for the existence and detection of subpermafrost groundwater. *J. Geophys. Res.* 115. doi:10.1029/2009JE003462.
- Costard, F.M., 1989. The spatial distribution of volatiles in the Martian hydrolithosphere. *Earth. Moon. Planets* 45, 265–290.

- Crown, D.A., Price, K.H., Greeley, R., 1992. Geologic evolution of the east rim of the Hellas basin, Mars. *Icarus* 100, 1–25. doi:10.1016/0019-1035(92)90014-X.
- Davis, P.A., Golombek, M.P., 1990. Discontinuities in the shallow Martian crust at Lunae, Syria, and Sinai Plana. *J. Geophys. Res.* 95, 14231–14248. doi:10.1029/JB095iB09p14231.
- Edwards, C.S., Nowicki, K.J., Christensen, P.R., Hill, J., Gorelick, N., Murray, K., 2011. Mosaicking of global planetary image datasets: 1. Techniques and data processing for Thermal Emission Imaging System (THEMIS) multi-spectral data. *J. Geophys. Res.* 116, E10008. doi:10.1029/2010JE003755.
- Fastook, J.L., Head, J.W., Forget, F., Madeleine, J.-B., Marchant, D.R., 2011. Evidence for Amazonian northern mid-latitude regional glacial landsystems on Mars: Glacial flow models using GCM-driven climate results and comparisons to geological observations. *Icarus* 216, 23–39. doi:10.1016/j.icarus.2011.07.018.
- Fuller, E.R., Head, J.W., 2002. Amazonis Planitia: The role of geologically recent volcanism and sedimentation in the formation of the smoothest plains on Mars. *J. Geophys. Res.* 107, 5081. doi:10.1029/2002JE001842.
- Gault, D.E., Greeley, R., 1978. Exploratory experiments of impact craters formed in viscous-liquid targets: Analogs for Martian rampart craters? *Icarus* 34, 486–495. doi:10.1016/0019-1035(78)90040-4.
- Greeley, R., Guest, J.E., 1987. Geologic map of the eastern equatorial region of Mars (1:15,000,000). USGS Misc. Inv. Ser. Map I-1802-B.
- Greeley, R., Crown, D.A., 1990. Volcanic geology of Tyrrhena Patera, Mars. *J. Geophys. Res.* 95, 7133–7149.
- Gregg, T.K.P., Farley, M.A., 2006. Mafic pyroclastic flows at Tyrrhena Patera, Mars: Constraints from observations and models. *J. Volcanol. Geotherm. Res.* 155, 81–89. doi:10.1016/j.jvolgeores.2006.02.008.

- Hartmann, W.K., Berman, D.C., 2000. Elysium Planitia lava flows: Crater count chronology and geological implications. *J. Geophys. Res.* 105, 15011 – 15025.
- Head, J.W., Kreslavsky, M.A., Pratt, S., 2002. Northern lowlands of Mars: Evidence for widespread volcanic flooding and tectonic deformation in the Hesperian Period. *J. Geophys. Res.* 107, 5003.
- Head, J.W., Mustard, J.F., Kreslavsky, M.A., Milliken, R.E., Marchant, D.R., 2003. Recent ice ages on Mars. *Nature* 426, 797–802. doi:10.1038/nature02114.
- Head, J.W., Neukum, G., Jaumann, R., Hiesinger, H., Hauber, E., Carr, M.H., Masson, P., Foing, B., Hoffmann, H., Kreslavsky, M., Werner, S., Milkovich, S., van Gasselt, S., 2005. Tropical to mid-latitude snow and ice accumulation, flow and glaciation on Mars. *Nature* 434, 346–351.
- Head, J.W., Marchant, D.R., Agnew, M.C., Fassett, C.I., Kreslavsky, M.A., 2006. Extensive valley glacier deposits in the northern mid-latitudes of Mars: Evidence for Late Amazonian obliquity-driven climate change. *Earth Planet. Sci. Lett.* 241, 663–671. doi:10.1016/j.epsl.2005.11.016.
- Head, J.W., Marchant, D.R., Dickson, J.L., Kress, A.M., Baker, D.M., 2010. Northern mid-latitude glaciation in the Late Amazonian period of Mars: Criteria for the recognition of debris-covered glacier and valley glacier landsystem deposits. *Earth Planet. Sci. Lett.* 294, 306–320. doi:10.1016/j.epsl.2009.06.041.
- Hiesinger, H., Head, J.W., 2004. The Syrtis Major volcanic province, Mars: Synthesis from Mars Global Surveyor data. *J. Geophys. Res.* 109, E01004. doi:10.1029/2003JE002143.
- Hill, J., Edwards, C.S., Christensen, P.R., 2014. Mapping the Martian surface with THEMIS global infrared mosaics. Eighth Int. Conf. Mars Abstract #1141.
- Hörz, F., Ostertag, R., Rainey, D.A., 1983. Bunte Breccia of the Ries: Continuous deposits of large impact craters. *Rev. Geophys. Sp. Phys.* 21, 1667–1725.

- Iverson, R.M., 1997. The physics of debris flows. *Rev. Geophys.* 35, 245–296.
- Iverson, R.M., 2003. The debris-flow rheology myth. 3rd Int. Conf. Debris-Flow Hazards Mitig. Mech. Predict. Assess. 303–314.
- Iverson, R.M., LaHusen, R.G., 1993. Friction in Debris Flows: Inferences from Large-scale Flume Experiments. in: *Hydraulic Engineering (1993)*. Hsieh Wen Shen, S.T. Su, Feng Wen (eds). Proc. 1993 Conf., San Fr. CA, July 25-30, 1993. Am. Soc. Civ. Eng. 1604–1609.
- Iverson, R.M., Logan, M., LaHusen, R.G., Berti, M., 2010. The perfect debris flow? Aggregated results from 28 large-scale experiments. *J. Geophys. Res.* 115, F03005. doi:10.1029/2009JF001514.
- Johansen, L.A., 1979. The latitude dependence of Martian splosted cratering and its relationship to water. *Rep. Planet. Geol. Prog. 1978-1979*, NASA Tech. Memo., 80339 123–125.
- Jones, E., Osinski, G.R., 2015. Using martian single and double layered ejecta craters to probe subsurface stratigraphy. *Icarus* 247, 260–278. doi:10.1016/j.icarus.2014.10.016.
- Kadish, S.J., Head, J.W., 2011. Impacts into non-polar ice-rich paleodeposits on Mars: Excess ejecta craters, perched craters and pedestal craters as clues to Amazonian climate history. *Icarus* 215, 34–46. doi:10.1016/j.icarus.2011.07.014.
- Kargel, J.S., 1986. Morphologic variations of Martian rampart crater ejecta and their dependencies and implications. *Lunar Planet. Sci.* XVII 410–411.
- Kargel, J.S., 1989. First and second-order equatorial symmetry of Martian rampart crater ejecta morphologies. *Fourth Int. Conf. Mars* 132–133.
- Komatsu, G., Ori, G.G., Di Lorenzo, S., Rossi, A.P., Neukum, G., 2007. Combinations of processes responsible for Martian impact crater “layered ejecta structures” emplacement. *J. Geophys. Res.* 112. doi:10.1029/2006JE002787.

- Kreslavsky, M.A., Head, J.W., 2002. Fate of outflow channel effluents in the northern lowlands of Mars: The Vastitas Borealis Formation as a sublimation residue from frozen ponded bodies of water. *J. Geophys. Res.* 107, 5121. doi:10.1029/2001JE001831.
- Li, L., Yue, Z., Di, K., Peng, M., 2015. Observations of Martian layered ejecta craters and constraints on their formation mechanisms. *Meteorit. Planet. Sci.* 50, 508–522. doi:10.1111/maps.12438.
- Lucchitta, B.K., Ferguson, H.M., Summers, C., 1986. Sedimentary deposits in the Northern Lowland Plains, Mars. *J. Geophys. Res.* 91, E166–E174. doi:10.1029/JB091iB13p0E166.
- MacKinnon, D.J., Tanaka, K.L., 1988. A two-layer hydrologic model for the impacted Martian crust. *Lunar Planet. Sci. Conf. XIX* 707–708.
- Madeleine, J.-B., Forget, F., Head, J.W., Levrard, B., Montmessin, F., Millour, E., 2009. Amazonian northern mid-latitude glaciation on Mars: A proposed climate scenario. *Icarus* 203, 390–405. doi:10.1016/j.icarus.2009.04.037.
- Major, J.J., 1997. Depositional Processes in Large-Scale Debris-Flow Experiments. *J. Geol.* 105, 345–366.
- Major, J.J., Iverson, R.M., 1999. Debris-flow deposition: Effects of pore-fluid pressure and friction concentrated at flow margins. *Geol. Soc. Am. Bull.* 111, 1424–1434.
- Malin, M.C., Bell, J.F., Cantor, B.A., Caplinger, M.A., Calvin, W.M., Clancy, R.T., Edgett, K.S., Edwards, L., Haberle, R.M., James, P.B., Lee, S.W., Ravine, M.A., Thomas, P.C., Wolff, M.J., 2007. Context Camera Investigation on board the Mars Reconnaissance Orbiter. *J. Geophys. Res.* 112, E05S04. doi:10.1029/2006JE002808.
- McGill, G.E., 1989. Buried topography of Utopia, Mars: Persistence of a giant impact depression. *J. Geophys. Res.* 94, 2753–2759. doi:10.1029/JB094iB03p02753.

- Mellon, M.T., Arvidson, R.E., Marlow, J.J., Phillips, R.J., Asphaug, E., 2008. Periglacial landforms at the Phoenix landing site and the northern plains of Mars. *J. Geophys. Res.* 113, E00A23. doi:10.1029/2007JE003039.
- Melosh, H.J., 1989. *Impact Cratering: A Geologic Process*. Oxford University Press, 245 p.
- Mouginis-Mark, P.J., 1979. Martian fluidized crater morphology: Variations with crater size, latitude, altitude, and target material. *J. Geophys. Res.* 84, 8011 – 8022. doi:10.1029/JB084iB14p08011.
- Mouginis-Mark, P.J., 1981. Ejecta emplacement and modes of formation of Martian fluidized ejecta craters. *Icarus* 45, 60–76. doi:10.1016/0019-1035(81)90006-3.
- Mouginis-Mark, P.J., 1987. Water or ice in the Martian regolith?: Clues from rampart craters seen at very high resolution. *Icarus* 71, 268–286. doi:10.1016/0019-1035(87)90152-7.
- Mouginis-Mark, P.J., Boyce, J.M., 2004. The unique characteristics of double layered ejecta craters on Mars. *Eos Trans. AGU*, 85, Fall Meet. Suppl. Abstract #P33B–04.
- Mustard, J.F., Erard, S., Bibring, J.-P., Head, J.W., Hurtrez, S., Langevin, Y., Pieters, C.M., Sotin, C.J., 1993. The surface of Syrtis Major: Composition of the volcanic substrate and mixing with altered dust and soil. *J. Geophys. Res.* 98, 3387 – 3400. doi:10.1029/92JE02682.
- Oberbeck, V.R., 1975. The role of ballistic erosion and sedimentation in Lunar stratigraphy. *Rev. Geophys. Sp. Phys.* 13, 337–362.
- Oberbeck, V.R., 2009. Layered ejecta craters and the early water/ice aquifer on Mars. *Meteorit. Planet. Sci.* 44, 43–54. doi:10.1111/j.1945-5100.2009.tb00716.x.
- Osinski, G.R., 2006. Effect of volatiles and target lithology on the generation and emplacement of impact crater fill and ejecta deposits on Mars. *Meteorit. Planet. Sci.* 41, 1571–1586. doi:10.1111/j.1945-5100.2006.tb00436.x.

- Osinski, G.R., Tornabene, L.L., Grieve, R.A.F., 2011. Impact ejecta emplacement on terrestrial planets. *Earth Planet. Sci. Lett.* 310, 167–181. doi:10.1016/j.epsl.2011.08.012.
- Osinski, G.R., Grieve, R.A.F., Tornabene, L.L., 2013. Excavation and impact ejecta emplacement, in: Osinski, G.R., Pierazzo, E. (Eds.), *Impact Cratering: Processes and Products*, pp. 43–59.
- Platz, T., Michael, G., 2011. Eruption history of the Elysium Volcanic Province, Mars. *Earth Planet. Sci. Lett.* 312, 140–151. doi:10.1016/j.epsl.2011.10.001.
- Plaut, J.J., Safaeinili, A., Holt, J.W., Phillips, R.J., Head, J.W., Seu, R., Putzig, N.E., Frigeri, A., 2009. Radar evidence for ice in lobate debris aprons in the mid-northern latitudes of Mars. *Geophys. Res. Lett.* 36, L02203. doi:10.1029/2008GL036379.
- Plescia, J.B., 1993. Wrinkle ridges of Arcadia Planitia, Mars. *J. Geophys. Res.* 98, 15049–15059. doi:10.1029/93JE01324.
- Rossbacher, L.A., Judson, S., 1981. Ground ice on Mars: Inventory, distribution, and resulting landforms. *Icarus* 45, 39–59. doi:10.1016/0019-1035(81)90005-1.
- Rotto, S., Tanaka, K.L., 1995. Geologic/geomorphologic map of the Chryse Planitia region of Mars (1:5,000,000). USGS map I-2441.
- Schaber, G.G., 1982. Syrtis Major: A Low-Relief Volcanic Shield. *J. Geophys. Res.* 87, 9852–9866.
- Schneeberger, D.M., Pieri, D.C., 1991. Geomorphology and stratigraphy of Alba Patera, Mars. *J. Geophys. Res.* 96, 1907–1930.
- Schultz, P.H., 1992. Atmospheric effects on ejecta emplacement. *J. Geophys. Res.* 97, 11623–11662. doi:10.1029/92JE00613.
- Schultz, P.H., Gault, D.E., 1979. Atmospheric effects on martian ejecta emplacement. *J. Geophys. Res.* 84, 7669–7687.

- Scott, D.H., Tanaka, K.L., 1986. Geologic map of the western equatorial region of Mars (1:15,000,000). USGS Misc. Inv. Ser. Map I-1802-A.
- Skinner, J.A., Hare, T.M., Tanaka, K.L., 2006. Digital renovation of the atlas of Mars 1:15,000,000-scale global geologic series maps. *Lunar Planet. Sci. XXXVII* Abstract #2331.
- Smith, D.E., Zuber, M.T., Frey, H. V., Garvin, J.B., Head, J.W., Muhleman, D.O., Pettengill, G.H., Phillips, R.J., Solomon, S.C., Zwally, H.J., Banerdt, W.B., Duxbury, T.C., Golombek, M.P., Lemoine, F.G., Neumann, G.A., Rowlands, D.D., Aharonson, O., Ford, P.G., Ivanov, A.B., Johnson, C.L., McGovern, P.J., Abshire, J.B., Afzal, R.S., Sun, X., 2001. Mars Orbiter Laser Altimeter: Experiment summary after the first year of global mapping of Mars. *J. Geophys. Res.* 106, 23689–23722. doi:10.1029/2000JE001364.
- Souness, C., Hubbard, B., 2012. Mid-latitude glaciation on Mars. *Prog. Phys. Geogr.* 36, 238–261. doi:10.1177/0309133312436570.
- Tanaka, K.L., 1997. Sedimentary history and mass flow structures of Chryse and Acidalia Planitiae, Mars. *J. Geophys. Res.* 102, 4131–4149. doi:10.1029/96JE02862.
- Tanaka, K.L., Skinner, J.A., Hare, T.M., Joyal, T., Wenker, A., 2003. Resurfacing history of the northern plains of Mars based on geologic mapping of Mars Global Surveyor data. *J. Geophys. Res.* 108, 8043. doi:10.1029/2002JE001908.
- Tanaka, K.L., Skinner, J.A., Dohm, J.M., Irwin, R.P., Kolb, E.J., Fortezzo, C.M., Platz, T., Michael, G.G., Hare, T.M., 2014. Geologic map of Mars (1:20,000,000). USGS Sci. Investig. Map 3292.
- Thomson, B.J., Head, J.W., 2001. Utopia Basin, Mars: Characterization of topography and morphology and assessment of the origin and evolution of basin internal structure. *J. Geophys. Res.* 106, 23209–23230. doi:10.1029/2000JE001355.
- Weiss, D.K., Head, J.W., 2013. Formation of double-layered ejecta craters on Mars: A glacial substrate model. *Geophys. Res. Lett.* 40, 3819–3824. doi:10.1002/grl.50778.

- Weiss, D.K., Head, J.W., 2014. Ejecta mobility of layered ejecta craters on Mars: Assessing the influence of snow and ice deposits. *Icarus* 233, 131–146. doi:10.1016/j.icarus.2014.01.038.
- Wohletz, K.H., Sheridant, M.F., 1983. Martian Rampart Crater Ejecta: Experiments and Analysis of Melt-Water Interaction. *Icarus* 37, 15–37.
- Wulf, G., Kenkmann, T., 2015. High-resolution studies of double-layered ejecta craters: Morphology, inherent structure, and a phenomenological formation model. *Meteorit. Planet. Sci.* 1–31. doi:10.1111/maps.12416.

Chapter 4

4 Conclusions

Layered ejecta morphologies on Mars have been an intriguing crater morphology since being first recognized by the Mariner 9 spacecraft in the early 1970's (e.g., McCauley, 1973). Even more so is why and how 3 different types of these morphologies are produced (i.e., SLE, DLE, and MLEs). While it may be easy to explain how one layer of ejecta is emplaced (i.e., SLE), two or more layers (i.e., DLEs and MLEs) has proven to be more difficult. Considering the current theory that layered ejecta morphologies are emplaced as a ground-hugging flow (e.g., Carr et al., 1977), the target must have some effect on this emplacement process which may influence the type of morphology formed (e.g., SLE, DLE, or MLE). This study did not focus on how or why one morphology forms over others, but to what effect the nature of the target has on final morphology and morphometry of DLEs. These results may provide insight into the nature of the emplacement process. DLEs in this study were split into two groups based on being situated on terrains that are largely interpreted as either volcanic or sedimentary. Analysis included measuring ejecta mobility (EM) and lobateness (Γ) of each ejecta layer in addition to the documentation of radial grooves. Major results from this study include:

- Not all DLEs display the radial groove pattern that was originally suggested as a characteristic DLE feature and that the majority of DLEs without grooves are located $\pm 25^\circ$ equatorward. Instead, a base surge mechanism occurring after the emplacement of ejecta layers is proposed where larger, stronger surges etch grooves into ejecta and smaller, weaker surges do not. The presence of surficial dust and abundant volatile content at higher latitudes may produce to a larger, stronger base surge which may etch grooves into ejecta layers. DLEs impacting into less dusty and volatile-poorer (but not absent) targets may have produced a smaller surge that is not strong enough to etch grooves into ejecta.

- Surficial dust and/or sediments may contribute to longer ejecta runout distances (i.e., EM). This is based off of studies over the Bunte Breccia (ejecta blanket) at the Ries Crater where ejecta ran out farther in areas where loose unconsolidated sediments were present at the surface and less in places where competent Malm limestone was present (e.g., Hörz et al., 1983). Results from this thesis suggests that this phenomenon may be analogous to layered ejecta emplacement on Mars, where DLEs situated on targets that are largely interpreted as unconsolidated sediments had slightly greater EM values than those situated on largely volcanic (e.g., basaltic lavas) targets. Thick accumulations of dust may produce similar results. Volcanic DLEs in heavily dusty areas had slightly greater EM values than volcanic DLEs in less dusty areas.
- EM of both ejecta layers generally increases with increasing latitude and is most apparent for the outer layers. This is consistent with near-surface volatile concentrations on Mars increasing with increasing latitude. More volatiles incorporated into an ejecta blanket will make ejecta less viscous and may enhance fluidization. Because EM increases with latitude for both volcanic and non-volcanic DLEs, volatile content is suggested to be the main variable controlling EM.
- The lobateness of both ejecta layers generally decreases with increasing latitude. Frictional resistance between the ejecta and target is suggested to contribute to this trend and is based on comparisons to debris flow rheology and deposition. Greater frictional resistance can be expected to produced more pronounced lobes, equating to a higher lobateness, while less frictional resistance may produce more subdued lobes and a lower lobateness. The combination of abundant volatiles and surficial sediment/dust at higher latitudes would reduce friction between ejecta and target while more friction would be expected at lower latitudes, where there is less volatiles and sediment/dust, leaving solid rock exposed at the surface.

- The outer layer of ejecta is likely emplaced first. Outer layer EM values show a notable distinction between the volcanic and non-volcanic DLEs, while inner layer EM values show less of a distinction between the two groups. This suggests that the outer layer was affected by the surface properties (e.g., cohesiveness) of the target much more than the inner layer and suggests that the inner layer is emplaced after the outer layer. An already emplaced outer layer may provide a similar surface (e.g., unconsolidated material that makes up the ejecta blanket) on which the inner layer can travel upon regardless of target type (e.g., basaltic rock or sediments).

4.1 Future Work

There are multiple studies that may be conducted as a continuation of the work and ideas presented in this thesis. Three are described below.

1. Interpretations from this work are based largely off of terrestrial analogs (i.e., Ries impact structure, Germany) and large-scale experimental debris flows. While debris flow rheology may be the best analog for layered ejecta during emplacement, it lacks a comparable mechanism for the initiation of movement of material. For example, debris flows are largely triggered by instability and failure that gain momentum from gravity (e.g., Iverson, 1997), whereas, the momentum for impact ejecta is initiated by being thrown out of the transient crater at high velocities (e.g., Melosh, 1989). In addition, before mobility of ejecta across the surface, it was airborne and inevitably struck the ground before becoming a mobile surface flow of material. How does the frictional resistance and rheology compare between layered ejecta and debris flows over various surface mediums (e.g., loose sediment vs competent rock)? Gault and Greeley (1978) conducted small-scale experiments on impacts into a mud target that replicated layered ejecta morphologies, but did not consider the effect frictional resistance has on these morphologies. Further impact cratering and/or debris flow experiments should be carried out to investigate frictional resistance behaviors between debris and target surface properties (e.g., unconsolidated sediments vs competent rock)

and its relationship to final morphology. This can be used to support or dismiss implications of this study.

2. DLEs analyzed in this study are situated on targets that are largely interpreted as being either volcanic or sedimentary (e.g., Greeley and Guest, 1987; Scott and Tanaka, 1986; Tanaka et al., 2014). In addition, the geologic units included are all Hesperian-aged or younger, cover roughly half the planet, and are largely located in the northern hemisphere. Not included is the older, Noachian-aged southern half of the planet which consists of heavily degraded, undifferentiated materials (e.g., Greeley and Guest, 1987; Scott and Tanaka, 1986; Tanaka et al., 2014). The strength properties between volcanic and sedimentary targets are greatly contrasted and as Chapter 3 has suggested effects the morphometric properties of ejecta. How would the morphometric properties of DLEs on these older heavily degraded, undifferentiated Noachian terrains compare to the younger terrains included in this study?
3. Results from this study of the radial groove pattern found on some DLEs suggest that they are primarily located on DLEs $\pm 25^\circ$ poleward. However, DLEs analyzed in this study were only a handful (206) of the over 1300 globally distributed ones (reevaluated from Robbins and Hynes (2012)) with a large portion of them being located in the northern hemisphere. In addition, careful investigation of burial or erosional processes on the DLEs with an absence of grooves was only examined in detail on a select few of these DLEs. Still, it is difficult to imagine a mere coincidence that grooves on the majority of DLEs in this study $\pm 25^\circ$ equatorward have all been obscured by burial or erosional processes. A complete quantitative study documenting the presence or absence of radial grooves on DLE ejecta blankets should be carried out to investigate whether the lack of grooves are a primary or secondary (e.g., burial or erosional) phenomenon.

4.2 References

- Carr, M.H., Crumpler, L.S., Cutts, J.A., Greeley, R., Guest, J.E., Masursky, H., 1977. Martian impact craters and emplacement of ejecta by surface flow. *J. Geophys. Res.* 82, 4055–4065. doi:10.1029/JS082i028p04055.
- Gault, D.E., Greeley, R., 1978. Exploratory experiments of impact craters formed in viscous-liquid targets: Analogs for Martian rampart craters? *Icarus* 34, 486–495. doi:10.1016/0019-1035(78)90040-4.
- Greeley, R., Guest, J.E., 1987. Geologic map of the eastern equatorial region of Mars (1:15,000,000). USGS Misc. Inv. Ser. Map I-1802-B.
- Hörz, F., Ostertag, R., Rainey, D.A., 1983. Bunte Breccia of the Ries: Continuous deposits of large impact craters. *Rev. Geophys. Sp. Phys.* 21, 1667–1725.
- Iverson, R.M., 1997. The physics of debris flows. *Rev. Geophys.* 35, 245–296.
- McCauley, J.F., 1973. Mariner 9 evidence for wind erosion in the equatorial and mid-latitude regions of Mars. *J. Geophys. Res.* 78, 4123–4137. doi:10.1029/JB078i020p04123.
- Melosh, H.J., 1989. *Impact Cratering: A Geologic Process*. Oxford University Press, 245 p.
- Robbins, S.J., Hynek, B.M., 2012. A new global database of Mars impact craters ≥ 1 km: 1. Database creation, properties, and parameters. *J. Geophys. Res.* 117. doi:10.1029/2011JE003966.
- Scott, D.H., Tanaka, K.L., 1986. Geologic map of the western equatorial region of Mars (1:15,000,000). USGS Misc. Inv. Ser. Map I-1802-A.
- Tanaka, K.L., Skinner, J.A., Dohm, J.M., Irwin, R.P., Kolb, E.J., Fortezzo, C.M., Platz, T., Michael, G.G., Hare, T.M., 2014. Geologic map of Mars (1:20,000,000). USGS Sci. Investig. Map 3292.

Appendices

Appendix A: Morphometry and location of each crater included in this study

Table A.0.1 - Volcanic DLEs

Latitude	Longitude (E)	Diameter (km)	Geologic unit	Out. EM	Out. Γ	In. EM	In. Γ
31.689	266.849	6.9	AHcf	2.347	1.394	1.588	1.386
40.766	254.606	7.3	Aam	2.269	1.557	1.263	1.382
38.152	276.030	18.3	Htl	2.922	1.578	1.548	1.553
38.144	272.914	3.0	Htl	2.620	1.374	1.314	1.264
39.003	258.274	8.9	Aam	2.321	1.478	1.405	1.334
44.133	268.867	6.8	Htm	2.714	1.357	1.515	1.255
45.269	272.010	5.9	Htm	2.576	1.591	1.620	1.345
46.049	266.701	4.6	Aam	2.861	1.537	1.353	1.303
56.399	263.175	12.9	Hal	2.961	1.505	1.615	1.316
32.828	259.455	8.7	AHcf	2.630	1.251	1.391	1.360
39.727	276.544	13.1	Htl	2.863	1.580	1.556	1.324
29.949	274.305	13.3	Ht2	2.728	1.397	1.465	1.443
28.593	272.729	6.5	Ht2	2.188	1.244	1.220	1.251
36.827	231.344	4.5	Hal	2.382	1.230	1.531	1.167
36.967	232.303	12.9	Hal	2.245	1.329	1.139	1.430
41.325	234.619	9.6	Hal	2.072	1.548	1.396	1.347
37.787	232.975	12.4	Hal	2.858	1.384	1.588	1.428
37.159	237.113	6.7	Hal	2.336	1.386	1.349	1.331
31.530	231.536	16.4	Hal	2.766	1.374	1.648	1.395
31.253	243.248	14.7	Hal	2.704	1.289	1.223	1.227
45.289	269.743	9.2	Hal	3.074	1.611	1.395	1.305
45.687	272.263	7.5	Htm	3.122	1.632	1.271	1.248
26.419	270.416	14.2	Hf	1.764	1.503	1.347	1.627
26.031	274.647	24.0	Ht2	1.930	1.603	1.160	1.496
43.245	225.798	6.4	Hal	2.723	1.288	1.533	1.213

32.547	281.983	5.7	Hr	2.674	1.230	1.376	1.191
40.531	214.605	17.8	Aa1	3.731	1.253	2.099	1.202
39.803	217.165	8.8	Aa3	2.764	1.391	1.440	1.204
44.661	210.402	8.9	Aa1	3.063	1.225	1.534	1.155
30.803	297.610	18.1	Hr	2.409	1.378	1.579	1.368
58.453	265.129	17.9	Hal	3.099	1.297	1.699	1.270
53.333	288.847	8.9	Aa1	2.423	1.335	1.381	1.211
30.497	283.362	14.8	Hr	2.921	1.209	1.517	1.267
55.584	268.691	11.7	Hal	2.882	1.313	1.607	1.187
53.273	283.154	9.5	Aa1	2.592	1.299	1.526	1.164
40.279	225.932	12.6	Aa3	3.246	1.526	1.978	1.240
38.044	213.677	13.3	Aa3	3.116	1.600	1.351	1.363
53.748	276.208	6.8	Hal	2.327	1.476	1.446	1.277
10.444	287.746	19.1	Hr	2.181	1.479	1.268	1.313
6.839	297.494	11.9	Hr	1.786	1.312	1.284	1.498
6.807	296.503	16.7	Hr	1.952	1.550	1.323	1.596
9.834	288.961	11.9	Hr	1.689	1.457	1.108	1.382
17.908	287.405	5.1	Hr	2.207	1.440	1.456	1.352
15.133	292.468	11.4	Hr	1.735	1.512	1.292	1.321
26.423	177.576	3.2	Hr	2.064	1.317	1.255	1.284
36.561	155.460	8.7	Ae11	3.468	1.830	1.429	1.168
25.970	166.631	9.6	Ae11	2.561	2.111	1.499	1.421
32.275	169.191	20.3	Aps	2.899	1.433	1.955	1.298
34.597	149.351	13.4	HNu	2.635	1.500	1.321	1.274
17.262	144.994	9.8	Ae11	1.923	1.607	1.197	1.502
16.384	146.190	6.4	Ae11	2.024	1.673	1.358	1.479
35.773	146.311	5.5	HNu	3.744	1.703	1.663	1.252
9.628	145.628	12.1	Ae11	2.056	1.469	1.304	1.380
6.642	142.693	13.2	Npld	1.902	1.452	1.253	1.398
16.848	156.325	8.5	Ae11	1.842	1.577	1.454	1.454
31.002	178.299	7.2	Hr	2.497	1.480	1.449	1.271

20.115	177.549	6.2	AHpe	2.101	1.471	1.554	1.576
34.051	167.099	5.3	Aps	2.749	1.263	1.353	1.213
31.151	175.602	4.8	Hr	2.424	1.354	1.388	1.316
35.443	158.989	7.7	Ael1	2.794	1.391	1.577	1.236
31.395	178.257	4.9	Hr	2.735	1.261	1.821	1.196
21.829	182.599	6.7	Hr	2.560	1.337	1.512	1.262
32.920	155.414	6.4	Ael1	2.469	1.283	1.500	1.223
34.321	172.016	10.3	Apk	2.776	1.410	1.727	1.222
32.909	165.510	4.3	Aps	2.500	1.231	1.700	1.187
25.279	160.669	17.9	Ael1	2.934	1.375	1.561	1.261
34.814	169.559	8.5	Aps	3.050	1.377	1.604	1.150
25.301	162.873	10.7	Ael1	1.866	1.373	1.417	1.260
-10.206	301.040	5.9	Hr	2.591	2.059	1.920	1.530
-8.721	257.144	19.6	Hsu	2.285	1.988	1.462	1.735
-30.015	303.939	13.2	Hr	2.484	1.348	1.727	1.317
-18.373	292.824	6.4	Hr	2.326	1.547	1.695	1.355
-28.311	306.780	9.9	Hr	2.260	1.480	1.419	1.329
-8.857	273.585	12.9	Hsu	1.717	1.618	1.301	1.533
-12.269	300.295	6.0	Hr	2.435	1.427	1.580	1.193
-15.858	288.776	16.7	Hr	2.613	1.599	1.698	1.719
-11.102	278.538	14.4	Hr	2.141	1.776	1.476	1.619
-18.308	305.221	8.4	Hr	2.045	1.957	1.567	1.851
-14.243	289.935	16.7	Hr	2.380	1.860	1.428	1.641
-15.651	292.439	15.2	Hr	2.591	1.475	1.348	1.463
-19.035	304.366	16.4	Hr	1.701	1.541	0.976	1.659
-21.978	286.497	11.5	Hr	1.737	1.397	1.200	1.380
-14.727	291.692	11.4	Hr	3.028	1.737	1.636	1.749
-17.175	295.738	10.5	Hr	2.186	1.318	1.581	1.315
-2.486	270.332	17.0	Hsu	2.276	1.522	1.347	1.426
-25.345	288.214	11.6	Hf	1.690	1.471	1.320	1.374
-0.471	296.217	19.6	Hr	2.885	1.645	1.685	1.501

-22.335	282.606	16.0	Hr	2.680	1.661	1.611	1.340
-16.893	298.226	4.6	Npl2	2.203	1.488	1.755	1.383
-15.798	275.229	19.2	Hsu	2.542	1.490	1.667	1.590
-21.549	287.807	11.7	Hr	1.983	1.400	1.280	1.332
-7.928	300.251	14.5	Hr	1.865	1.491	1.311	1.433
-9.388	293.337	11.7	Npl2	2.120	1.389	1.545	1.405
-10.523	278.816	8.6	Hsu	2.887	1.983	1.960	1.627
-25.720	294.996	11.7	Hr	2.735	1.271	1.439	1.246
-19.453	266.860	18.3	Hsu	2.427	1.790	1.158	1.315
-23.807	277.774	7.6	Hr	1.863	1.431	1.214	1.255
-23.801	292.058	4.0	Hr	2.007	1.366	1.365	1.249
-35.496	295.290	7.0	Hpl3	2.294	1.352	1.342	1.226
10.423	72.763	16.3	Hs	2.263	1.700	1.549	1.604
9.605	75.466	14.7	Hs	2.312	1.682	1.355	1.649
13.056	72.663	11.6	Hs	2.670	1.569	1.466	1.462
18.459	73.344	15.1	Hs	2.672	1.871	1.399	1.403
14.368	70.048	12.5	Hs	2.085	1.549	1.317	1.362
6.673	74.724	8.1	Hs	1.545	1.529	1.145	1.507
13.896	69.457	10.8	Hs	1.957	1.535	1.316	1.536
8.915	74.328	23.7	Hs	2.491	1.592	1.426	1.442
3.428	76.957	10.2	Hs	2.051	1.559	1.581	1.549
9.999	70.667	15.4	Hs	1.963	1.436	1.526	1.410
-19.330	118.328	16.2	Hr	2.226	1.544	1.299	1.655
-23.236	119.512	14.8	Hr	2.013	1.820	1.323	1.482
-23.801	110.244	14.9	Hr	2.131	1.597	1.192	1.550
-28.547	101.979	8.6	Hr	2.561	1.725	1.437	1.417
-30.141	100.438	12.8	Hr	2.161	1.695	1.208	1.613
-29.799	104.144	7.5	Hr	2.318	1.440	1.366	1.213
-28.217	113.251	8.1	Hr	2.640	1.760	1.433	1.281
-27.175	115.509	9.5	Hr	1.575	1.462	1.085	1.361
-28.225	116.842	15.1	Hr	2.091	1.543	1.169	1.508

-29.723	118.947	14.8	Hr	1.948	1.549	1.182	1.469
-31.314	113.667	5.5	Hr	1.999	1.517	1.442	1.552
-32.638	114.456	19.7	Hr	2.069	1.651	1.253	1.551
-34.880	119.530	8.2	Hr	2.797	1.480	1.468	1.360
-36.647	117.104	9.9	Hr	2.877	1.616	1.542	1.270
-37.115	119.545	6.6	Hr	2.686	1.422	1.509	1.359
-37.906	113.755	8.5	Hr	2.570	1.371	1.420	1.275
-39.644	123.073	7.2	Hr	2.717	1.212	1.727	1.412
-30.618	127.120	4.7	Hr	2.369	1.211	1.437	1.199

Table A.0.2 - Non-volcanic DLEs

Latitude	Longitude (E)	Diameter (km)	Geologic unit	Out. EM	Out. Γ	In. EM	In. Γ
43.461	319.322	14.1	Hvm	2.572	1.396	1.662	1.261
29.999	316.371	14.2	Aa1	2.991	1.500	1.548	1.529
43.356	351.038	12.1	Aa1	3.519	1.347	1.594	1.176
44.269	333.727	12.2	Hvg	3.763	1.503	1.974	1.370
42.542	308.864	10.8	Nple	2.458	1.392	1.573	1.280
63.406	313.745	9.7	Hvk	3.140	1.522	1.925	1.265
35.417	311.208	9.4	Hchp	2.399	1.567	1.695	1.501
44.016	306.741	8.6	Nple	2.709	1.606	1.618	1.289
50.735	303.874	7.7	Npl1	2.646	1.472	1.327	1.279
43.521	339.027	7.3	Hvg	3.386	1.594	1.433	1.170
39.943	305.322	5.7	Nple	1.997	1.326	1.411	1.234
42.926	348.191	5.5	Hvg	3.996	1.380	1.393	1.176
44.896	320.613	4.7	Hvm	3.087	1.327	1.785	1.237
44.302	342.055	4.6	Hvg	3.452	1.246	1.506	1.176
45.172	338.326	4.4	Hvg	2.892	1.280	1.568	1.170
43.561	321.052	4.3	Hvm	3.294	1.257	1.629	1.191
43.403	320.556	4.1	Hvm	2.954	1.409	1.605	1.156

44.296	338.772	3	Hvg	3.474	1.326	1.622	1.178
47.266	4.822	13.2	Hvk	3.323	1.366	1.712	1.180
49.956	5.805	8.2	Hvk	3.545	1.265	1.726	1.187
22.998	308.762	8.1	Hchp	2.921	1.547	1.732	1.227
20.66	319.873	16.7	Hchp	2.629	1.502	1.578	1.560
56.792	307.591	6.4	Hvm	4.459	1.347	1.904	1.163
53.296	300.718	4.8	Hchp	2.609	1.227	1.435	1.178
54.278	320.917	9	Hvm	2.766	1.272	1.568	1.154
40.251	312.187	17.4	Hchp	2.482	1.541	1.647	1.343
46.03	327.156	3.6	Hvg	3.092	1.354	1.465	1.182
45.063	337.328	4.5	Hvg	3.300	1.213	1.266	1.204
44.301	339.812	4.2	Hvg	3.403	1.353	1.638	1.189
45.876	346.414	12.8	Hvg	3.573	1.355	1.579	1.230
46.318	348.215	14.4	Hvg	4.053	1.490	1.660	1.238
61.031	24.135	11.9	Hvk	3.444	1.414	1.777	1.214
72.992	38.303	10.8	Hvk	3.283	1.459	1.538	1.288
38.532	99.201	18.4	Hvg	4.402	1.416	1.463	1.176
58.221	74.745	17	Hvm	3.131	1.334	1.608	1.203
44.039	101.71	16.2	Hvg	3.894	1.267	1.755	1.132
58.532	116.812	15.9	Hvm	3.890	1.207	1.897	1.200
58.27	67.709	14.5	Hvm	3.375	1.187	1.583	1.149
34.898	102.582	13.5	Hvg	3.527	1.200	1.615	1.124
48.466	89.276	12.1	Hvm	3.429	1.139	1.884	1.095
36.622	81.676	11.2	Aps	3.604	1.280	1.718	1.152
57.001	95.714	10.7	Hvm	3.092	1.366	1.720	1.152
37.427	115.364	10.2	Ael3	3.069	1.339	1.410	1.180
33.072	86.166	10.6	Aps	3.107	1.189	1.272	1.200
43.675	79.586	6.4	Apk	3.633	1.223	1.719	1.199
38.997	103.676	4.9	Hvg	3.425	1.291	1.544	1.231
34.706	120.533	12.2	Ael3	2.937	1.281	1.474	1.153
34.066	129.4	8	Ael3	2.753	1.342	1.388	1.189

36.886	124.277	5.8	Ael3	4.017	1.322	1.700	1.172
37.597	128.919	4.9	Ael3	2.770	1.262	1.474	1.168
37.108	133.128	4	Ael3	2.975	1.292	1.487	1.182
26.763	120.964	14.5	Hvg	3.454	1.371	1.874	1.225
45.491	63.705	3.9	Aps	2.670	1.292	1.544	1.297
50.824	41.685	17.2	Aps	3.396	1.400	1.618	1.245
51.096	54.187	21.4	Apk	3.327	1.280	1.833	1.294
49.137	76.305	7.6	Hvm	3.402	1.303	1.514	1.169
49.903	94.849	10	Hvm	4.129	1.283	1.401	1.116
40.951	98.296	14.7	Hvg	3.485	1.364	1.711	1.184
31.034	102.254	9.3	Hvg	2.947	1.572	1.659	1.198
28.722	119.947	10.2	Hvg	2.048	1.701	1.187	1.424
34.645	125.597	12.8	Ael3	2.725	1.633	1.533	1.329
32.987	118.605	20.7	Aps	3.261	1.602	1.699	1.392
36.399	127.842	3.3	Ael3	3.128	1.277	1.578	1.221
38.593	137.222	18.5	Ael3	4.404	1.639	1.529	1.162
54.939	175.115	5.1	Hvm	3.038	1.187	1.559	1.122
66.967	252.049	9.2	Hvk	2.785	1.277	1.492	1.156
70.44	227.832	7.3	Am	2.557	1.226	1.482	1.197
68.434	189.325	11.6	Hvk	3.387	1.304	1.766	1.145
69.027	199.283	7.4	Am	2.708	1.292	1.646	1.189
70.81	200.327	6.5	Am	2.548	1.303	1.500	1.191
34.051	167.099	5.4	Aps	2.608	1.263	1.287	1.186
48.366	167.419	7.1	Aps	3.443	1.283	1.446	1.194
32.27493	169.19096	20.3	Aps	2.899	1.433	1.955	1.298
34.59711	149.35078	13.4	HNu	2.635	1.500	1.321	1.274
35.77289	146.31133	5.5	HNu	3.744	1.703	1.663	1.252
34.051	167.099	5.3	Aps	2.749	1.263	1.353	1.213
34.321	172.016	10.3	Apk	2.776	1.410	1.727	1.222
32.909	165.51	4.3	Aps	2.500	1.231	1.700	1.187
34.814	169.559	8.5	Aps	3.050	1.377	1.604	1.150

Curriculum Vitae

Name: Ryan Schwegman

Post-secondary Education and Degrees: Oklahoma State University
Stillwater, Oklahoma
2009-2012 B.Sc.

Rogers State University
Claremore, Oklahoma
2005-2008 A.A.

Related Work Experience

Teaching Assistant
University of Western Ontario
2013-2015

Research Assistant
University of Western Ontario
2013-2015

Intern
Planetary Science Institute
2012

Teaching Assistant
Oklahoma State University
2011-2012

Publications:

Schwegman, R.D., Osinski, G. R., Tornabene, L.L., Jones, E., Harrison, T.N. (2015). A comparative morphologic and morphometric study of double layered ejecta craters in volcanic terrains on Mars. *Meteoritics & Planetary Science* (*submitted*).

Schwegman, R.D., Osinski, G.R., Tornabene, L.L. (2015). A morphometric comparison of Martian double layered ejecta craters and implications for the effect of target lithology. Lunar and Planetary Science Conference XLVI, Abstract #2607.

Schwegman, R.D., Osinski, G.R., Tornabene, L.L. (2015). Layered ejecta morphologies on Syrtis Major and implications for regional geology. Lunar and Planetary Science Conference XLVI, Abstract #2645.

Schwegman, R.D., Osinski, G.R., Tornabene, L.L. (2014). A comparison of the morphometry of double layered ejecta crater in different volcanic regions on Mars. 8th International Conference on Mars, Abstract #1046.

Schwegman, R.D., Osinski, G.R., Jones, E., Tornabene, L.L. (2014). Assessing the morphology of double layered ejecta craters at equatorial regions on Mars. Lunar and Planetary Science Conference XLV, Abstract #2385.

Schwegman, R.D., Bourke, M.C. (2013). Analysis of rock breakdown features at Gusev Crater, Mars. Lunar and Planetary Science Conference XLIV, Abstract #3086.